



University  
of Glasgow

Welsh, Elizabeth (2011) *A novel method of cadaveric data acquisition from a dissection of the male lower limb using the Perceptron ScanWorks® V5 scanner.*  
MSc(R) thesis.

<http://theses.gla.ac.uk/2824/>

Copyright and moral rights for this thesis are retained by the author

A copy can be downloaded for personal non-commercial research or study, without prior permission or charge

This thesis cannot be reproduced or quoted extensively from without first obtaining permission in writing from the Author

The content must not be changed in any way or sold commercially in any format or medium without the formal permission of the Author

When referring to this work, full bibliographic details including the author, title, awarding institution and date of the thesis must be given



**UNIVERSITY**  
*of*  
**GLASGOW**

**A Novel Method of Cadaveric Data Acquisition from a  
Dissection of the Male Lower Limb Using the Perceptron  
ScanWorks® V5 Scanner**

**THESIS**

for

**MSc (by Research)**

by

**Elizabeth Welsh (0506726)**

Supervisor: Dr Paul Rea

# Abstract

**Introduction:** Under the current pressures of an expanding medical curriculum, the time allocated to anatomical training in medical education has been greatly reduced, resulting in an increasing number of doctors qualifying from medical school with an inadequate, and arguably unsafe level of anatomical understanding. Given the limited time now available for cadaveric dissection in medical training, future rectification of these deficits is becoming heavily dependent on supplementation from virtual anatomical training tools. In light of this, many attempts have been made to acquire cadaveric data for the creation of realistic virtual specimens. Until now however, the educational value of these training tools has been heavily scrutinised, with many sharing the view that they are over simplified and anatomically inaccurate.

The main problems associated with the usability of pre-existing datasets arise primarily as a result of the methodology used to acquire their cadaveric data. Projects in this field have previously approached the task of cadaveric data acquisition by creating comprehensive libraries of anatomical cross-sections, from which three-dimensional processing can be technically difficult and not always successful for the reconstruction of fine or complex anatomical structures.

**Aim:** The aim of this study therefore was to approach cadaveric data acquisition, for the purpose of creating a digital cadaveric specimen, in an unconventional manner, by obtaining three-dimensional data directly from cadaveric tissues with a Perceptron ScanWorks®V5 non-contact laser scanner.

**Methods:** To do this, a carefully planned dissection of the lower limb was performed on a 68 year old male cadaver, and laser scanning of all clinically relevant structures was undertaken at sequential stages throughout. In addition to this, colour and texture information was collected from the cadaveric tissues by high-resolution digital photography.

**Results:** A comprehensive three-dimensional dataset was acquired from all clinically relevant anatomy of the lower limb as a result of the methodology used in this study. Data was obtained at extremely high point to point resolutions, with a measurement accuracy of  $24\mu\text{m}$ ,  $2\sigma$ .

**Discussion:** By obtaining cadaveric data in this way, the problems associated with the three-dimensional processing of conventional cross-sectional data, such as image segmentation, are largely overcome and fine anatomical details can be accurately documented with high precision. This data can be processed further to create an accurate and realistic virtual reconstruction of the lower limb for both three-dimensional anatomical training and surgical rehearsal in the future.

**Conclusion:** Whilst the value of cross-sectional datasets in their own right should not be disputed, the methodology used for cadaveric data acquisition in this study has proved a very successful in collecting three-dimensional data directly from the specimen, and could be used to acquire detailed datasets for the reconstruction of other complex body regions for virtual anatomical training in the future.

# Acknowledgements

First and foremost, I would like to express my gratitude to my supervisor, Dr Paul Rea, for his invaluable guidance and support throughout this project.

I would also like to show thanks to the Royal College of Physicians and Surgeons Glasgow, for their kind financial support.

I should also take this opportunity to thank Professor Paul Anderson and Mr Duncan Kay, who are responsible for the high quality digital imaging documented in this study, and also to the rest of the digital design team from the Digital Design Studio, Glasgow School of Art, who's fine expertise continues to make this project such a great success.

Finally, I would like to acknowledge my friends and colleagues in the Laboratory of Human Anatomy, University of Glasgow, including the technical staff for their help and cooperation, Dr John Shaw- Dunn for his invaluable advise on various aspects of the dissection, and Dr Ahmed Khalid Raheem for his helpful input throughout the year.

# Contents

<b>Chapter</b>	<b>Page No.</b>
<b>Declaration of Originality</b>	<b>i</b>
<b>Abstract</b>	<b>ii</b>
<b>Acknowledgements</b>	<b>iv</b>
<b>Contents</b>	<b>v</b>
<b>List of Figures and Tables</b>	<b>vii</b>
<b>1: Introduction</b>	<b>1</b>
1.1: General Overview	2
1.2: The Requirement for ‘Virtual Cadavers’	4
1.3: Project Motive	6
1.4: Laser Scanning (Theory Behind the Project)	8
1.5: Projects Aims and Approach	11
1.5.1: The Scanner	11
1.5.2: The Dissection	13
1.5.3: Research Hypothesis	14
1.6: Research Team	15
<b>2: Materials and Methods</b>	<b>17</b>
2.1: Materials	18
2.1.1: Cadaveric Dissection	18
2.1.2: Cadaveric Data Acquisition	19
2.2: Methods	20
2.2.1: Cadaveric Dissection	20

<b>Full Account of Cadaveric Dissection</b>	<b>22</b>
<b>Block A:</b> The Inguinal Canal	22
<b>Block B:</b> The External Genitalia	26
<b>Block C:</b> The Anterior and Medial Compartments of the Thigh	30
<b>Block D:</b> The Anterior and Lateral Compartments of the leg and Dorsum of the foot	37
<b>Block E:</b> The Gluteal Region and Posterior Compartment of the Thigh	43
<b>Block F:</b> The Posterior Compartment of the Leg	48
<b>Block G:</b> The Sole of the Foot	50
<b>Block H:</b> Articulations	55
<b>Block I:</b> Bones	58
<b>2.2.2:</b> Cadaveric Data Acquisition	59
<b>3: Results</b>	<b>62</b>
<b>3.1:</b> Cadaveric Dissection	63
<b>Block A:</b> The Inguinal Canal	63
<b>Block B:</b> The External Genitalia	66
<b>Block C:</b> The Anterior and Medial Compartments of the Thigh	68
<b>Block D:</b> The Anterior and Lateral Compartments of the Leg and Dorsum of the	70
<b>Block E:</b> The Gluteal Region and Posterior Compartment of the Thigh	73
<b>Block F:</b> The Posterior Compartment of the Leg	75
<b>Block G:</b> The Sole of the Foot	77
<b>Block H:</b> Articulations	79
<b>Block I:</b> Bones	81
<b>3.2:</b> Cadaveric Data Acquisition	83
<b>4: Discussion</b>	<b>90</b>
<b>4.1:</b> Overview of Results	91
<b>4.2:</b> How Can this Data be Used?	93
<b>4.3:</b> Previous Work in Cadaveric Data Acquisition	95
<b>4.4:</b> Advantages of Present Study	102
<b>4.5:</b> Potential for Research Development	106
<b>4.6:</b> Summary and Conclusion	110
<b>References</b>	<b>112</b>
<b>Appendices</b>	<b>117</b>
<b>Appendix I:</b> ScanWorks V5 Datasheet	118
<b>Appendix II:</b> Perceptron Accuracy Statement	119
<b>Appendix III:</b> Cimcore Infinite 2.0 Arm Datasheet	122
<b>Appendix IV:</b> Description of Cimcore Accuracy Terminology	124
<b>Appendix V:</b> LHA Embalming Protocol	125

# List of Figures and Tables

	Page
<b>Figure 1:</b> Selected key stages of dissection Block A	65
<b>Figure 2:</b> Selected key stages of dissection Block B	67
<b>Figure 3:</b> Selected key stages of dissection Block C	69
<b>Figure 4:</b> Selected key stages of dissection Block D	72
<b>Figure 5:</b> Selected key stages of dissection Block E	74
<b>Figure 6:</b> Selected key stages of dissection Block F	76
<b>Figure 7:</b> Selected key stages of dissection Block G	78
<b>Figure 8:</b> Selected key stages of dissection Block H	80
<b>Figure 9:</b> Selected key stages of dissection Block I	82
<b>Figure 10:</b> An example of how a polygon mesh surface is created from the point cloud data collected at each stage of the cadaveric dissection.	84
<b>Figure 11:</b> Imaging of selected inguinal canal dissections (Block A) by digital photography and laser scanning.	85
<b>Figure 12:</b> Imaging of anterior thigh dissection from Block C (vi)	86
<b>Figure 13:</b> Imaging of selected dissections of the anterior and lateral compartment of the leg and dorsum of the foot (Block D).	87
<b>Figure 14:</b> Imaging of selected dissections from gluteal and posterior compartment of thigh regions (Block E).	88
<b>Figure 15:</b> Imaging of selected dissections from the sole of the foot (Block G)	89
<b>Figure 16:</b> Prototype reconstruction derived from point cloud data acquired from inguinal canal, external genitalia and anterior thigh dissections by digital design experts at the Digital Design Studio, Glasgow School of Art.	94
<b>Table 1:</b> A Comparison of Methods in Cadaveric Data Acquisition	109

# 1: Introduction

## **1.1: General Overview**

The ancient art of cadaveric dissection dates back to a time before 500 BC with the initial writings of Hippocrates II (Molamo et al., 2006), and has been seen as a corner-stone in anatomical training ever since. In recent decades however, the profile of anatomy and cadaveric dissection has been tainted by claims that it is an exhausted area of research, and in the midst of a global curricular reform, has fallen under scrutiny as an essential component of medical training (Fasel,1993; Malamed & Seiden, 1995; Moosman & Arbor, 1980). The drastic reduction in hours now allocated to cadaveric dissection and anatomical teaching in the modern medical curriculum has raised concerns that young doctors are graduating from medical school with an insufficient understanding of three-dimensional anatomy, and it is feared that this level of training has now fallen below that which supports safe medical practice (Kluchova et al., 2000; Turney, 2007). These issues have indicated the requirement for new ways of teaching in anatomy, and in the midst of a digital revolution, educators are looking to the concept of virtual cadavers to help rectify these deficits. In light of this, many projects have pursued the challenge of acquiring real cadaveric data to create accurate anatomical reconstructions, by sectioning cadavers and using the extensive two-dimensional datasets to build three-dimensional models for use in anatomical training. Whilst acquiring cadaveric data in this way is useful for cross-sectional anatomy training for radiology per say, three-dimensional reconstruction from this data remains a great technical challenge, and important anatomical details are often lost in the process. As a result, the standard of digital cadavers produced from these datasets have left many traditionalists sceptical about the value of virtual specimens, with many of them sharing the view that they are oversimplified and non-representative of real anatomy (Garg et al., 1999; Nicholson et al., 2006).

This report therefore, describes a study which aims to overcome some of these problems by employing a completely unique approach to cadaveric data acquisition.

## **1.2: The Requirement for ‘Virtual Cadavers’**

It can be strongly argued that a profound knowledge of the human anatomy is crucial for the safe and effective execution of many techniques seen in clinical examination, diagnostics, radiology, therapeutics, anaesthetics, emergency medicine and of course, surgery, to mention but a few (Kilroy & Driscoll, 2006; Turney, 2007). Given the relevance of anatomy in its clinical context, it is not surprising that this basic science is a historical component of medical training. Regardless of recent claims that it is outdated and didactic, the majority of clinicians, educationalists and students agree that it is still an important and relevant part of the basic medical curriculum, and often sparks a great deal of enthusiasm amongst students (Cottam, 1999; Mitchell & Batty, 2009; Moxham & Plaisant, 2007; Patel & Moxham, 2006).

Anatomy is largely a practical based discipline and has traditionally been taught in medical schools by the time-honoured method of cadaveric dissection. Anatomical dissection has been praised over the years as an educational tool for, not only bestowing anatomical knowledge on the student, but also for providing them with the essential humanistic values and transferable skills required by a professional and compassionate doctor (Evans & Watt, 2005; Newell, 1995; Older, 2004; Rizollo & Stewart, 2006; Shaw Dunn, 1995). Traditionally, anatomy teaching from the dissection table has, until the advent of digital technologies, been the only method of providing the student with an awareness of three-dimensional spatial relationships, physical differences between specific tissues types, and a means of developing their manual dexterity (Older, 2004; Rizollo, 2002; Rizollo & Stewart, 2006; Shaw Dunn, 1995). Despite the advent of computerised cadavers, dissection still remains the best way of highlighting the concept of anatomical variation, and introducing the student to the concept of mortality (Finkelstien & Mathers, 1990).

Despite the important role which dissection has played in the medicine and science over the generations, its place in the medical curriculum has been in steady decline for many decades (Malamed & Seiden, 1995; Moosman & Arbor, 1980). A number of reasons for this decline have been proposed, however those most commonly stipulated in the literature are; reduced time allocation for anatomical teaching, a significant shortage of qualified teachers and a drastic shift in teaching methods (Cahill et al., 2000; Evans & Watt, 2005; McLachlan et al., 2004; Older, 2004; Pryde & Black, 2005; Rizollo & Stewart, 2006). This decline has been global, and now presents the medical and lay person communities with the worrying prospect of doctors qualifying from their undergraduate, and even specialist training, with a level of anatomical knowledge below that which supports safe medical practice (Kluchova et al., 2000; Turney, 2007). For example, In Cottam's (1999) study of US residency programs, it was indicated that 57% of residency program directors believed their surgical trainees were in need of a refresher course in anatomy upon arrival to their specialist training, and 14% felt that new trainees were seriously lacking in anatomical knowledge. These findings are significant and reflect a similar situation in the UK. There was also a seven-fold increase in claims associated to the physician's anatomical error reported to the Medical Defence Union between 1999 and 2000 (Older, 2004). Rectification of the discrepancies in anatomical knowledge at postgraduate level is also becoming more difficult. Given the recent changes to the structure of postgraduate training in the UK, and the limitations on work placement training imposed by the European Working Time Directive, the time for further anatomical training in postgraduate programmes is greatly limited (Older, 2004; Standring, 2008). It would also appear that as well as clinicians and academic professionals, students share a similar concern with regards to the current level of anatomical tuition in the medical curriculum (Mitchel & Battey, 2009; Prince et al., 2003). In light of this serious problem, educators are turning more and more frequently to virtual cadavers to try and rectify these growing deficits in anatomical education.

## **1.3: Project Motive**

Whilst digital anatomy now has a crucial role to play in medical education, educators remain largely sceptical about its educational value, with many claiming that virtual cadavers are oversimplified, inaccurate and unrealistic (Garg et al., 1999; Nicholson et al., 2006). Many previous attempts have been made to create accurate cadaveric reconstructions for anatomical training by obtaining data from real cadaveric specimens. The idea was in fact first coined in the 1970's by Professor Robert A. Chase at Stanford University, who digitally reconstructed a female pelvic specimen by serially sectioning a cadaveric female pelvis and imaging the slices. (University of Stanford, 1974). This method of cadaveric data collection has since however, been pursued on a much greater scale, in projects such as the Visible Human Project (VHP), the Chinese Visible Human (CVH) and the Korean Visible Human (KVH) (Park et al., 2006; Spitzer & Whitlock, 1998; Zhang et al., 2003). The first of these projects, which remains to this day a benchmark in the field of cadaveric data collection, was the University of Colorado's Visible Human Project, funded The National Library of Medicine (NLM). This project was initiated in 1989 and aimed to obtain a fully comprehensive dataset for the definitive male and female for use in teaching and research projects across the globe. The VHP researchers approached this task by freezing and cross sectioning the male and female cadavers into slices of one millimetre and one-third of a millimetre slices respectively, obtaining a total of 1878 slices for the male, completed in 1994, and 5189 slices for the female in 1995. Prior to cryosectioning, the cadavers were imaged by CT and MRI scanning in transverse and coronal planes, and these radiographic images were then coupled with colour photographs of the corresponding cryosectioned slices (Spitzer & Whitlock, 1998). Though the advent of this data was revolutionary, many problems have since been identified with the Visible Human data (VHD) and the methodology used to acquire it. Freezing of the cadavers caused distortion of neural tissue, and the cryosectioning technique resulted in

elements of data loss and ‘streaking’ of tissues across the photographed slices. The KVH and CVH followed this attempt with similar approaches to data acquisition, making slight alterations to the methodology in a bid to improve the quality and the usability of the cross-sectional data in three-dimensional processing (Park et al., 2006; Zhang et al., 2003). Whilst the advent of these datasets has indeed proved invaluable in many areas of research such as the development of medical imaging techniques, computer assisted surgery and radiological training, the use of cross-sectional data for creating three-dimensional anatomical reconstructions for general training purposes, remains a complex technical problem. The greatest challenge exists in that, in order to use this data for three-dimensional reconstruction, it must undergo a meticulous process of image segmentation, whereby each cadaveric slice must be carefully delineated into its anatomical components and is then aligned in sequence to create a stacked three-dimensional frame. Given the compositional complexity of each anatomical cross-section, combined with the poor colour differentiation of frozen cadaveric tissues, this process can be extremely time consuming and is not always successful in creating detailed reconstructions of spatially complex anatomy (Imelińska & Molholt, 2005; López-Cano et al., 2007; Sakellariou et al., 2009). Even when three-dimensional surfaces can be successfully reconstructed in this way, the visual surface textures produced by these means are often lacking in realism (Beylot et al., 1996). For these reasons, a fully comprehensive and coherent 3D anatomical library has yet to be produced from the VHD (Jastrow & Vollrath, 2003). Given the pressing requirement to produce more adequate digital cadavers for anatomical training in the current educational climate, these problems must somehow be overcome.

## **1.4: Laser Scanning (Theory Behind the Project)**

The study in hand therefore, aims to overcome some of the problems associated with the use of previous cadaveric datasets, by approaching cadaveric data acquisition, not with a conventional sectioning technique, but using state of the art three-dimensional laser scanning technology instead. Three-dimensional laser scanning is already a standard modality of data acquisition in industries such as car manufacturing and mechanical engineering and is commonly used in these disciplines as a means of reverse engineering for mechanical part inspection.

Like an 'ordinary' digital camera, a laser scanner has a cone shaped field of view and can only obtain information in its direct line of sight. Unlike simple digital photography however, laser scanning does not capture an image using reflected colour information, but documents an objects three-dimensional surface profile using distance information, instead. This works on the mathematical principle of triangulation, whereby; if the scanner emits a laser beam onto a solid physical surface, and the reflected light spot is monitored by an appropriately placed sensor (at a known distance and angle from the emitter), then the distance between the emitter and the point of intersection (by the physical surface) can be determined. Each surface point can then be plotted (by appropriate compatible scanning software) in three-dimensional space to create a dataset called a point cloud, which represents an accurate geometric profile of the objects surface. Whilst modern laser scanners often use a laser stripe to increase the speed of data acquisition, a number of scans must usually be performed (from various angles) before an objects entire surface topography can be documented. Each point cloud produced must therefore be translated into a common co-ordinate frame and aligned with the corresponding profiles collected. This is usually done using an external tracking device such as a Co-ordinate Measuring Machine (CMM) (to which the scanner is often

physically attached) which can determine the exact position of the scanner in three-dimensional space at any one time throughout the process of data collection. Once an objects complete surface profile has been obtained, the collective point cloud can then be ‘joined-up’ by a series of straight lines to create a three-dimensional triangulated-mesh frame, or polygon-mesh. This mesh can then be used as a basis for further modelling or for a variety of different purposes, depending on the target end-use of the data (Hieu et al., 2010; Pfeifer & Briese, 2007).

Developed on the basis of these relatively simple laws of physics, this technology offers one of the most precise and accurate means of digital imaging available, and for this reason, is already a well established three-dimensional imaging modality within a number of different industries. As mentioned however, it is perhaps best known for its use in mechanical reverse engineering and car manufacturing, where laser scanning is commonly employed as a means of inspection and quality assurance of physical mechanical parts (Gerth & Brueckner, 2005; Gerth, 2005; Hieu et al., 2010). In addition to its precision, non-contact laser scanning can accurately document an objects three-dimensional surface without physically modifying or damaging the object in any way. This makes it a popular choice of imaging technique for the digital reconstruction of ancient historical artefacts, art restoration or any other project which involves precision three-dimensional modelling of deformable solid objects (Europac3Dimensional, 2011; Pfeifer & Briese, 2007).

Whilst non-contact laser scanning has not yet been documented in the literature as a means of cadaveric data acquisition, it has already established its place in a number of the biomedical and clinical production lines, including the production of customised hearing devices, orthotic implants, dental prosthetics and even in the development of contact lenses (Hieu et al., 2010).

Based on the physical principles of laser scanning, along with its frequently documented success in the aforementioned areas, the idea behind this study was that laser technology could also be used as a means of obtaining highly accurate three-dimensional data directly from the deformable human tissues of a cadaveric specimen for the purpose of digitally reconstructing those tissues for anatomical training. This would then be useful in that the requirement for cadaveric sectioning and subsequent image segmentation prior to specimen reconstruction would be eliminated.

## **1.5: Project Aims and Approach**

To investigate this theory, and attempt to overcome the problems associated with the use of previous datasets in the production of digital cadavers for anatomical training, the aim of this study was to use high-end non-contact laser scanning to obtain three-dimensional surface data from all clinically relevant anatomical structures within a designated anatomical region of a cadaveric specimen. The laser scanner of choice was the Perceptron ScanWorks<sup>®</sup> V5 scanner attached to a Cimcore Infinite 2.0 (seven axis) Portable Co-ordinate Measuring Machine Arm (PCMM), and the designated anatomical region from which data was to be collected was the male lower limb. To approach this task, the specimen was to be carefully dissected in progressive stages and data collected from all clinically relevant structures at each stage, via laser imaging and digital photography.

### **1.5.1: The Scanner**

The Perceptron ScanWorks<sup>®</sup> V5 scanner used in this study has been approved by government and military engineers and is frequently quoted by experts as being one of the most advanced laser scanners of its kind (Gerth, 2005; Perceptron, 2011). For this reason, it is already a popular choice of digital imaging modality in many disciplines, such as automotive, animation, aeronautical engineering and many more (Gerth, 2005; Europac3Dimensional, 2011). Whilst there are many features which deemed the ScanWorks<sup>®</sup> V5 scanner suitable for the study in hand, the main reasons for this choice were:-

- It can capture surface data with a mean point to point resolution of up to 12 $\mu$ m, thus making it capable of facilitating high resolution data acquisition of fine anatomical details (see Appendix. I)
- As mentioned, it has been approved by both military and government engineers (Perceptron, 2011) and performs surface data collection with a measurement accuracy of 24 $\mu$ m  $2\sigma$  throughout its entire field of view. Additionally, both the scanner and Cimcore arm are issued with guaranteed accuracy measures (see Appendix. II for details on scanner accuracy statement, and Appendices III and IV for details on Cimcore arm accuracy measures)
- It has the fastest point collection system of any line scanner, with the ability to collect up to 458400 surface points per second, potentially reducing the time required to acquire large amounts of cadaveric data (See Appendix. I)
- Unlike many other laser scanners, it can be used to obtain data from moist or reflective surfaces without the use of ‘dulling’ agents, and thus is a more suitable choice for scanning moist cadaveric tissues) (See Appendix. I)
- It provides the operator with various visible and audible cues while scanning which they can use to achieve optimal data acquisition and reduce the collection of redundant data. (See Appendix. I)

In addition to laser-facilitated data acquisition, the cadaveric structures were also to be photographed using a high-resolution Panasonic™ DMC TZ7 Lumix digital camera (12 x

Optical Zoom, 10.1 Megapixels), in order to support the three-dimensional data with corresponding surface colour and texture information.

### 1.5.2: The Dissection

The region of anatomy from which laser facilitated data acquisition was to be performed in this study was the male lower limb. The lower limb is a spatially complex part of the human anatomy with many clinical applications, including the correction of circulation disorders, sports injury repair, anaesthetics and inguinal hernia repair (Fagan & Awad, 2004), making this region an ideal focal point for this study. More specifically however, the main reasons behind choosing this anatomical region for this particular study were:-

- The lower limb is relatively accessible by simple dissection techniques
- This region incorporates the inguinal canal which features complex spatial anatomical relationships
- Lower limb anatomy is extremely relevant to modern clinical teaching
- There exists a distinctive lack of musculoskeletal and inguinal canal training applications which have been successfully derived from previous cadaveric datasets

The basic criteria for this dissection, determined prior to the study, was that it had to demonstrate all clinically relevant anatomy at a level of detail sufficient for further digital modeling, and to do so in such a way that offers an accurate representation of ‘normal’ lower limb anatomy.

### 1.5.3: Research Hypothesis

Based on the physical principles of laser scanning, and on the well documented success of this technology in other areas of research, it was hypothesised that, providing the cadaveric dissection of the lower limb met the above criteria, laser scanning would facilitate the collection of a comprehensive, accurate and high resolution three-dimensional dataset for the male lower limb, including all clinically relevant anatomy, which can be used in the future production of a virtual specimen for anatomical training.

## **1.6: Research Team**

This project involves a unique collaboration between the Digital Design Studio (DDS), Glasgow School of Art (GSA), the Royal College of Physicians and Surgeons Glasgow (RCPSG) and the Laboratory of Human Anatomy (LHA), University of Glasgow.

### **The Laboratory of Human Anatomy**

LHA is one of the largest and most reputable of its kind in the UK, and provides a venue for many well established surgical and anatomical training courses for professionals from around the globe, training in plastic and reconstructive surgery, podiatry, anaesthesia and physiotherapy.

### **The Digital Design Studio**

The DDS is the largest postgraduate research centre of the Glasgow School of Art, and features one of the top 6 interactive 3D visualisation laboratories in the world. Their extensive knowledge in advanced 3D visualisation and their vast experience in the use of laser-scanning technology has led them into high profile associations within the art, science and engineering disciplines. As a result of its expertise in the field of digital visualisation, the DDS is the leading part in the recently established Scottish Medical Visualisation Network (SMVN) (Digital Design Studio, 2007). This is an interdisciplinary expert group who have already undertaken projects in the creation of anatomical training packages such as haptic lumbar puncture, the foot and ankle in teaching musculoskeletal ultrasound, lung collapse and the management of breast cancer (Digital Design Studio, 2007; Sakellariou et al., 2009;

Ward et al., 2009). Research undertaken by the SMVN has also touched upon the creation a virtual inguinal canal package for surgical training, using cross sectional CT and MRI scan data (Sakellariou et al., 2009) and it is hoped that further development of this training package, and others like it will benefit greatly from the results of this study.

## The Royal College of Physicians and Surgeons Glasgow

Having been founded on the 29th November 1599, the college has a substantial background of excellence in medicine and prides itself in promoting high standards of healthcare, from disciplines in clinical medicine, dentistry and travel medicine across the globe. It is a vastly multidisciplinary organisation with 9500 members from research, clinical and educational backgrounds from various locations across the world. The research documented in this study was fully supported and funded by this prestigious organisation (RCPSG, 2011).

# 2:Materials & Methods

## 2.1: Materials

### 2.1.1: Cadaveric Dissection

The cadaver used for all of the dissection documented in this study was a 68 year old male, selected from the general stock in the Laboratory of Human Anatomy, University of Glasgow. The cadaver chosen died from pulmonary fibrosis, and demonstrated no obvious abdominal or lower limb abnormalities prior to, or after dissection had taken place. The specimen was embalmed following the normal embalming protocol at the Laboratory of Human Anatomy before any dissection commenced (see Appendix. IV for further details on the Laboratory of Human Anatomy embalming procedure).

#### Dissection Kit:

- Swann- Morton<sup>®</sup> scalpel handle (size 4)
- Swann- Morton<sup>®</sup> surgical blades (size 24, 11)
- Dissection forceps (fine, blunt)
- Dissecting scissors (small)
- Dissection pins
- Wooden dissection block (approx. 30 x 10 x 15 cm)
- Dissection lamp
- Embalming fluid spray
- Polythene body cover

### 2.1.2: Cadaveric Data Acquisition

- Perceptron ScanWorks<sup>®</sup> V5 Scanning Probe
- Cimcore Infinite 2.0 (Seven axis) Portable Co-ordinate Measuring Machine Arm (PCMM).
- Panasonic<sup>™</sup> DMC TZ7 Lumix digital camera (12 x Optical Zoom, 10.1 Megapixels)
- Dell<sup>™</sup> portable laptop PC
- ScanWorks<sup>®</sup> V5-compatible Software

## **2.2: Methods**

### **General Approach**

A full dissection of the lower limb was planned according to the initial criteria and carried out on the selected male specimen. Throughout this period, three-dimensional surface data and colour digital photography was acquired from all clinically relevant anatomical structures exposed during dissection, using the Perceptron ScanWorks<sup>®</sup> V5 scanner, and Panasonic<sup>™</sup> Lumix digital camera, respectively.

### **2.2.1: Cadaveric Dissection**

The cadaveric dissection for the purpose of this study was carried out in nine consecutive blocks, each focussing on a separate anatomical sub-region of the lower limb. These sub-regions were:-

- (A)** The Inguinal Canal
- (B)** The External Genitalia
- (C)** The Anterior and Medial Compartments of the Thigh
- (D)** The Anterior and Lateral Compartments of the Leg and Dorsum of the Foot
- (E)** The Gluteal Region and Posterior Compartment of the Thigh
- (F)** The Posterior Compartment of the Leg
- (G)** The Sole of the Foot

## **(H)** Articulations

## **(I)** Bones

Prior to the dissection, all clinically relevant anatomical structures within the male lower limb were listed and placed in a timetabled dissection agenda. Using this as a guide, each body region was dissected in sequential stages, with the view of progressively demonstrating all clinically relevant anatomy for subsequent data collection. For blocks 1- 4 the cadaver was maintained in a supine position and from block 5 onwards the specimen was turned 180° in order to facilitate access to the gluteal and posterior lower limb compartments. The dissection was performed entirely by the author, and full details of the dissection methodology, including a list of all anatomical structures demonstrated for data collection, are given on pages 22-58.

At intermittent periods between dissections, the specimen was sprayed with embalming spray to maintain the tissues in a moist condition and as close to their natural state as possible. Skin flaps were retained and replaced over exposed tissue, and the polythene body cover was used between every dissection to prevent moisture evaporation and tissue drying. It was ensured however, that the specimen was not sprayed within a twenty-four hour period prior to imaging to prevent excessive levels of moisture from interfering with the functionality of the laser scanner.

# **Full Account of Cadaveric Dissection**

The concept of “imaging”, referred to throughout this account, includes both three-dimensional laser scanning and digital photography of the cadaveric structures in question.

## **Block A: The Inguinal Canal**

### **(i) Exposure of Subcutaneous Fat**

A vertical midline skin incision was made from the umbilicus to the mons pubis and from either end of this incision, another two horizontal skin incisions were made, the first from umbilicus to right mid-flank region, and the second from the mons pubis to left lumbar region. This rectangular area of skin was then reflected to expose the subcutaneous tissue on the lower left abdominal wall.

Another vertical skin incision was then made from mid-way along the inferior horizontal abdominal incision, to mid-way down the anterior aspect of the thigh. From here, a perpendicular incision was made across the midpoint of the thigh, and the skin on either side was then fully reflected to expose the subcutaneous fat of the superior and anterior portion of the thigh. The entire area of exposed subcutaneous fat overlying the abdominal and thigh regions were then imaged.

### **(ii) Exposure of Superficial Veins and Inguinal Ligament**

The great saphenous, superficial external pudendal, superficial epigastric and superficial circumflex iliac veins were identified within the subcutaneous tissue and defined by way of

blunt dissection. Once the superficial veins had been successfully identified within surrounding fatty tissue of the groin and proximal thigh region, subcutaneous fat and superficial fascia overlying the proximal thigh was removed in a superior to inferior direction, from the inguinal ligament, downwards. In addition to the superficial veins and deep fascia, care was taken to identify and define various other structures such as the superficial inguinal lymph nodes, (anterior femoral veins) and the lateral cutaneous nerve of the thigh. All aforementioned structures were subsequently imaged.

### (iii) Exposure of Rectus Sheath, External Oblique Aponeurosis, Superficial Inguinal Ring and Proximal Spermatic Cord

All remaining abdominal fat was removed to reveal the underlying rectus sheath, and the lower portion of the external oblique muscle (and aponeurosis), taking care not to damage the cutaneous branches of the iliohypogastric and ilioinguinal nerves. The proximal spermatic cord (external spermatic fascia), and superficial inguinal ring were identified and defined, and the aforementioned structures were scanned.

Between the superficial inguinal ring and the cords point of entry into the groin region, a small section of the external spermatic fascia was carefully removed to expose the underlying ilioinguinal nerve and the cremasteric fascia for subsequent imaging.

### (iv) Exposure of Internal Oblique, Iliohypogastric Nerve and Conjoined Tendon

The external oblique aponeurosis (including the remaining anterior wall of the inguinal canal) was removed in a medial to lateral direction from an area immediately lateral to the linea alba, to the medial boundary of the external oblique muscle fibres. In doing this, the

underlying internal oblique muscle, its aponeurosis, and the conjoint tendon were identified and imaged. The iliohypogastric nerve was observed emerging from the internal oblique muscle fibres, and was traced medially to the point at which it passes through the external oblique aponeurosis. Additionally, the ilioinguinal nerve was traced back from the inguinal canal to the point at which it pierces the internal oblique muscle fibres. The course of these nerves was then defined for laser scanning.

#### (v) Exposure of Rectus Abdominis, Transversus Abdominis, Transversalis Fascia Aperture and Deep Inguinal Ring

The muscle fibres of the external oblique were dissected from the underlying internal oblique and the former was then reflected laterally to expose the underlying internal oblique layer for subsequent imaging. The anterior wall of the rectus sheath was then removed to expose the underlying rectus abdominis and from the lateral border of this muscle, the internal oblique aponeurosis was carefully dissected from the underlying aponeurosis of transversus abdominis. Following this, the iliohypogastric nerve was cut midway along its exposed length (reflecting the distal portion medially) and the internal oblique was then reflected laterally to expose the underlying transversus abdominis and the proximal course of the nerve along the anterior surface of the deep muscle layer. At this stage, the transversalis fascia aperture and the deep inguinal ring were also identified and defined by blunt dissection. All aforementioned structures were then subject to imaging.

(vi) Exposure of Inferior Epigastric Vessels, Lower Thoracic Nerves and Posterior Rectus Sheath

The rectus abdominis was divided along the border of the superior horizontal abdominal incision (see A(i)), and was then reflected inferiorly taking care only to cut neurovasculature associated with the posterior surface of the muscle. A horizontal incision was made along the inferior border of the rectus abdominis (immediately superior to the left pubic tubercle) and the muscle was then completely removed to expose the posterior rectus sheath, inferior epigastric vessels, and thoracic and subcostal nerves (T 11 and T12), all of which were subsequently imaged.

## **Block B: The External Genitalia**

### (i) Exposure of the Superficial Veins of the Penis

In continuation with the previous vertical abdominal skin incision (see section A(i)), a shallow skin incision was made down the dorsal aspect of the penis to the neck of the glans. Perpendicular to this, another skin incision was then made around the base of the prepuce, allowing the skin covering the body of the penis to be reflected laterally on either side. The superficial penile fascia was then carefully removed in a proximal to distal direction to expose the superficial dorsal veins, which were then defined by blunt dissection for imaging.

### (ii) Exposure of Deep Dorsal Vessels, Dorsal nerve, and External Spermatic Fascia of the Scrotum

The superficial dorsal vein was divided at the base of the penis and was then removed. Another skin incision was then made down the ventral aspect of the penis from the frenulum to the base, and then from here, down the raphe of the scrotum, allowing the skin on the ventral aspect of the penis and the left portion of the scrotum to be reflected inferiorly (to the base of the penis on the right, and to the posterior boundary of the scrotum on the left). The external spermatic fascia was then identified. The linea alba was cut horizontally at its distal attachment to the pubic symphysis and reflected superiorly and following this, the dorsal arteries, nerves and deep dorsal vein were identified emerging from the sub-pubic angle at the base of the penis. These structures were then traced in a distal direction along the dorsal penile shaft by careful removal of the deep fascia. All aforementioned structures were then defined and subsequently imaged.

### (iii) Exposure of Corpus Caverosum, Cremasteric Fascia and Genital Branch of the Genitofemoral Nerve

The deep dorsal vein and dorsal nerves were dissected from the dorsal surface of the penis and were then divided and removed at the penis base. Any remaining fascia and neurovasculature on the ventral shaft were also removed in a distal to proximal direction to demonstrate the corpus cavernosum and spongiosum, for imaging.

A longitudinal incision was then traced down the remaining external spermatic fascia of the distal spermatic cord, from the point at which it had been previously dissected (see section A(iii)) to the inferior surface of the exposed scrotum. The external spermatic fascia was then reflected on either side of this incision to expose the underlying cremasteric fascia and genitofemoral nerve, and these structures were then imaged. On reflection of the external spermatic fascia surrounding the testicle, an area of fascial attachment on the medial aspect of the testicle, to the testicular septum, was preserved to maintain the testicle in position for documentation.

### (iv) Exposure of Corpus Spongiosum and Internal Spermatic Fascia

On the left hand side of the penis, the fundiform ligament was divided horizontally, and was then reflected superiorly and inferiorly to expose the base. The corpus spongiosum was identified emerging from the pubic angle on the ventral aspect of the penis and from here, along with the glans penis, this structure was then separated from the corpus cavernosum in a proximal to distal direction, by blunt dissection. The corpus spongiosum was then reflected laterally to facilitate full exposure of the corpus spongiosum, which was subsequently imaged.

The fascial attachment on the medial aspect of the left testis (see section B(iii)), and any remaining connections between the spermatic cord and the body wall were divided with a scalpel to liberate the testis and distal spermatic cord from the body wall and perineum. Following this, a longitudinal incision was made through the cremasteric fascia, from the abdominal wall to the medial aspect of the left testicle. The testicle was then returned to its true position and fixed with a pin to the testicular septum for visual clarity during scanning. The internal spermatic fascia of the testis and cord was then identified and imaged.

#### (v) Exposure of Parietal and Visceral Layers of Tunica Vaginalis

Once the pin had been removed, and the testis released from its anatomical position, the internal spermatic fascia was divided with a circular horizontal incision around the superior margin of the testis. All internal spermatic fascia below this incision was then carefully removed to expose the parietal layer of the tunica vaginalis, after which the testicle was fixed in its anatomical position with a pin and then imaged. Following this, the testicle was released once again by removal of the pin, and the parietal layer was removed to expose the underlying visceral layer of the tunica on the anterior, lateral and medial testicular surfaces. Care was taken at this stage to preserve a small portion of the parietal layer on the posterio-medial surface of the testis to demonstrate the folding of the tunica vaginalis on the posterior aspect of the testicle. The liberated testis was then lay flat on the anterior thigh to allow scanning of both its lateral and medial surfaces, thus imaging the visceral tunica, and the folding at the posterior border of the testicle.

(vi) Exposure of Tunica Albuginea, Epididymis, Vas Deferens, Testicular Nerves, Testicular Arteries and Pampiniform Plexus

The internal spermatic fascia surrounding the distal spermatic cord and the remaining leaf of parietal tunica vaginalis on the postero-medial aspect of the testicle, was removed, and the visceral layer of the tunica vaginalis on the superior aspect of the testicle was cut away to expose the underlying head of epididymis. From this point, the epididymis was traced and dissected down the postero-lateral aspect of the testicle and then onto its inferior surface by way of blunt dissection, taking care not to damage the efferent ductules or any associated neurovasculature in this region. From the tail of the epididymis, the ascending vas deferens was identified, and dissected by blunt dissection in a proximal direction, up the postero-medial surface of the testis, into the distal portion of the spermatic cord. In doing this, care was taken to preserve and define the associated branch of the testicular artery. All other testicular nerves and vessels, namely the pampiniform plexus, and the testicular artery, veins and nerves were identified and defined, by blunt dissection, along the posterior and superior border of the testicle, to their point of ascent into the distal spermatic cord. Towards the posterior portion of the testicle, tough connective tissue was removed to expose the underlying tunica albuginea, and this was differentiated from the remaining portion of the tunica vaginalis on the anterior portion of the testicle, along its cut edge. The testicle was then mounted on the anterior aspect of the thigh, and was imaged on both its medial and lateral surfaces, thus allowing all aforementioned structures to be fully documented.

## **Block C: The Anterior and Medial Compartments of the Thigh**

### (i) Exposure of Fascia Lata

From mid way along the previous horizontal mid-thigh incision (see section A(i)), a vertical skin incision was made down the anterior surface of the distal thigh to the superior border of the patella. Perpendicular to this, a horizontal incision was then made from the medial to the lateral femoral condyle, immediately superior to the anterior aspect of the knee. The skin on the distal portion of the thigh was then reflected on either side of the vertical incision to expose the subcutaneous fat layer of the lateral, anterior and medial aspects of the lower thigh. The great saphenous vein was traced and defined by blunt dissection, in a proximal to distal direction from the level up to which it had previously been dissected (see section A(ii)). The vein was then cut midway along its exposed length and was then reflected superiorly and inferiorly to facilitate subsequent removal of the newly exposed subcutaneous fat in a proximal to distal direction. In doing this, fascia lata of the lateral, anterior and medial aspects of the thigh was fully exposed for imaging. At this stage the saphenous opening was identified and defined by blunt dissection. The upper and lower portions of the divided saphenous vein were then returned to their anatomical position and fixed in place with a pin through the underlying fascia. The fascia lata, the saphenous opening and the visible portion of the great saphenous vein were subsequently imaged.

(ii) Exposure of Quadriceps, Gracilis, Sartorius, Distal Portion of Adductor Longus, Pectineus, Tensor Fascia Latae, Iliotibial Tract, Femoral Triangle and Saphenofemoral Junction

The pin from the previous stage of dissection was removed and the two portions of the great saphenous vein were reflected in opposing directions. A vertical incision was made in the fascia lata from the inferior border of the saphenous opening to the horizontal skin incision on the distal aspect of the thigh. At the distal end of this incision, (along the line of the previous horizontal skin incision made in Block C(i)) a horizontal incision was then made across the top of the knee from the medial to the lateral condyles. The fascia lata was then reflected on either side of the thigh, medially as far as possible and laterally as far as the anterior margin of the iliotibial tract. In reflecting the lateral sheet of the fascia lata, the lateral cutaneous nerve was reflected superiorly. At this stage, the gracilis, adductor longus, sartorius, pectineus, vastus medialis, rectus femoris, and vastus lateralis muscles were all identified and cleaned for visual clarity. Following this, the femoral artery, vein and nerve were located within the femoral triangle and any visible branches were traced into the sartorius and proximal portions of the quadriceps. All of the aforementioned musculature and neurovasculature was then imaged.

(iii) Removal of Sartorius

Mid-way along the distal horizontal thigh incision, immediately superior to the patella, a vertical skin incision was made down the anterior aspect of the knee to the tibial tuberosity. A horizontal incision was then created below the knee joint from the lateral, to the medial condyles of the tibia. The skin overlying the anterior knee surface was then reflected on either side to expose the distal attachment of sartorius onto the medial tibial condyle. The sartorius

was then imaged in its entirety. Following this, the sartorius was then dissected from underlying musculature by blunt dissection and was then divided mid- way down its length to allow reflection of its superior and inferior parts in opposing directions. In doing this, any neurovascular connections from the femoral vessels and nerve were cut, as appropriate. Once fully reflected, the sartorius was divided at both its proximal and distal attachments for complete removal.

Following this, the connective tissue sheath overlying the adductor canal was removed, and the femoral artery, femoris profunda, femoral vein, lateral circumflex femoral vessels, saphenous nerve and the nerve to vastus medialis were exposed and defined for visual clarity. Minor blood vessels and nerve branches in the region of the femoral triangle were removed at this stage for visual clarity. On the lateral aspect of the thigh, the iliotibial tract was dissected from the vastus lateralis, was divided at either end and was then removed to expose the extent of the lateral quadriceps muscle. Imaging was carried out at this stage to document the components of the adductor canal, as listed above, and all of the quadriceps with the exception of vastus intermedius.

The distal fibres of the rectus femoris were dissected from the quadriceps tendon and the muscle was reflected to expose the vastus medialis and the underlying vastus intermedius. On reflection of rectus femoris, care was taken to preserve its neurovascular connections to the lateral circumflex femoral artery, lateral circumflex femoral vein, and the femoral nerve. The neurovascular supply to the vastus intermedius from the femoral nerves and vessels were then identified and defined by blunt dissection and removal of intermuscular adipose tissue. The neurovascular supply to the vastus intermedius and reflected rectus femoris was subsequently imaged.

#### (iv) Exposure of Adductor Longus and Vastus Intermedius

Blood vessels and nerves supplying the rectus femoris were cut adjacent to the lateral circumflex femoral artery and vein, and femoral nerve root respectively. Nerves and blood vessels associated with the vastus lateralis and vastus medialis muscles were also cut in a similar manner to facilitate the pending removal of these muscles. The reflected rectus femoris was divided at its proximal attachment and was subsequently removed to expose the origin of the vastus lateralis. From the anterior border of the vastus lateralis, immediately inferior to the greater trochanter, a large continuous incision was then made around the superior, posterior and inferior edges of the muscle. This incision was then carried in a medial direction across the quadriceps tendon and finally, along the inferior border of the vastus medialis. A vertical midline incision was then made, in a proximal to distal direction along the length of the tendinous attachment between the vastus lateralis and medialis, taking care not to damage the underlying tendinous attachment of the vastus intermedius on the anterior shaft of the femur. The bulk of the vastus lateralis was then removed by reflecting the muscle laterally from the midline incision, using a scalpel to separate fusing muscle fibres from the surface of the vastus intermedius. The vastus medialis was then removed by reflection in a medial direction, similarly using a scalpel to separate it from the intermedius, and the tendinous roof of the adductor canal. Following this, the roof of the canal was mostly removed with the exception of a 10 cm portion at its distal end to demonstrate part of this structure for documentation.

Within the newly exposed section of the adductor canal, perforating arteries were identified and defined by blunt dissection. All aforementioned structures, namely the extent of the vastus intermedius and the perforating arteries, were then imaged.

### (v) Exposure of Adductor Brevis, Anterior Division of Obturator Nerve, Shaft of Femur and Adductor Hiatus

The tensor fasciae latae was divided horizontally mid-way down its length, and the distal portion of the muscle removed (to facilitate better access to the origins of the vastus lateralis and intermedius). With the exception of a small area of muscle at the muscles proximal attachment, the remaining border of the vastus lateralis was removed to expose the underlying intermuscular septum.

The vastus intermedius was divided at both its origin and insertion, and all associated neurovascular connections cut, to allow complete removal of the muscle and subsequent exposure of the anterior shaft of the femur. Care was taken in dividing the distal portion of the vastus intermedius to preserve the common quadriceps tendon for dissection of the knee joint at a later stage.

On the medial aspect of the thigh, the remaining distal part of the vastus medialis was removed to expose the tendon of the adductor magnus and the adductor hiatus, which was then carefully defined by blunt dissection.

On the proximal thigh, the adductor longus and pectineus were cut along their proximal and distal muscular attachments, and all neurovascular connections to these muscles cut, allowing the bulk of each to be removed. In removing the adductor longus, the associated obturator nerve branch was identified, and cut for complete removal of the muscle. At this stage, the anterior division of the obturator nerve was identified and its branches traced into the gracilis, and adductor brevis. All aforementioned structures were defined by blunt dissection and were subsequently imaged.

#### (vi) Exposure of Adductor Magnus and Posterior Division of Obturator Nerve

Branches of the anterior division of the obturator nerve and blood vessels associated with the adductor brevis were cut adjacent to the muscle (and those overlying the adductor brevis removed) and the remaining branch of the anterior division of the obturator nerve was then divided 3 cm from its point of emergence from the superior border of the obturator externus. The adductor brevis was then cut at its origin, reflected laterally (taking care not to damage the underlying posterior division of the obturator nerve), and divided again along its distal attachment to the linea aspera, before being completely removed. The adductor magnus was identified fully, and perforating arteries from the profunda femoris were defined along its longitudinal attachment to the shaft of the femur. The obturator externus, posterior division of the obturator nerve, and medial circumflex artery and vein were identified and defined for visual clarity. The posterior division of the obturator nerve, and branches of the medial circumflex artery and vein were then carefully traced into the adductor magnus. Branches from these vessels were also traced into a small remaining portion of the adductor brevis at the muscles proximal attachment, demonstrating the vascular supply to this muscle also. The adductor magnus, perforating arteries, the posterior division of the obturator nerve, and the medial circumflex artery, and vein were all then subject to imaging.

#### (vii) Exposure of the Obturator Externus

The iliopsoas was cut immediately below the inguinal ligament and was then reflected in an inferior direction to its distal attachment onto the lesser trochanter. This section of muscle was then divided along its distal attachment and was subsequently removed to expose a larger area of the obturator externus. Care was taken at this stage not to damage the branch of the medial circumflex artery passing dorsally to the hip joint. Branches of the medial circumflex

femoral artery and vein supplying the adductor magnus and adductor brevis (imaged in the previous dissection) were then cut and the remaining part of the adductor brevis was removed. Prior to imaging, the femoral artery, profunda femoris and femoral vein were pulled in a lateral direction and fixed with a pin, to the tendinous insertion of the adductor magnus, in order to facilitate a clear view of the obturator externus. Imaging of the obturator externus then followed.

## **Block D: The Anterior and Lateral Compartments of the Leg and Dorsum of the Foot**

To facilitate better access with the scanner head for the purpose of imaging in this block, the lower limb was supported by a wooden dissection block, placed beneath the ankle joint, elevating the limb to an angle of 45°.

### (i) Exposure of Subcutaneous Fat, Long Saphenous Vein, Saphenous Nerve and Superficial Peroneal Nerve

A vertical skin incision was made down the anterior aspect of the leg and dorsum of the foot, from the tibial tuberosity to an area midway between the second and third metatarsophalangeal joints. This incision was then intersected with a horizontal incision over the anterior surface of the ankle joint, from the medial to the lateral aspect of the calcaneal tendon (passing inferiorly to the level of the medial and lateral malleoli). Another horizontal skin incision was then made across the dorsum of the foot, from the first to the fifth metatarsophalangeal joints and from this level, a vertical skin incision was made down the dorsal aspect of each toe. The skin on the anterior surface of the leg and the dorsal surface of the foot (including digits) was then fully reflected to expose the underlying subcutaneous fat layer of these areas. The smaller skin flaps from the dorsum of the foot were folded under the sole of the foot and held in place with a pin through the plantar fat pad.

From the medial aspect of the knee, the great saphenous vein, saphenous nerve, and associated branches, were traced down the medial aspect of the leg and dorsum of the foot, and were made visible by the removal of overlying fat (only subcutaneous fat overlying these structures was removed at this stage).

On the dorsum of the foot, smaller vessels draining into the venous dorsal arch from the five digits were then identified and carefully defined by blunt dissection.

On the anterior aspect of the leg, the superficial peroneal nerve was also identified and defined in a proximal to distal direction as far as possible onto the dorsum of the foot. The same technique was used to identify and define the terminal portion of the deep peroneal nerve, lying just laterally to the first metatarsal. The subcutaneous fat and superficial neurovasculature of the leg and foot as described was then subject to imaging.

### (ii) Exposure of Deep Fascia

All remaining subcutaneous fat on medial, anterior and lateral surfaces of the leg, and dorsum of the foot was removed in a proximal to distal direction, taking care to preserve the previously dissected neurovasculature. The deep fascia of the leg and foot and perforating veins were identified and subsequently defined by blunt dissection. The points at which the deep and superficial peroneal nerves emerge from the deep fascia of the foot and leg, respectively, were also located and defined for visual clarity. The aforementioned structures were then imaged.

### (iii) Exposure of Musculature in Anterior and Lateral Leg Compartments and Retinacula of Ankle

The great saphenous vein (from an area immediately below lateral malleolus) and the superficial portion of the peroneal nerve were both cut and removed. A longitudinal incision was then made through the deep fascia, from the tibial tuberosity to the superior border of the extensor retinaculum, along the anterior shaft of the tibia. A horizontal incision was then

made along the superior border of the extensor retinaculum over the anterior surface of the leg, from the medial to the lateral portion of the calcaneal tendon. All deep fascia lying superiorly to the extensor retinaculum was then reflected on either side of the mid-line incision (as far as the level of skin reflection on either side), and was then removed. The peroneus longus and brevis, extensor digitorum longus and hallucis longus, tibialis anterior, subcutaneous shaft of tibia, medial portion soleus, medial head of gastrocnemius, flexor digitorum longus and the tendon of tibialis posterior were all identified and cleaned by blunt dissection for visual clarity.

On the dorsum of the foot, a horizontal incision was made along the inferior border of the inferior extensor retinaculum, from the lateral surface of the calcaneus to the medial border of the plantar aponeurosis. All deep fascia, inferior to this incision, on the dorsal surface of the foot, was then removed (up to the level of the previous skin reflection) to expose the tendons of extensor hallucis longus, extensor digitorum longus, peroneus tertius, tibialis anterior, extensor digitorum brevis, as well as the extensor hoods on the dorsal surface of all five digits. Following this, finer structures on the foot, such as the sural and deep peroneal nerves, and the dorsalis pedis were located and carefully defined by blunt dissection.

On the remaining section of fascia covering the anterior surface of the ankle, the inferior and superior extensor retinacula were identified separately by closely examining the direction of the collagenous fibres under the dissecting lamp. The upper and lower bands of the inferior, and the inferior border of the superior extensor retinaculum were traced out with a scalpel, and all non-contributing fascia in the region was removed. On the medial surface of the ankle, the flexor retinaculum was also dissected using a similar technique. All aforementioned structures were imaged at this stage.

A vertical incision was made along the medial boundary of the extensor retinacula, and both the superior and inferior bands were reflected laterally to expose the underlying synovial

sheaths of the extensor hallucis longus, extensor digitorum longus and peroneus tertius tendons. These sheaths were then removed, to facilitate clear identification of the tendons. Deeper structures in this region, including the anterior tibial artery and venae comitantes were also located and defined by blunt dissection. On the medial surface of the calcaneal tendon, visible contents of the tarsal tunnel passing deep to the flexor retinaculum were also cleaned for imaging. On the medial side of the foot, subcutaneous fat was removed to expose the superior portion of the adductor hallucis muscle. This muscle, along with the tarsal tunnel and those structures deep to the extensor retinacula were all then subject to further imaging.

#### (iv) Exposure of the Common Peroneal Nerve and Anterior Tibial Artery

The tendons of extensor digitorum longus were divided adjacent to the proximal metatarsophalangeal joints, and the muscle was then detached at its proximal attachments to the tibia and fibula, and was then completely removed by separating the muscle from the interosseous membrane. The peroneus tertius was removed using a similar technique, dividing the muscle at its proximal and distal attachments. The anterior tibial artery and vein, and the deep peroneal nerve were then identified and traced into the tibialis anterior and extensor hallucis longus, and then carefully defined by blunt dissection for visual clarity.

Inferiorly to the lateral malleolus, the superior and inferior extensor retinaculum and surrounding connective tissue were completely removed to demonstrate the tendons of the peroneus longus and brevis on the lateral aspect of the ankle.

On the lateral aspect of the leg, the peroneus longus was divided 2cm from its most proximal point of origin, adjacent to the neck of the fibula, and the muscle fibres were then retracted slightly on either side of this incision to expose the neck of the common peroneal nerve at this location. The main branches of this nerve (namely the three articular, the lateral sural

cutaneous and the superior and deep peroneal (motor) branches) were then identified and defined by blunt dissection (taking care to demonstrate the path of its branches into surrounding musculature). On the medial aspect of the ankle, the flexor retinaculum was completely removed to expose the tibialis posterior, flexor digitorum longus, flexor hallucis longus, tibial nerve, posterior tibial artery (including calcaneal branches) and posterior tibial veins, and these structures were identified and defined by blunt dissection. The common peroneal nerve (and main branches), extensor digitorum brevis, the tendons of the peroneus longus and brevis, tarsal tunnel and the calcaneal branches of the posterior tibial artery and tibial nerve, mentioned above, were all subsequently imaged.

#### (v) Removal of Extensor Hallucis Longus

All blood vessels and nerve branches supplying the extensor hallucis longus were divided and the muscle tendon was cut adjacent to the first metatarsophalangeal joint. The muscle was then completely removed by separating the muscle in a superior to inferior direction at its proximal attachment, from the interosseous membrane. Care was taken at this stage to preserve the anterior tibial artery and deep peroneal nerve running adjacent to this membrane. The extensor digitorum brevis, deep peroneal nerve, and anterior tibial artery were all located, defined and imaged at this stage.

#### (vi) Removal of Peroneus Longus, Peroneus Brevis, Tibialis Anterior and Extensor Digitorum Brevis

The tibialis anterior was cut in a proximal to distal direction along its proximal attachment to the tibia, and was divided again at its distal attachment before being completely removed. In

doing this, care was taken not to damage the recurrent tibial artery and vein. The interosseous membrane was cleaned of any remaining muscle fibres and the proximal aperture (with associated anterior tibial vessels) was carefully defined by blunt dissection. On the lateral aspect of the ankle, the tendons of the peroneus longus and brevis were divided, adjacent to the lateral malleolus, retaining the distal portions of these tendons for visual clarity. Both muscles were then removed in a proximal to distal direction along their proximal attachments to the fibula and interosseous membrane, thus exposing the extent of the interosseous membrane, and the anterolateral surfaces of the tibia and fibula.

On the dorsal aspect of the foot, the extensor digitorum brevis was divided at each of its tendons, adjacent to each metatarsophalangeal joint. Each muscle belly was then reflected proximally, using a scalpel to separate the fascial connections to the underlying dorsal interosseous muscles. Once fully reflected, the extensor digitorum brevis was divided at its proximal attachment, and was then completely removed. The dorsal shafts of the metatarsal bones, dorsal interossei, anterior medial and lateral malleolar, medial and lateral tarsal, and arcuate arteries were identified and defined, and all aforementioned structures of the leg and foot were then imaged.

## **Block E: The Gluteal Region and Posterior Compartment of the Thigh**

### (i) Exposure of Subcutaneous Fat Over Gluteal Region and Posterior Aspect of Thigh

From the terminal point of the previously made horizontal skin incision on the left flank (see section A(i)), an incision was made along the lumbar region, immediately superior to the margin of the iliac crest. This incision then followed the downwards curvature of the iliac crest to the midline of the sacrum, and then to the intergluteal crest. Another skin incision was then made through the existing skin flap on the lateral aspect of thigh, along the gluteal fold, towards the perineum. Another horizontal incision was then made through the lateral skin flap, directly below the knee joint, across the proximal portion of the leg, and then through the medial skin flap on the opposing side. The skin overlying the gluteal and thigh compartments was then reflected medially to expose the underlying subcutaneous fat layer of these regions for subsequent imaging.

### (ii) Exposure of Gluteus Maximus, Posterior Cutaneous Nerve of Thigh and Fascia Lata

In a proximal to distal direction, the subcutaneous fat overlying the gluteal and posterior thigh regions was removed to expose the underlying deep fascia. The deep fascia overlying the gluteus maximus was then removed to demonstrate the muscle fibre orientation for imaging. Care was taken in removing the deep fascia around the sacral region to preserve and define the cutaneous sacral nerves and recurring branches of the posterior cutaneous nerve of

the thigh around the inferior border of the gluteus maximus. The gluteus maximus, posterior fascia lata and cutaneous nerves were all then imaged at this stage.

### (iii) Reflection of Gluteus Maximus and Removal of Fascia Lata

Using blunt dissection, the upper and lower borders of the gluteus maximus were separated from underlying connective tissue, taking care not to damage underlying gluteal nerves and vessels. The muscle was then divided along its proximal attachment (taking care not to damage the sacrotuberous ligament), and was then reflected laterally to expose its under-surface, piriformis, gluteus medius and the superior and inferior gluteal nerves and vessels, all of which were then defined by blunt dissection. On reflection of gluteus maximus, inferior gluteal nerves and vessels were divided 1cm from their point of entry into the under-surface of the muscle. The muscle pedicle and trochanteric bursa were then identified and defined on the under-surface of the gluteus maximus. A small “L” shaped incision was created in the connective tissue overlying the bursa and a small corner reflected, to demonstrate the cavity of the bursa for visual clarity. The aforementioned structures were then imaged.

Following reflection of the gluteus maximus, the proximal portions of the posterior cutaneous and sciatic nerves were identified, and traced in a distal direction into the posterior thigh region. A vertical mid-line incision was made down the length of the fascia lata, to the superior boundary of the popliteal fossa. Care was taken at this stage not to damage the posterior cutaneous nerve or underlying musculature of the thigh. The fascia lata was then fully reflected on either side of this incision, and removed, to expose the ischial tuberosity, hamstrings (excluding distal attachments at this stage) and the extent of the posterior cutaneous nerve of the thigh for subsequent imaging.

Deep to the sciatic nerve, the lateral hip rotators, namely the gemelli, the obturator internus and the quadratus femoris were all identified and cleaned of connective tissue and said structures then imaged.

#### (iv) Reflection of Gluteus Medius

From its posterior border, the under-surface of the gluteus medius muscle was separated from the gluteus minimus, using blunt dissection, taking care not to damage associated neurovasculature within the muscular plane. An oblique incision was then made through the gluteus medius from midway along its posterior border, to midway along its proximal attachment to the iliac crest. The medial portion of the gluteus medius was then removed and the lateral portion reflected, thus exposing the gluteus minimus and the deep branches of the superior gluteal nerves and vessels. These were then defined by blunt dissection and subsequently imaged. Care was taken in reflecting the remaining portion of the gluteus medius to preserve any of its associated neurovasculature for visual clarity.

#### (v) Removal of Gluteus Maximus, Medius and Inferior Portion of Sacrotuberous Ligament

The remaining attachment of the gluteus maximus was divided and the entire muscle was then removed. Superior gluteal nerve branches and vessels associated with the gluteus medius were then cut, and its distal muscle attachment to the greater trochanter was divided allowing complete removal of the muscle. The gluteus minimus was then cleared of connective tissue for imaging. Following this, the inferior portion of the sacrotuberous ligament was removed and its neurovascular supply defined. The named structures were then imaged.

## (vi) Removal of Gluteus Minimus, Piriformis and Remainder of Sacrotuberous Ligament

The piriformis was divided in a superior to inferior direction along its point of emergence from the lateral border of the sacrum, and again at its distal attachment, and was then completely removed. Neurovasculature associated with the sacrotuberous ligament was cleared and the remaining superior portion of the ligament was divided along the lateral border of the sacrum and removed. Following this, the sacrospinous ligament and pudendal nerve and vessels were identified and defined for imaging.

The superior gluteal arteries and nerves associated with the gluteus minimus were divided at their point of emergence from the greater sciatic foramen, and the gluteus minimus was reflected to expose the underlying surface of the ilium. The gluteus minimus was then divided at its distal attachment (just superiorly to the acetabular rim to avoid damage to the joint capsule) and was subsequently removed. The newly exposed surface of the ilium was then cleaned of any remaining muscle fibres or connective tissue prior to imaging.

## (vii) Removal of Hamstrings

The posterior cutaneous nerve of the thigh was divided at its point of emergence from the greater sciatic foramen and removed. The hamstrings were divided at their common origin, and at their distal attachments to the medial and lateral tibial condyles. The short head of biceps femoris was detached from its attachment to the linea aspera, and all of the hamstrings were then completely removed, cutting neurovascular connections from the sciatic nerves and perforating arteries as necessary. In doing this, care was taken to preserve the underlying sciatic nerve. The newly exposed surfaces of the ischial tuberosity, femoral shaft and the posterior aspect of the adductor magnus were then cleaned for visual clarity. The popliteal

artery and vein, and the bifurcation of the sciatic nerve into the tibial and common peroneal branches, as well as genicular branches of the above were all identified and defined by blunt dissection. All aforementioned structures were then subject to imaging.

## **Block F: The Posterior Compartment of the Leg**

### **(i) Subcutaneous Fat of Posterior Leg**

The remaining attachment of skin on the posterior aspect of the leg was reflected in an inferior direction, then cut horizontally along the calcaneal tendon and removed. Once imaged, the subcutaneous fat layer was then removed from the posterior compartment of the leg, taking care to preserve and define the small saphenous vein, between the level of the popliteal fossa superiorly, and the lateral malleolus inferiorly. In doing this, the sural nerve was identified emerging from the deep fascia and was subsequently defined by blunt dissection. The deep fascia of the posterior leg, small saphenous vein and sural nerve were all then imaged.

### **(ii) Exposure of Gastrocnemius**

The small saphenous vein was divided at its point of branching from the popliteal vein and removed. A vertical incision was then created up the length of the remaining deep fascia, from the point where the sural nerve emerges, to the popliteal fossa. Care was taken at this point not to damage the proximal portion of the sural nerve deep to the fascia. From the distal end of this incision, another incision was made down the distal portion of the leg, to the calcaneal tubercle. The deep fascia was then reflected on either side, and subsequently removed, to expose the gastrocnemius. The medial and lateral heads of gastrocnemius, and neurovascular connections from the tibial nerve and sural blood vessels were then defined by blunt dissection for subsequent imaging.

### (iii) Exposure of Soleus

Tibial nerve branches and sural blood vessels associated with the medial and lateral heads of gastrocnemius were cut, and both heads were then separated from their attachments to the medial and lateral condyles of the femur, respectively. Care was taken at this point not to damage the underlying plantaris or the nerve and blood supply to soleus. The gastrocnemius was then reflected in an inferior direction towards the foot, and was then cut and removed at the calcaneal tendon, thus fully exposing soleus, plantaris and their neurovascular connections to the tibial nerve and sural blood vessels. The aforementioned structures were defined by blunt dissection and subsequently imaged.

### (iv) Exposure of the Deep Muscles of the Posterior Compartment of the Leg

All remaining neurovascular connections to the remaining portion of the soleus were cut. The proximal attachment of the muscle was divided, first along its lateral attachment to the fibula, and then along its medial attachment to the tibia. Following this, the calcaneal tendon was cut 3cm from its distal attachment, and the remaining portion of the muscle was then completely removed to expose the flexor digitorum longus, hallucis longus and the tibialis posterior. These structures were then cleaned by blunt dissection and subsequently imaged. On the proximal aspect of the leg, the plantaris was divided 2cm from its proximal attachment to the lateral femoral condyle and the distal portion was removed. The posterior tibial artery and the tibial and peroneal nerves were identified and traced distally down the posterior aspect of the leg to the tarsal tunnel. The branch point of the anterior tibial artery and the proximal aperture of the interosseous membrane were also identified, and all aforementioned structures were defined by blunt dissection prior to imaging.

## **Block G: The Sole of the Foot**

### (i) Exposure of Subcutaneous Fat

From the area of remaining skin attachment on the heel of the foot, the skin of the sole was reflected forward, toward the toes, where it was then detached with a horizontal incision along the base of each digit. From this incision, a vertical cut was made down the plantar surface of each toe, and the skin removed on either side, thus exposing the extent of subcutaneous fat over the sole and all five digits, which was then imaged.

### (ii) Plantar Aponeurosis, Digital Slips, Digital and Cutaneous Nerves

Working from the posterior border of the calcaneus, forwards, the subcutaneous fat over the sole was removed to expose the underlying plantar aponeurosis (and deep fascia on either side of it). Care was taken in doing this to preserve the cutaneous branch of the medial and lateral plantar nerves, which were then further defined by blunt dissection. Loose connective tissue between each digital slip was carefully removed to define the digital slips and to expose distal portions of the digital plantar nerves and arteries, which were then traced down the plantar surface of each toe. All aforementioned structures were subsequently imaged.

### (iii) First Layer of the Sole

The plantar aponeurosis was divided at its proximal attachment to the calcaneus and reflected in a forwards direction, by separating it from the underlying flexor digitorum brevis, and from its fascial connections to the intermuscular septa (between muscle bellies of flexor digitorum brevis). Once fully exposed, the flexor digitorum brevis was defined by blunt

dissection and its tendons traced as far distally as possible into digits two, three four and five, by opening up the four digital fibrous sheaths with a scalpel. On the great toe, the tendon of the flexor hallucis longus was identified and traced proximally, to the medial border of the flexor digitorum brevis, retaining its fibrous sheath for visual clarity. The distal portions of the lumbricals could be visualised at this stage. The deep fascia on both the lateral and medial aspects of the sole was then carefully removed to expose the abductor digiti minimi and the distal portions of the abductor hallucis for imaging. On the medial aspect of the foot, the medial plantar nerve and artery were identified on emergence from the medial border of the flexor digitorum brevis and traced distally into the digital plantar nerves and arteries respectively. On the lateral surface of the sole, the superficial branch of the lateral plantar nerve and the proximal portion of the lateral plantar artery were located emerging from the lateral border of the flexor digitorum brevis and were then traced distally. In doing this, the nerve was traced into its superficial digital branches towards the clefts of the toes, where the metatarsal plantar arteries were also identified and traced distally into the plantar digital arteries. All of the structures documented above were then subject to imaging.

#### (iv) Second Layer of the Sole

The flexor digitorum brevis was cut along its proximal attachment to the calcaneus and was then turned forwards toward the toes, dividing associated connections from the medial plantar nerve and artery as appropriate. The muscle was divided at each of its tendinous insertions onto digits two - five, and was subsequently removed. The underlying flexor accessorius, and the tendons of the flexor digitorum longus and flexor hallucis longus then clearly identified. The tendons of the two later structures were then traced distally towards the toes. The extent of the lumbricals were clearly identified at this stage, and these were defined by blunt dissection prior to imaging. In completing this stage of the dissection, care was taken to

preserve, where possible, the previously dissected portions of the plantar nerves and arteries, and these were traced proximally to their point of emergence from the medial and lateral borders of the accessorius.

#### (v) Third Layer of the Sole

The abductor digiti minimi was divided 3cm from the posterior border of the calcaneus and was turned forwards towards its distal attachment, dividing neurovascular connections from the lateral plantar nerve and artery as appropriate, onto the lateral side of the proximal phalynx, where it was subsequently detached. In doing this, the underlying flexor digiti minimi brevis was exposed, and cleaned by blunt dissection for imaging. On the medial aspect of the sole, the abductor hallucis longus was divided at its proximal attachment to the medial calcaneal tubercle and was then reflected forwards (cutting neurovascular connections from medial nerve and artery as appropriate), towards its distal attachment to the medial surface of the proximal phalynx, where it was divided again and removed. At this stage, the contents of the tarsal tunnel, namely the tendons of tibialis posterior, flexor digitorum longus, flexor hallucis longus, and the posterior tibial artery and nerve were observed passing onto the plantar surface of the foot. The two heads of the flexor hallucis brevis were also identified and all aforementioned structures were defined by blunt dissection for visual clarity. The superficial branches of the medial and lateral plantar nerves (including those supplying the toes) were cut and removed. The aforementioned structures were then imaged.

Following this, the tendons of the flexor digitorum longus and hallucis longus were divided along the anterior border of the flexor accessorius, and the distal portions of these muscles reflected forwards towards the toes, where they were divided once again at their insertions onto the distal phalanges (following opening of the fibrous flexor sheaths with a scalpel), and

removed. The flexor accessorius was then detached from its origin. The transverse and oblique heads of the adductor hallucis, and opened flexor sheaths were then observed and defined by blunt dissection prior to subsequent imaging.

#### (vi) Extent of Plantar Artery

The flexor hallucis brevis was separated from its proximal attachment to the cuboid, lateral cuneiform and tibialis posterior tendon and was then reflected towards its two distal attachments on either side of the proximal phalanx, where it was divided and removed. Care was taken at this stage to preserve the first metatarsal plantar artery beneath. The first metatarsal bone was identified and cleaned for visual clarity. The oblique and transverse heads of the adductor hallucis were detached from their proximal attachments to the associated metatarsals and were then reflected in a forward direction towards their common insertion onto the base of the great toe, dividing any neurovascular connections from the lateral plantar nerves and vessels. On the lateral aspect of the foot, the flexor digiti minimi brevis was detached from its proximal attachment to the fifth metatarsal and was then reflected forward towards its insertion onto the fifth proximal phalanx, where it was divided again and removed. Care was taken at this stage not to damage the closely associated plantar interosseous muscle. The plantar interosseous muscles were identified in full and their fascial covering was removed for visual clarity. The lateral plantar arch and metatarsal arteries were all identified and defined by blunt dissection. The deep branch of the lateral plantar nerve was also identified and traced into the interosseous muscles. All aforementioned structures were then imaged.

#### (vii) Fourth Layer of the Sole

The deep branch of the lateral plantar nerve, and the lateral and medial plantar arteries, including the plantar arch and plantar metatarsal arteries were cut and removed between the lateral malleolus and the lateral border of the first metatarsal (where plantar arch joins dorsalis pedis). On the proximal portion of the sole, the long plantar, calcaneocuboid and calcaneonavicular ligaments were identified and cleaned for visual clarity. From directly beneath the lateral malleolus, the tendon of the peroneus longus was traced onto the sole of the foot, and the distal portion of the plantar ligament was removed to demonstrate the course of the peroneus longus tendon underneath. From the tarsal tunnel, the tendon of tibialis posterior was traced onto the tuberosity of the navicular bone, and subsequently defined, along with its tendinous slips by blunt dissection. On the anterolateral aspect of the sole, the plantar interosseous muscles were detached from their proximal and distal attachments to the metatarsals, and were then removed to expose the dorsal interossei. All of the structures dissected above were then imaged.

## **Block H: Articulations**

### (i) Removal of Soft Tissue

The femoral blood vessels were divided just below the inguinal ligament, and all remaining vasculature on the thigh, leg and foot were removed. In the gluteal region, the remaining gluteal vessels and the sciatic nerve were divided at their point of emergence from the greater sciatic foramen, and from here, all remaining nerves were removed between the gluteal region and the foot, rendering the all regions completely free of any neurovasculature. Following this, all remaining musculature was completely detached from its bony attachments, and the interosseous membrane was removed to demonstrate the extent of the articulated skeleton of the lower limb.

### (ii) The Hip Joint

The capsule of the hip joint (including the ischiofemoral, iliofemoral, and pubofemoral ligaments) and the greater and lesser trochanter of the femur were identified and defined by blunt dissection for imaging. Following this, a firm incision was made around the capsule, and the hip joint was gently hyperflexed, until breaking of the ligament of the head of femur was sounded. The head of the femur was then pulled free of the hip joint. At this stage, the head and neck of the femur, the distal portion of the ligament of head of femur and the fovea capitis were all clearly identified. The remainder of the joint capsule still attached to the acetabulum at this stage was then removed, so the inside of the joint was fully exposed. In doing so, the acetabular labrum and fossa, lunate cartilage and the proximal portion of the ligament of head of femur were all identified. Prior to imaging, fat and connective tissue in the region of the ischiofemoral fossa and proximal perineum were removed in order to define

the ischial tuberosity and ischiopubic ramus. Any remaining fibres of the obturator externus were removed from the obturator membrane. All aforementioned structures of the hip joint were subsequently imaged.

### (iii) The Knee Joint

On the anterior aspect of the knee, the quadriceps tendon was traced out with a scalpel from the surrounding fibrous capsule, from the distal end of the femur, to the tibial tuberosity. The tendon, complete with patella, was then reflected inferiorly, and the synovial infrapatellar fold cut, to expose the suprapatellar, and infrapatellar bursae, the articulating surface of the patella, and the tibiofemoral joint. The remainder of the fibrous capsule was then removed. At this stage, the collateral ligaments were identified and defined on either side of the knee joint for imaging. Just deep to the fibular collateral ligament, the remaining portion of the popliteus tendon was also located and defined for visual clarity. On the anterior articulating knee joint, the medial and lateral menisci and the transverse ligament of the knee were located, and defined, ensuring that their anatomical relationships with proximal menisci were clearly demonstrated. The knee joint was then flexed fully, to expose the anterior and posterior cruciate ligaments deep within the joint, and these were subsequently defined for imaging. On the posterior aspect of the knee, the synovial capsule was removed from the femoral epicondyles. The posterior menisiofemoral ligament was then traced from the lateral meniscus to the medial surface of the medial femoral epicondyle, and deep to this, the posterior surface of the cruciate ligaments were also observed. The relationships between these structures were then defined for imaging. Finally, the collateral, posterior menisiofemoral and cruciate ligaments were all divided and the tibiofemoral joint was disarticulated to demonstrate the opposing articulating surfaces of the femur and tibia. All of the knee structures described, were then imaged.

#### (iv) The Ankle Joint

Following removal of all tendons and neurovasculature from around the ankle joint, the anterior and posterior tibiofibular ligaments, posterior tibiotalar, deltoid, anterior and posterior talofibular, calcaneofibular and inferior transverse ligaments were all identified and defined for subsequent imaging. On the dorsal surface of the foot, now void of all neurovasculature, the talonavicular, bifurcated, and the lateral part of the interosseous talocalcaneal ligaments were all located and further defined also, for visual clarity. The ligaments spanning the ankle joint (namely the posterior tibiotalar, the deltoid, anterior and posterior talofibular, calcaneofibular and inferior transverse ligaments, listed above) were then divided to allow disarticulation of the talocrural joint. The articulating surfaces of the tibial, fibula and talus were all identified and all aforementioned structures were then imaged.

## **Block I: Bones**

All ligamentous tissue was removed from the femur, tibia and fibula, and the dorsal surfaces of the bones of the foot. Small ligamentous attachments were preserved on the plantar surface of the foot in order to maintain the bones in an anatomical position for imaging. The proximal and distal talofibular ligaments were then divided, and the tibia and fibula were disarticulated. The femur, tibia and fibula were all imaged individually from multiple angles, and the dorsal surface of the foot bones were imaged in their anatomical position.

## 2.2.2: Cadaveric Data Acquisition

### Equipment Set-up

Following each key stage of the dissection, three-dimensional topographical data was collected from all exposed anatomical structures using the Perceptron ScanWorks<sup>®</sup> V5 Scanning Probe, attached to the Cimcore Infinite 2.0 (Seven axis) CMM Arm. Handling of digital equipment including set-up, calibration, cadaveric scanning and management of digital data was performed entirely by a designated digital design expert who had previously undertaken sufficient training specific to the equipment used. Additionally, scanning was performed in a designated laboratory with a concrete floor to minimize the risk of vibrations interfering with data acquisition, and the equipment was stored and used at ambient room temperature throughout the study. Lighting was kept at a constant level for the purpose of digital photography, however the functionality of the ScanWorks<sup>®</sup> V5 scanner is unaffected by ambient light (See Appendix I).

The scanning equipment was set up in accordance with the manufacturer guidelines, and field calibration of the sensor hard probe was performed using the position of the PCMM to align the sensor into a common co-ordinate frame. (For details on factory rectification procedure of V5 sensor, see Appendix II).

Following equipment set-up and field calibration of the hard probe, the specimen was moved to a position where the articulated PCMM arm and attached probe could comfortably reach the relevant area of dissection. It was then ensured that the specimen itself was in a position which optimised the exposure of the relevant structures, and this position was maintained throughout the scanning process to avoid the appearance of artefacts during automated

alignment of the scan data. Once these criteria had been met and clarified, scanning could proceed.

## Laser Scanning

To commence three-dimensional data collection, the laser stripe projected by the hard probe was swept steadily over the dissected region in a rostral to caudal direction. This action was repeated several times until a sufficient level of point cloud data had been collected from relevant anatomical surfaces. Following each scan, the point cloud data obtained was aligned into a common co-ordinate from using the position of the PCMM in three-dimensional space.

Evaluation of the cadaveric data being obtained was based primarily upon a visual representation of the surface data on the Dell™ lap-top computer screen. This visual representation was a grey polygon-mesh model, derived directly from the point cloud data from the cadaveric surfaces. This graphical output could be magnified and rotated in any axis following each scan to ensure an adequate level of surface data was being obtained from the dissection. Black areas on the polygon-mesh reconstruction signalled areas where topographical information was lacking, and if associated with an important anatomical structure, further scanning of said area was pursued. When examining the on-screen model, care was taken to ensure not only that enough point cloud data had been gathered from the appropriate structures for subsequent modelling, but also that the acquisition of excessive redundant data was avoided. To make the scans as efficient as possible, the operator was guided by a visual representation of the lasers cone-shaped field of view, which signalled to them the optimal scanning offset distance from the probe face. In addition to this, the operator used an audible tone produced by the scanning software, which changed pitch in accordance with the proximity of the scanning probe to the surface of the cadaveric tissues.

When enough topographical data had been collected from the relevant anatomical structures for subsequent modelling, scanning for that stage of the dissection could be terminated. Each scanning session took approximately 10 scans of the dissected area, and lasted approximately 10 minutes. (This varied slightly for each session depending on the intricacy of the anatomical structures being imaged).

### Digital Photography

Following each session of laser scanning, the anatomical structures of interest were photographed from various angles using the Panasonic™ DMC TZ7 Lumix digital camera.

# 3: Results

## **3.1: Cadaveric Dissection**

The dissection performed in this study allowed a thorough and clear demonstration of all clinically relevant anatomical structures associated with the male lower limb, for the purpose of collecting a comprehensive topographical dataset by way of high-end laser scanning and digital photography. Throughout the dissection, the cadaver presented almost completely normal anatomy, with the exception of a small amount of arthritic change on the articulating surfaces of the knee joint, which are detailed in Figure 8. Figures 1-9 illustrate selected examples from each stage of the dissection, and illustrate the level of intricacy and detail, which was achieved in each. The key stage from which each example has been taken is indicated, and a simple numbering system has been used to indicate the relevant anatomical structures, which have been demonstrated.

### **Block A: The Inguinal Canal**

The first block of dissection successfully demonstrated all clinically relevant areas of anatomy associated with the male inguinal canal. The anterior abdominal wall layers which comprise the canal and spermatic cord, including the external and internal obliques, transversus abdominis and the transversalis fascia, were all clearly demonstrated for subsequent imaging. Figure 1(a) demonstrates the how the superficial inguinal ring, formed by an occlusion in the aponeurosis of the external oblique, was visible following the reflection of skin, and the removal of superficial fascia and subcutaneous fat. The spermatic cord could be clearly seen emerging from this opening and removal of the external spermatic fascia (continuous with the external oblique aponeurosis), proximal to the superficial ring allowed the ilioinguinal nerve to be visualised passing through the superficial ring, along

with the spermatic cord. As shown in Figure 1(b), the deep inguinal ring and the transversalis aperture, were visible just deep to the arching fibres of the transversus abdominis following reflection of the external and internal oblique muscles. The ilioinguinal and iliohypogastric nerves could also be seen penetrating the transversus abdominis, and passing into the plane between this muscle and the internal oblique. In Figure 1(c), it can be seen that removal of the lower rectus abdominis facilitated good exposure of the inferior epigastric vessels, the lower thoracic nerves (T11 and T12), and the transversalis fascia, comprising the lower portion of the posterior rectus sheath. Figure 1(d) shows that the extent of the spermatic cord, and the continuation between the internal spermatic fascia and the transversalis fascia was clearly defined following reflection of the cremasteric fascia. The genital branch of the genitofemoral nerve supplying the cremaster, was also clearly visualised at this stage.

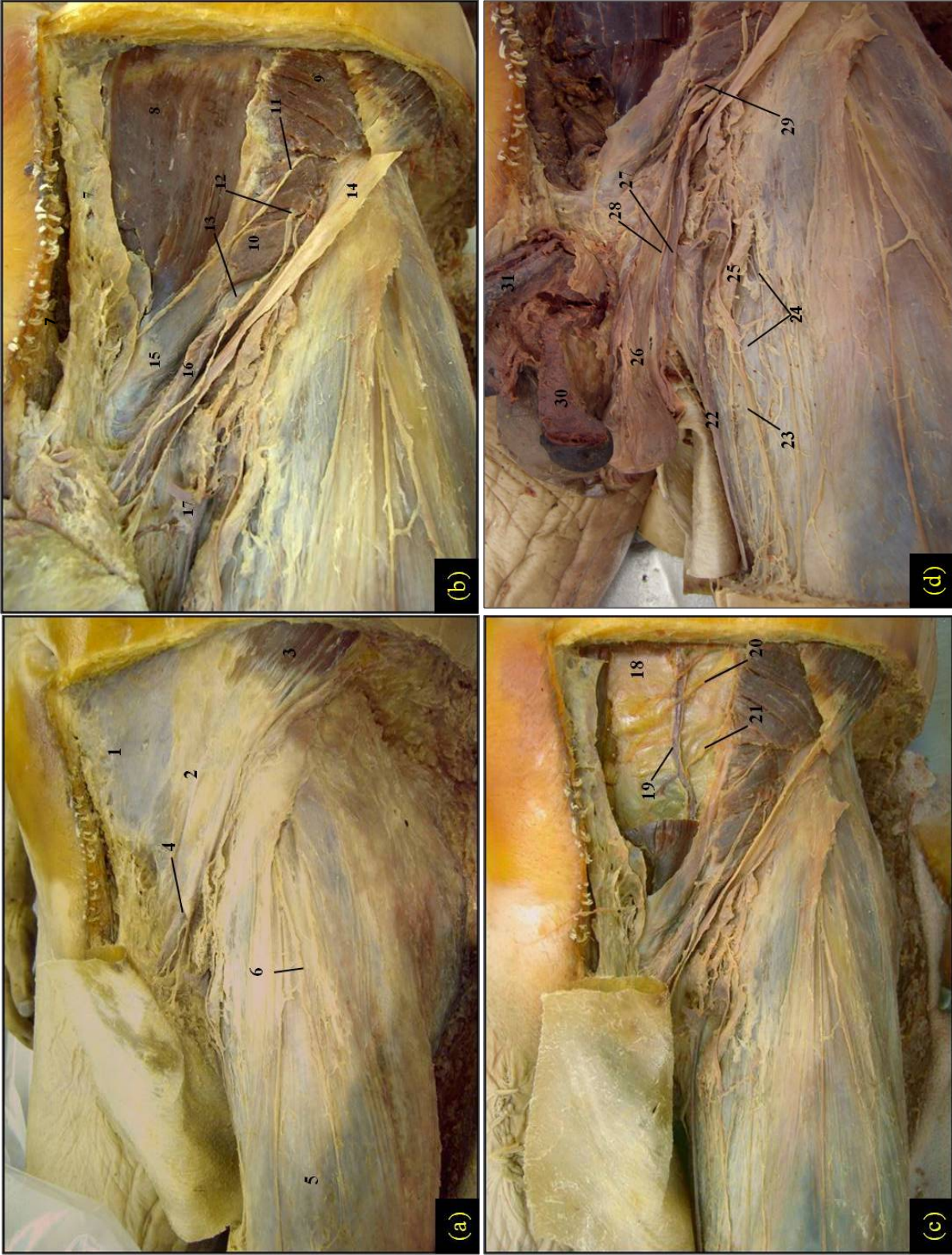


**Figure 1. Selected key stages of dissection Block A: The Inguinal Canal (a) Block:A(i), (b) Block:A(ii), (c) Block A(iii), (d) Block A(iv)** (1) rectus sheath; (2) external oblique aponeurosis; (3) external oblique; (4) superficial inguinal ring; (5) fascia lata; (6) lateral femoral cutaneous nerve. (7) linea alba; (8) rectus abdominis; (9) internal oblique; (10) transversus abdominis; (11) iliohypogastric nerve; (12) ilioinguinal nerve; (13) deep inguinal ring; (14) inguinal ligament (reflected); (15) conjoint tendon; (16) spermatic cord; (17) saphenofemoral junction; (18) transversalis fascia; (19) inferior epigastric vessels, (20) thoracic nerve 11; (21) thoracic nerve 12; (22) great saphenous vein; (23) anterior femoral vein; (24) lymph vessels; (25) inguinal lymph node; (26) internal spermatic fascia; (27) cremasteric fascia; (28) genital branch of genitofemoral nerve; (29) deep inguinal ring; (30) corpus spongiosum; (31) corpus cavernosum.

## **Block B: The External Genitalia**

This stage of the dissection provided adequate exposure of all clinically relevant anatomical components of the male external genitalia for subsequent data acquisition. Following reflection of the skin, the superficial dorsal vein of the penis was clearly identifiable for imaging. Figure 2(a) illustrates the penis following removal of the superficial fascia and superficial dorsal vein, after which dorsal arteries, nerves and the deep dorsal vein were all visible. In Figure 2(b), all neurovasculature has been removed from the dorsal aspect of the penis to expose the corpus cavernosum. The removal of the external, and cremasteric fascia from the spermatic cord facilitated a clear view of the internal spermatic fascia, and the genital branch of the genitofemoral nerve. Following this, dissection of the corpus cavernosum from the underlying corpus spongiosum, facilitated subsequent imaging of both structures. Figure 2(c) presents the lateral aspect of the left testis following complete removal of all layers of the spermatic cord, and the parietal layer of the tunica vaginalis, which was demonstrated at a previous stage. This dissection clearly illustrated all major contents of the male spermatic cord including the vas deferens, testicular artery, and the testicular veins and nerves, as shown.

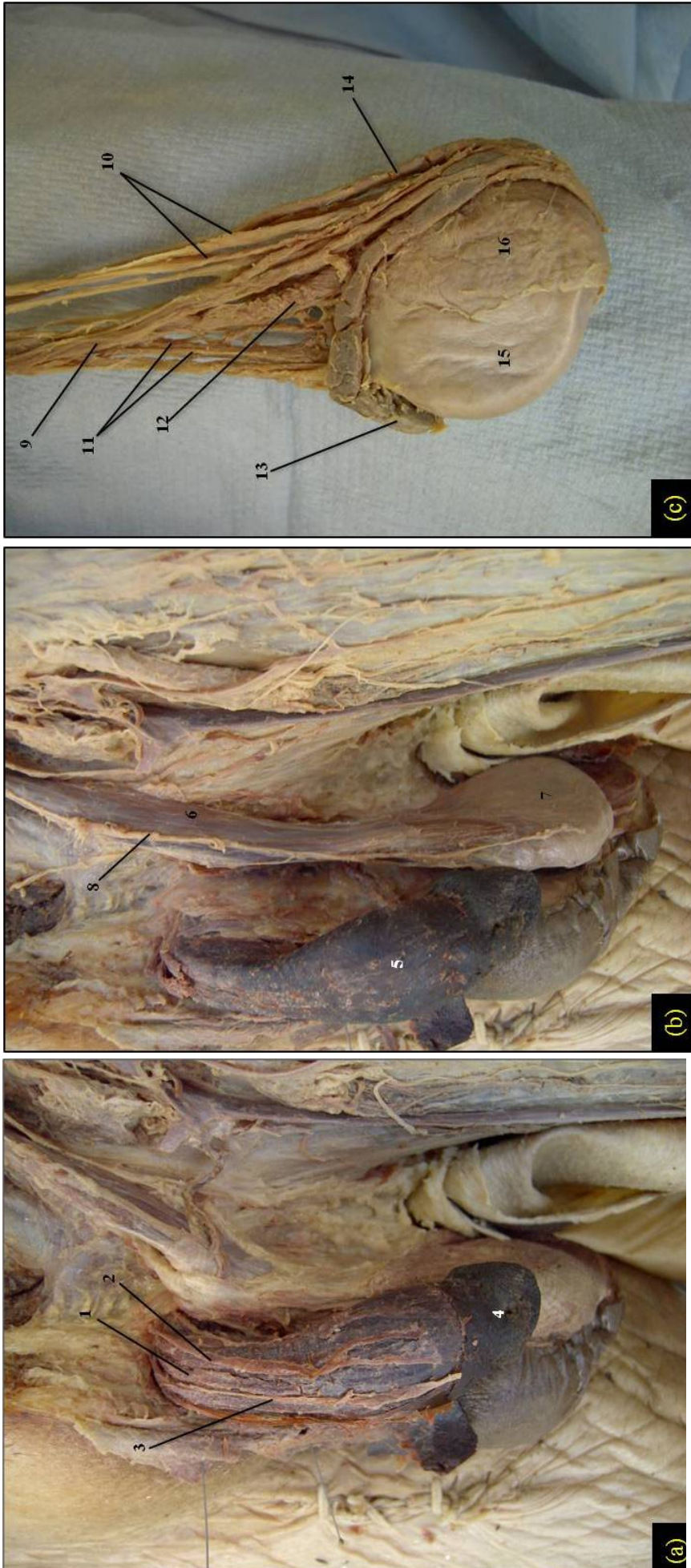


**Figure 2. Selected key stages of dissection Block B: The External genitalia. (a) Block B(ii), (b) Block B(iii) and (c) Block B(vi)** (1) dorsal vein; (2) dorsal artery; (3) dorsal nerve; (4) prepuce; (5) corpus cavernosum; (6) spermatic cord (with internal spermatic fascia); (7) testis; (8) genitofemoral nerve; (9) testicular artery; (10) testicular vein; (11) testicular nerve; (12) pampiniform plexus; (13) head of epididymis; (14) vas deferens; (15) visceral layer of tunica vaginalis; (16) tunica albuginea.

## **Block C: The Anterior and Medial Compartments of the Thigh**

In Block C of the dissection, all major anatomical components of the anterior and medial compartments of the thigh were demonstrated for imaging. Figure 3(a) shows the superficial musculature of the thigh immediately after removal of the deep fascia. With all musculature of the thigh in tact at this stage, the boundaries of the femoral triangle could be clearly visualised. Although the majority of the fascia lata overlying the anterior aspect of the thigh was removed here, the iliotibial band was successfully preserved and defined for imaging.

Figure 3(b) demonstrates how the contents of the femoral canal including the femoral vein, artery and nerve which were all clearly defined, following removal of the rectus femoris, sartorius, and femoral sheath. At this stage, the femoris profunda could be clearly identified as a branch of the femoral artery, and both the lateral and medial circumflex femoral arteries (though the medial not visible in this image), were also demonstrated. Nerve and blood supply to the sartorius and quadriceps from the femoral vessels, and the femoral nerve were clearly identifiable for imaging. Figure 3(c) demonstrates the extent of the vastus intermedius and its neurovascular supply from the lateral femoral circumflex artery and femoral nerve following removal of the medial and lateral vasti. The extent of the adductor longus was also demonstrated at this stage. Figure 3(d) taken from the final stage of Block C, successfully shows the posterior and (cut) anterior branches of the obturator nerve passing through the obturator externus, and the posterior branch could be clearly seen innervating the adductor magnus. At a previous stage of the dissection, the anterior branch and its connections with the adductor longus, brevis and gracilis was also successfully displayed for imaging.

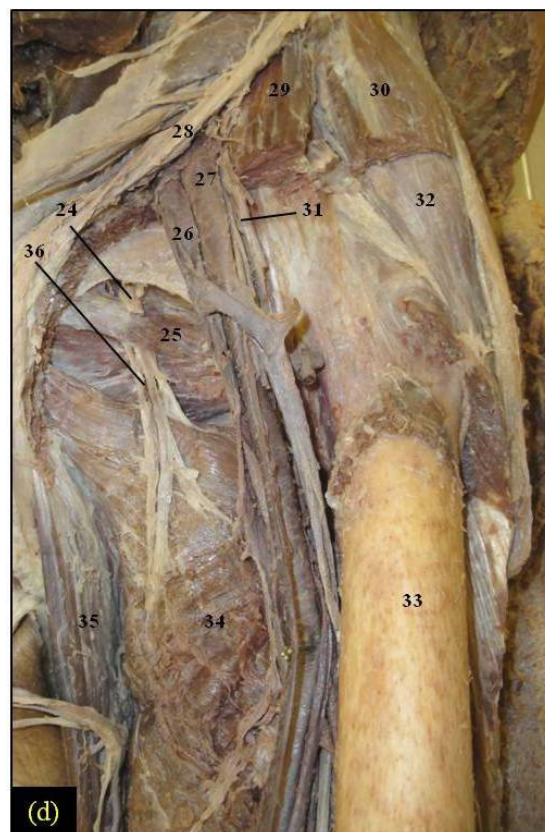
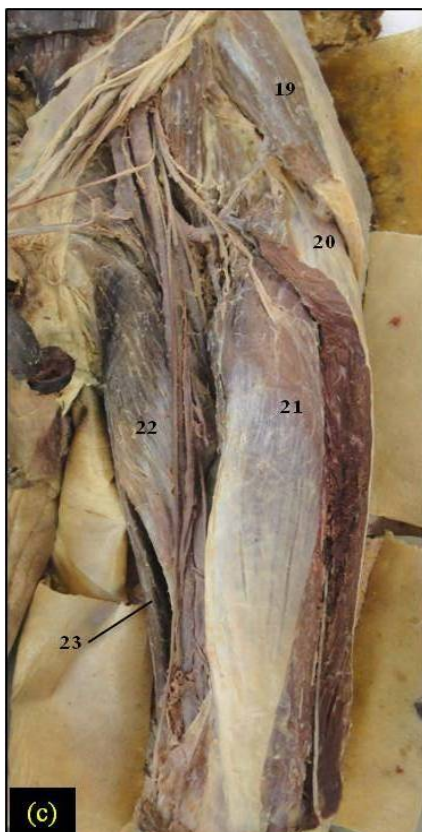
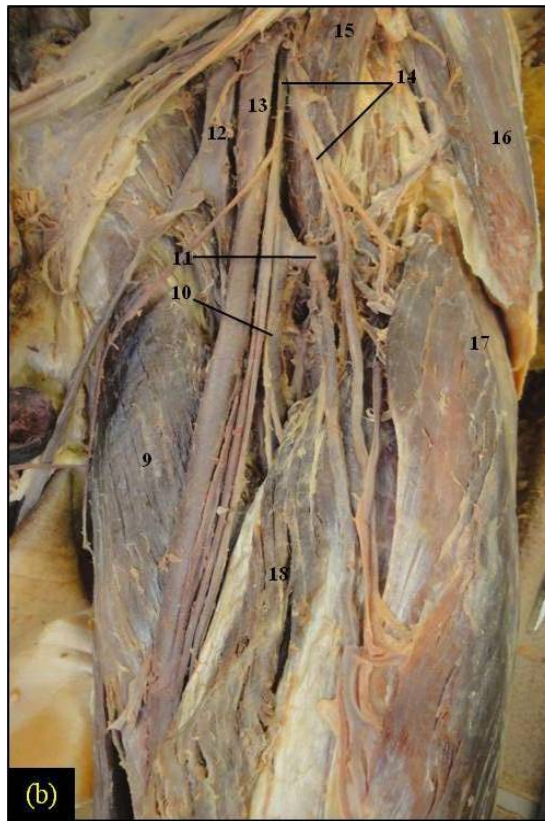


**Figure 3: Selected key stages of dissection Block C: The Anterior and Lateral Compartments of Thigh.** (a) Block C(ii), (b) Block C(iii), (c) Block C(iv), and (d) Block C(vi). (1) Sartorius; (2) adductor magnus; (3) tensor fascia latae; (4) iliotibial tract; (5) rectus femoris; (6) vastus medialis; (7) quadriceps tendon; (8) vastus lateralis; (9) adductor longus; (10) femoris profunda; (11) lateral circumflex femoral artery; (12) femoral vein; (13) femoral artery; (14) femoral nerve; (15) iliopsoas; (16) tensor fascia latae; (17) vastus lateralis; (18) vastus intermedius; (19) tensor fascia lata (cut); (20) vastus lateralis (cut); (21) vastus intermedius; (22) adductor longus; (23) gracilis; (24) anterior branch of obturator nerve; (25) obturator externus; (26) femoral vein; (27) femoral artery; (28) inguinal ligament; (29) iliopsoas; (30) tensor fascia latae(cut); (31) femoral nerve; (32) gluteus medius; (33) femur; (34) adductor magnus; (35) gracilis.

## **Block D: The Anterior and Lateral Compartments of the Leg and Dorsum of the Foot**

At this stage of the dissection, all relevant musculature and neurovasculature of the anterior and lateral leg compartments, and dorsum of the foot was successfully demonstrated for subsequent imaging. Figure 4(a) illustrates a medial view of the deep fascia leg following removal of subcutaneous fat, where the great saphenous vein and saphenous nerve branches on either side, and the dorsal venous arch on the dorsal aspect of the foot, could be clearly visualised upon dissection. Though not shown in this image, the superficial peroneal nerve was also clearly identifiable on emergence from the deep fascia on the anterior aspect of the leg. Following removal of the deep fascia, with the exception of the superior and inferior extensor retinacula, as shown in Figure 4(b), all of the musculature in the anterior and lateral leg compartments were successfully demonstrated, and tendons of the tibialis anterior, extensor hallucis longus, extensor digitorum longus and the three peroneal muscles could be seen spanning the ankle joint. With the exception of the peroneus longus, the insertions of these muscles were also clearly demonstrated on the dorsal aspect of the foot for imaging. These tendons were demonstrated in full, following removal of the retinacula at a different stage. On the medial aspect of foot, though not shown, here, the flexor retinaculum was also successfully demonstrated for imaging at this stage of the dissection. Figure 4(c) demonstrates the deep anterior tibial artery and veins of the leg, and the deep peroneal nerve following removal of the extensor digitorum longus, hallucis longus and peroneus tertius muscles. At this stage, the extensor digitorum brevis and interossei were also clearly demonstrated for imaging. Removal of the extensor digitorum brevis muscle at a later stage then facilitated a good visual demonstration of the dorsalis pedis passing through to the plantar surface of the foot. On removal of the lateral compartment of the leg, the common

peroneal nerve was successfully demonstrated looping round the head of the fibula, and its deep, superficial and genicular branches were clearly displayed for imaging.

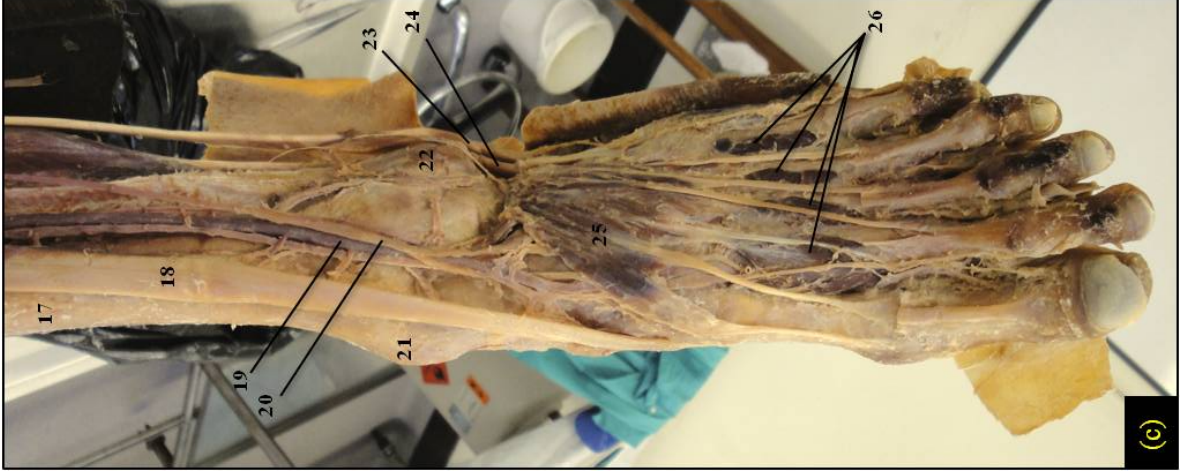
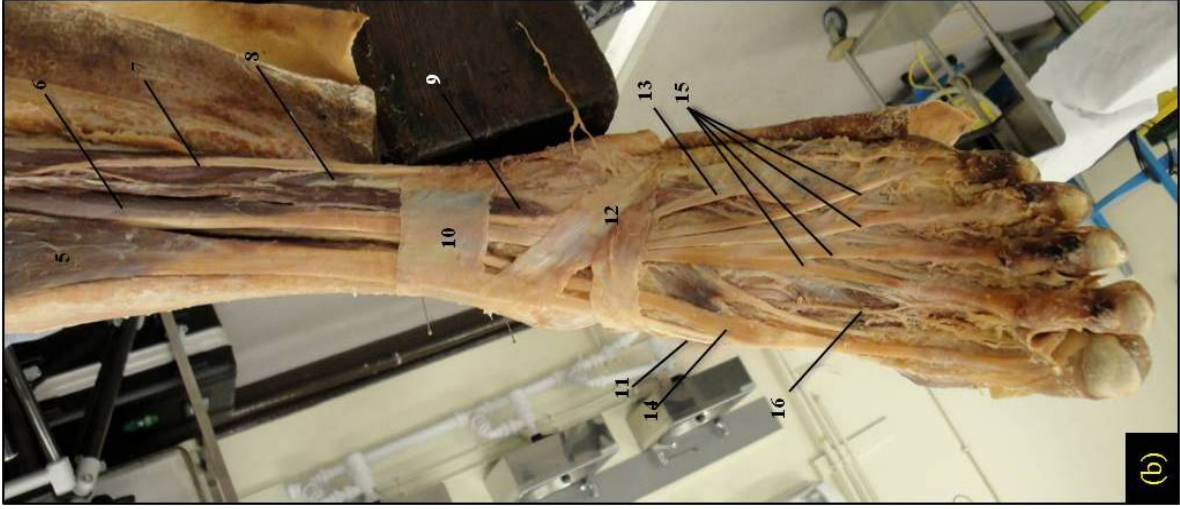
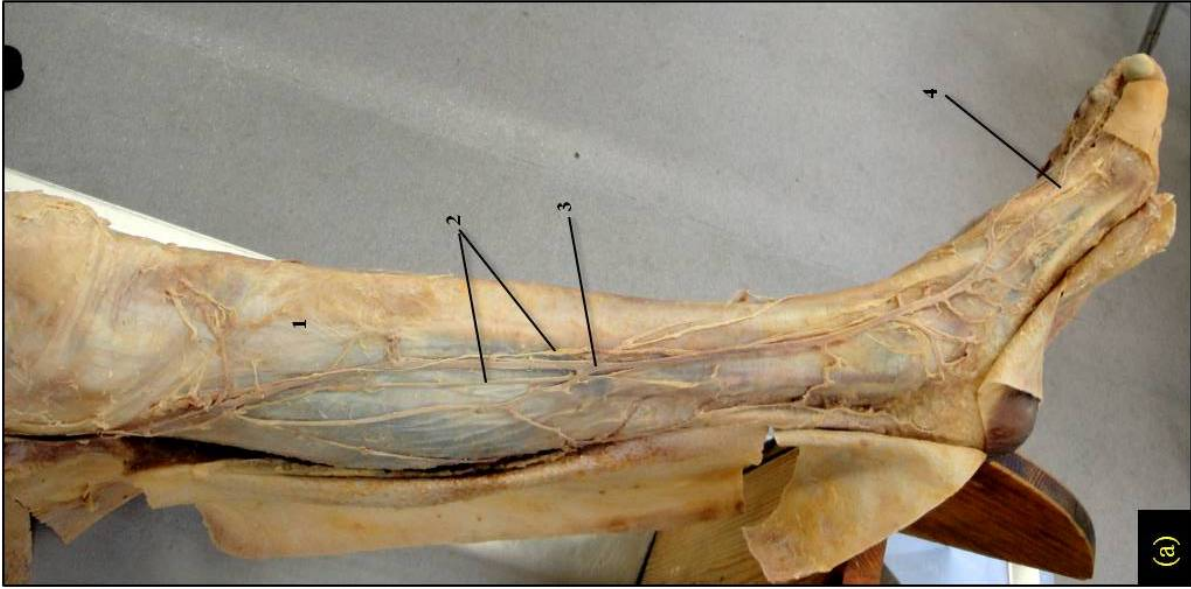


**Figure 3: Selected key stages of dissection Block D: The Anterior and lateral Compartments of the Leg and Dorsum of the foot. (a) Block D(ii), (b) Block D(iii), (c) Block D(v).** (1) deep fascia; (2) saphenous nerve; (3) peroneus tertius; (4) dorsal venous arch; (5) great saphenous vein; (6) tibialis anterior; (7) peroneus longus; (8) peroneus longus; (9) peroneus brevis; (10) tendon of peroneus brevis; (11) inferior extensor retinaculum; (12) superior extensor retinaculum; (13) tendon of tibialis anterior; (14) deep peroneal nerve; (15) tendons of extensor digitorum longus; (16) deep peroneal nerve; (17) tibia; (18) tibialis anterior (tendon); (19) anterior tibial artery; (20) deep peroneal nerve; (21) medial malleolus; (22) lateral malleolus; (23) peroneus longus (tendon); (24) peroneus brevis (tendon); (25) extensor digitorum longus; (26) dorsal interosseal.

## **Block E: The Gluteal Region and Posterior Compartment of the Thigh**

Following completion of this block of dissection, all clinically relevant anatomical structures within the gluteal region and posterior thigh compartments were clearly demonstrated for imaging. Figure 5(a) shows the first stage of this dissection in which the skin was reflected to reveal the subcutaneous fat layer in relation to the deep fascia (fascia lata) underneath. Figure 5(b) demonstrates the dissection following removal of this fat layer, which was done to expose the gluteus maximus and the extent of the fascia lata on the posterior aspect of the thigh. Both the muscle fibre orientation, and the relationship between the gluteus maximus and the fascia lata were clearly visible at this stage. Removal of the fascia lata and sequential dissection of the gluteal muscle layers, facilitated a thorough display of all relevant neurovasculature associated with the region. This included the posterior cutaneous nerve of the thigh, the sciatic nerve and the inferior and superior gluteal nerves and vessels, the spatial relationship between these structures, and the greater and lesser sciatic foramen. Though not displayed in these images, the hamstrings were also clearly demonstrated for imaging, following removal of the deep fascia. Figure 5(c) and (d) demonstrate the final stages of the gluteal and posterior thigh dissection, in which the gluteal muscles and hamstrings had been completely removed. At this stage, the lateral hip rotators, ischial tuberosity and the extent of the sciatic nerve were successfully demonstrated for imaging.

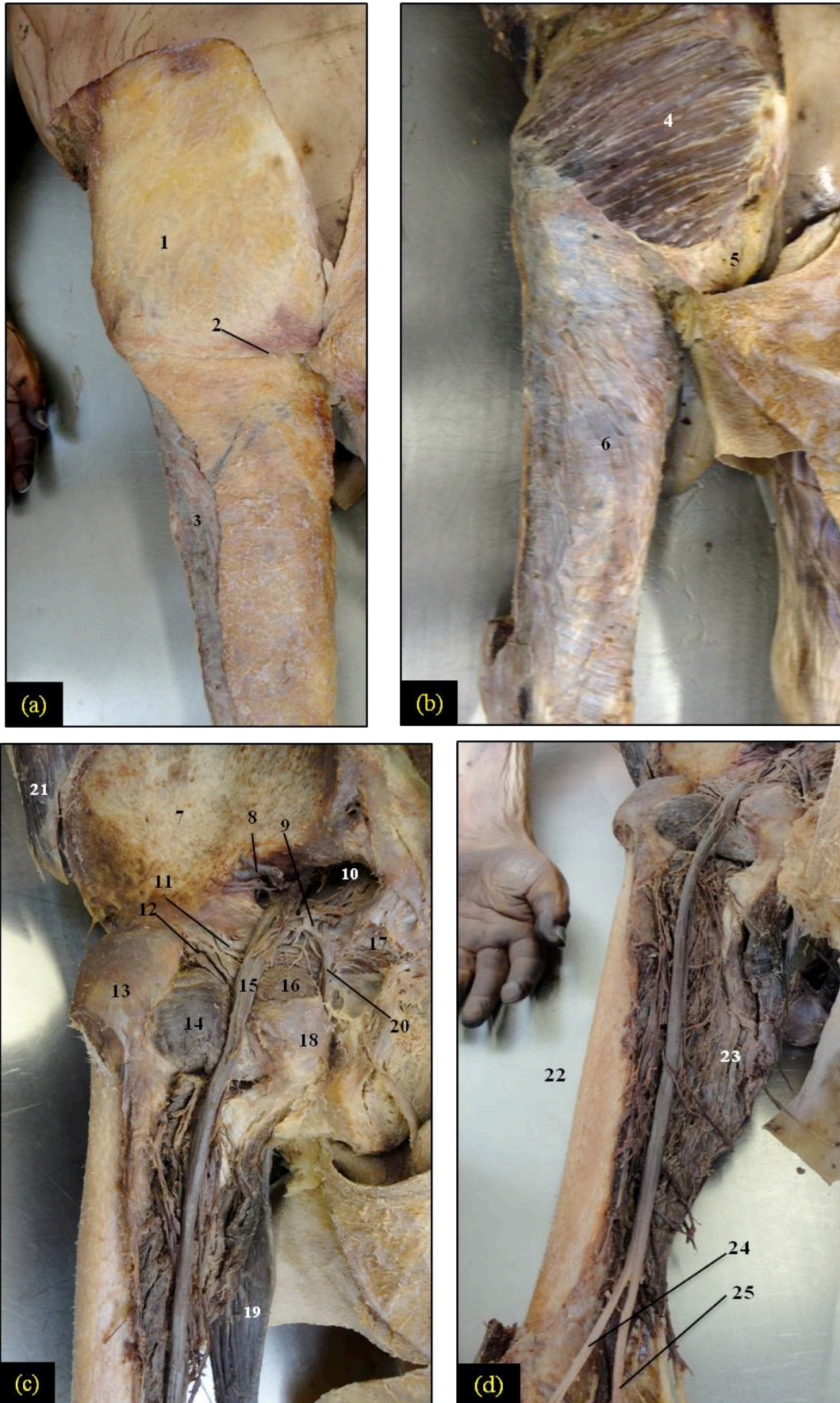


**Figure 4. Selected key stages of dissection Block E: The Gluteal Region and the Posterior Compartment of the Thigh. (a) Block E(i), (b) Block E(ii), (c) Block E(vi) and (d) Block E(vii). (1) subcutaneous fat; (2) gluteal fold; (3) fascia lata; (4) gluteus maximus; (5) ischiorectal fossa; (6) fascia lata; (7) ilium; (8) superior gluteal artery (cut); (9) inferior gluteal artery; (10) greater sciatic foramen; (11) superior gemellus; (12) inferior gemellus; (13) greater trochanter; (14) quadratus femoris; (15) sciatic nerve; (16) obturator externus; (17) sacrospinous ligament; (18) ischial tuberosity; (19) gracilis; (20) pudendal artery; (21) external oblique; (22) sciatic nerve; (23) adductor magnus; (24) common peroneal nerve; (25) tibial nerve.**

## **Block F: The Posterior Compartment of the Leg**

In Block F of the dissection, all relevant musculature and neurovasculature associated with the popliteal fossa and posterior compartment of the leg was successfully presented for imaging. Figure 6(a) illustrates the posterior aspect of the leg following removal of the deep fascia to expose the superficial muscles of the calf. At this stage, the spatial relationship between the gastrocnemius and soleus could be clearly visualised and their point of merging to form the calcaneal tendon was demonstrated. The saphenous nerve was also clearly identifiable for imaging. Within the popliteal fossa, the popliteal vessels, and bifurcation of the sciatic nerve into the common peroneal, and tibial branches, were clearly defined, and the neurovascular associations between these structures and the muscles of the calf were displayed. Figure 6(b) illustrates the popliteal fossa following removal of the gastrocnemius, where all aforementioned structures could be clearly identified. Figure 6(c) demonstrates the deep muscles of the posterior compartment following removal of the gastrocnemius, soleus and plantaris muscles, at which stage the extent of the tibial nerve and posterior tibial artery, coursing down the posterior aspect of the thigh, was successfully shown. At this stage, the tendons of the tibialis posterior, flexor digitorum longus, tibial artery, posterior tibial nerve and flexor hallucis longus, were demonstrated passing through the tarsal tunnel. Removal of all deep musculature at this stage then facilitated good exposure of the interosseous membrane for imaging.

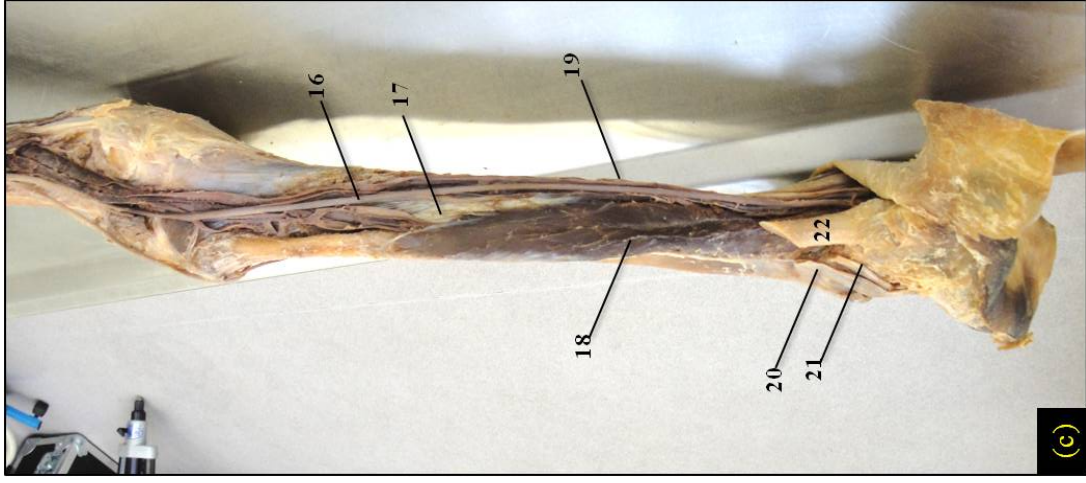
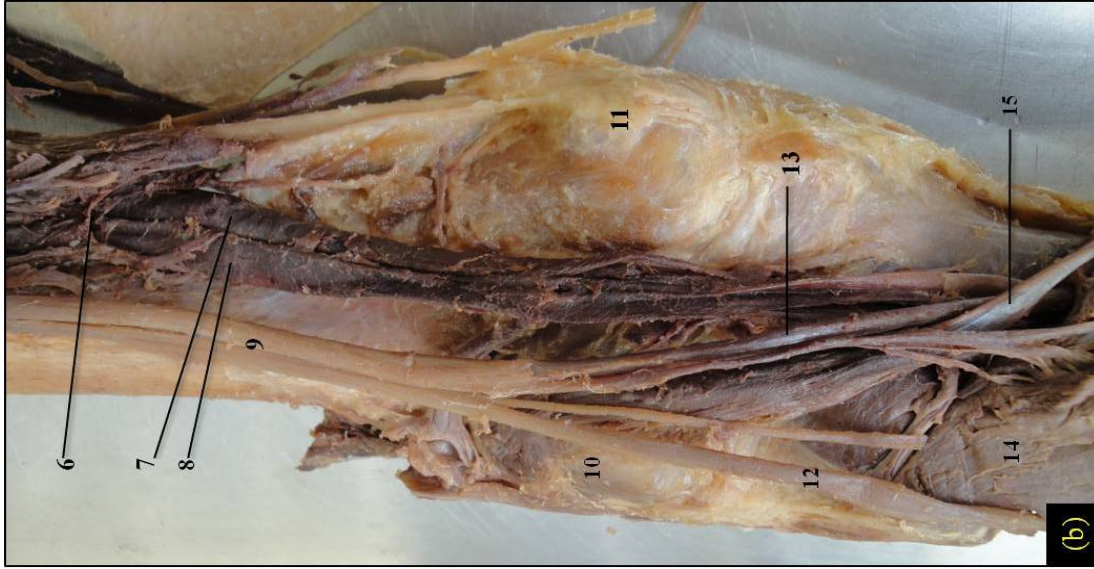


**Figure 5: Selected key stages of dissection Block F: Posterior compartment of leg. (a) Block F(i), (b) Block F(ii), (c) Block F(iii) and (d) Block F(iv)** (1) gastrocnemius; (2) soleus; (3) sural nerve; (4) fibula; (5) calcaneal tendon; (6) adductor hiatus; (7) popliteal vein; (8) popliteal artery; (9) adductor hiatus; (10) lateral condyle of femur; (11) medial condyle of femur; (12) common peroneal nerve; (13) tibial nerve; (14) soleus; (15) plantaris; (16) plantaris; (17) tibialis posterior; (18) flexor hallucis longus; (19) flexor digitorum longus; (20) tendon of peroneus longus (cut); (21) tendon of peroneus brevis (cut); (22) calcaneal tendon (cut).

## **Block G: The Sole of the Foot**

This dissection facilitated a fully comprehensive demonstration of all relevant anatomy within all four layers of the sole of the foot. Figure 7(a) clearly illustrates the first layer of the sole following removal of the plantar aponeurosis, which was previously shown for imaging. At this stage, the flexor digitorum longus, abductor digiti minimi, and abductor hallucis were all clearly discernable. Digital nerve branches were also shown. Figure 7(b) shows the next stage of dissection, which facilitated visualisation of the second layer of the sole layer. Here, the lumbricals were visible and the flexor digitorum longus tendons could be seen passing into the flexor sheaths. The medial and lateral plantar nerves and arteries, and their association with surrounding musculature was also clearly shown. Removal of the flexor digitorum longus tendons, the lumbricals, accessorius, and the abductor digiti minimi at the next stage exposed all anatomical structures associated with the third layer of the sole which is shown in Figure 7(c). At this stage, the abductor digiti minimi brevis, plantar interossei, transverse and oblique heads of adductor hallucis, and the medial and lateral heads of flexor hallucis brevis, were clearly presented for imaging. The removal of the transverse and oblique heads of the adductor hallucis during the next stage of dissection successfully demonstrated the extent of the lateral plantar artery and the plantar arch. Finally, Figure 7(d) shows the fourth layer of the sole, featuring the major plantar ligaments and the tendon of peroneus longus, following the removal of all musculature and neurovasculature from the plantar surface of the foot.

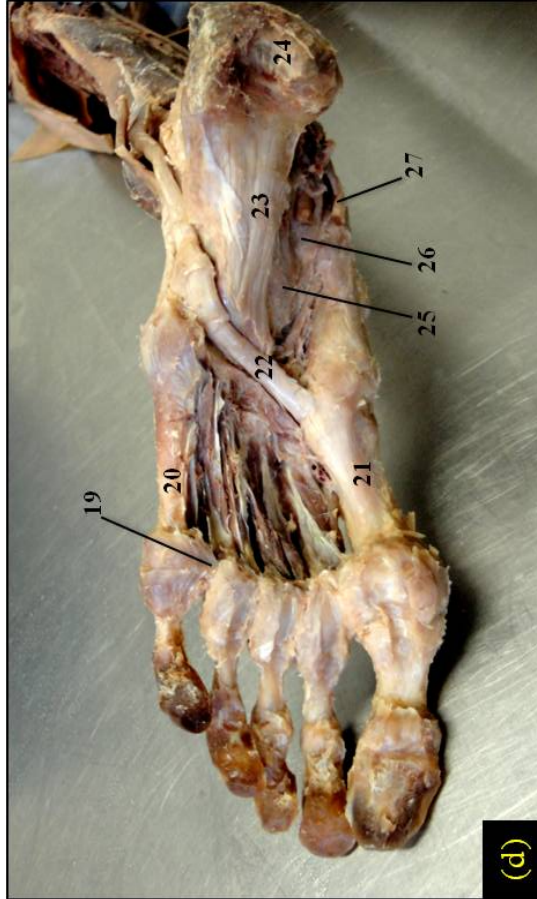
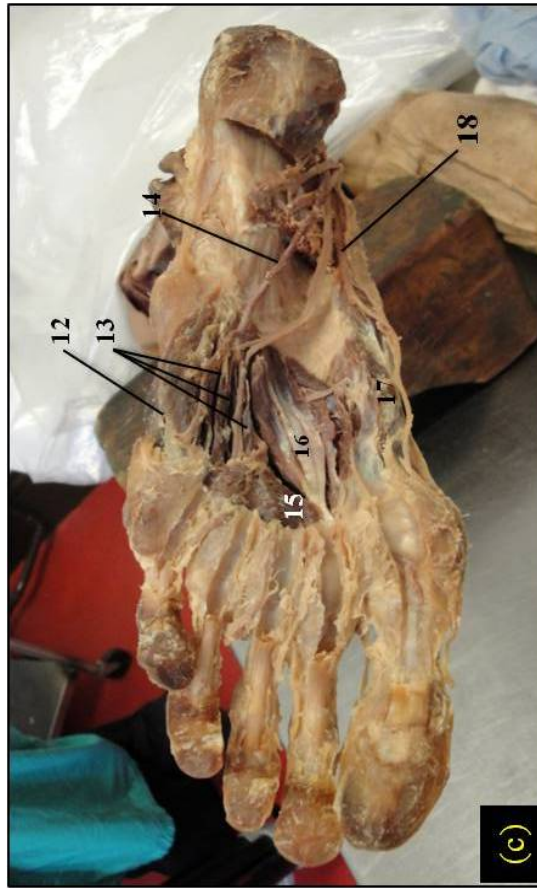


**Figure 6. Selected key stages of dissection Block G: The Sole of the Foot. (a) Block G(iii), (b) Block G(vi), (c) Block G(vii) and (d) Block G(vii).** (1) fibrous flexor sheaths; (2) digital nerves; (3) tendon of flexor hallucis longus; (4) abductor digiti minimi; (5) flexor digitorum brevis; (6) abductor hallucis; (7) lumbricals; (8) tendons of flexor digitorum longus; (9) lateral plantar artery; (10) lateral plantar nerve; (11) medial plantar nerve; (12) abductor digiti minimi brevis; (13) plantar interseus; (14) lateral plantar interseus; (15) transverse head of adductor hallucis; (16) oblique head of adductor hallucis; (17) flexor hallucis brevis (medial and lateral heads); (18) medial plantar artery; (19) deep transverse metatarsal ligament; (20) fifth metatarsal; (21) first metatarsal; (22) tendon of peroneus longus; (23) long plantar ligament; (24) calcaneus; (25) calcaneocuboid ligament; (26) calcaneonavicular ligament; (27) tendon of tibialis posterior.

## **Block H: Articulations**

This block of the dissection facilitated a good demonstration of all of the major joints of the lower limb, including the hip, knee and ankle joints. Removal of all remaining muscle, vascular and neural tissue and facilitated easy disarticulation of the hip, knee and ankle, thus providing a good demonstration of all relevant ligaments and articulating surfaces, associated with each joint. Figure 8(a) shows the posterior aspect of the articulating surface of the head of the femur, and illustrates how a portion of the joint capsule and ligament of head of femur were presented for imaging. Fig 8(b) features a superior view of the articulating surface of the tibia, where the collateral and cruciate ligaments and both menisci can be clearly visualised. This figure also shows arthritic degeneration of the proximal articulating cartilage of tibia, which was also found on that of the patella and distal femur. Figure 8(c) offers a posterior view of the disarticulated foot and shows how the articulating surface of the talus was presented for imaging. Although not visible in the examples provided, all ligaments associated with the ankle joint, and those on the dorsum of the foot, such as the posterior tibiofibular, posterior tibiotalar, deltoid, anterior and posterior talofibular, calcaneofibular and inferior transverse ligaments, were presented clearly for imaging.

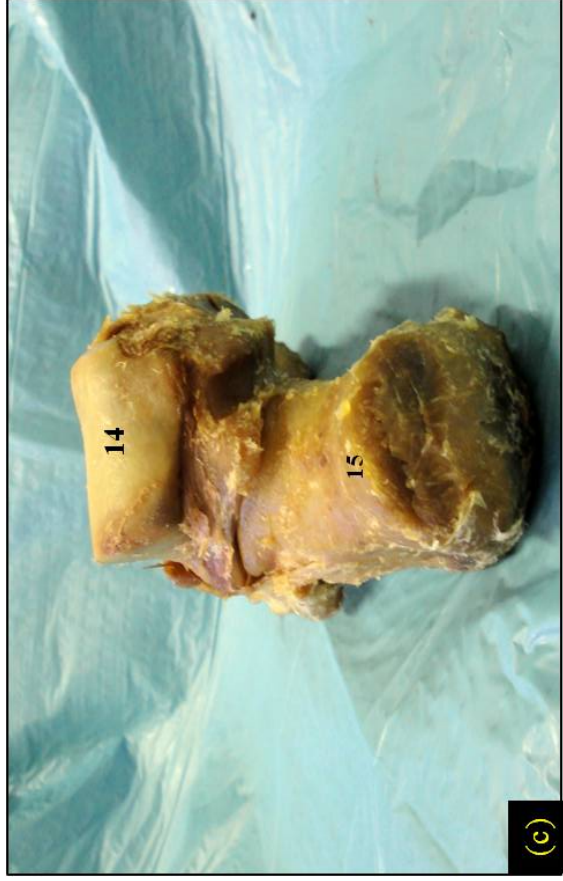
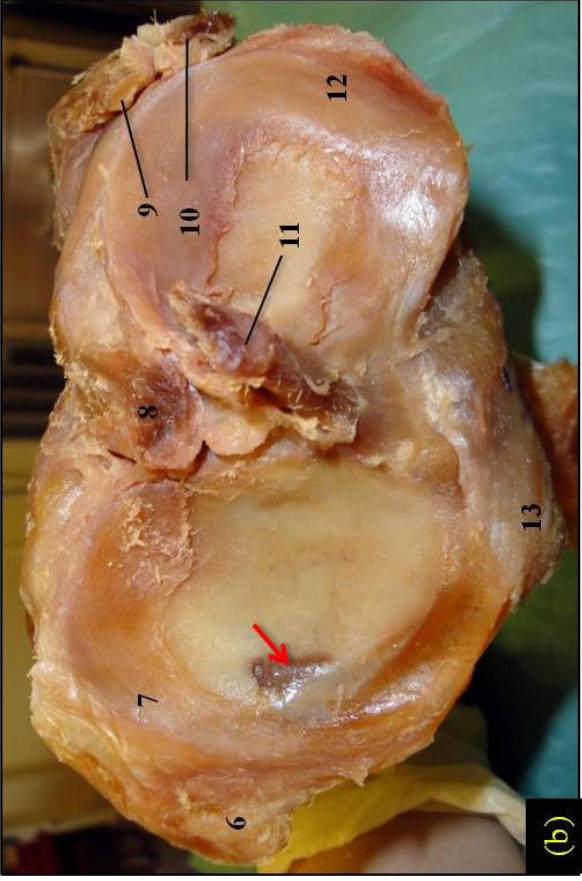


**Figure 7. Selected key stages of dissection Block H: Articularions. (a) Block H(ii), (b) Block H(iii) and (c) Block H(iv).** (1) greater trochanter; (2) head of femur; (3) ligament of head of femur; (4) joint capsule (cut); (5) lesser trochanter; (6) tibial collateral ligament; (7) medial meniscus; (8) posterior cruciate ligament; (9) fibular collateral ligament; (10) tendon of popliteus; (11) anterior cruciate ligament; (12) lateral meniscus; (13) trochlea of talus; (14) tibial tuberosity; (15) calcaneus; (*red arrow*) arthritic degeneration of articulating cartilage.

## **Block I: Bones**

Following the final block of dissection, the individual bones of the lower limb were clear of almost all remaining tissue, offering a clear view of the topography of each bone, and a clear demonstration of all clinically relevant bony landmarks. Figure 9(a) demonstrates a posterior view of the femur in its entirety after being stripped of all ligamentous tissue proximal to its articulating surfaces. Figure 9(b) and (c) offer individual anterior views of the tibia and fibula following disarticulation from each other. Figure 9 (c) shows a superior view of the bones of the foot in their anatomical position, following complete removal of all associated ligaments around the ankle and the dorsum of the foot.

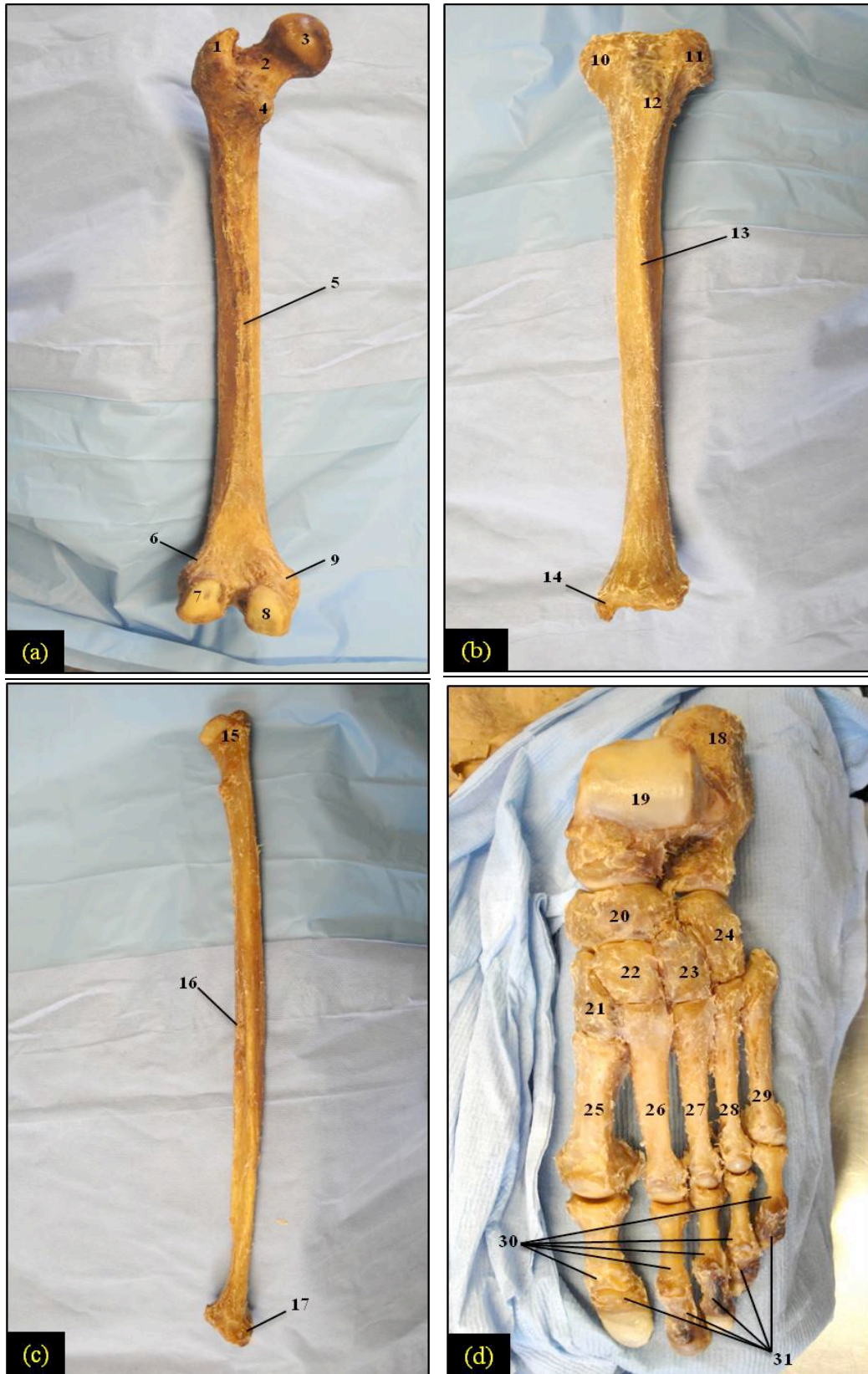


**Figure 8. Selected key stages of dissection Block I: Bones. (a) femur, (b) tibia, (c) fibula and (d) bones of the foot.** (1) greater trochanter; (2) neck of femur; (3) head of femur; (4) lesser trochanter; (5) linea aspera; (6) lateral epicondyle; (7) lateral condyle; (8) medial condyle; (9) medial epicondyle; (10) medial condyle; (11) lateral condyle; (12) tibial tuberosity; (13) anterior margin of tibia; (14) medial malleolus; (15) head of fibula; (16) interosseous crest; (17) lateral malleolus; (18) calcaneus; (19) talus; (20) navicular; (21) medial cuneiform; (22) intermediate cuneiform; (23) lateral cuneiform; (24) cuboid; (25) first metatarsal; (26) second metatarsal; (27) third metatarsal; (28) fourth metatarsal; (29) fifth metatarsal; (30) proximal phalanges; (31) distal phalanges.

## **3.2: Cadaveric Data Acquisition**

Following systematic laser scanning and digital photography of all key stages of the dissection, accurate three-dimensional topographical data, sufficient for subsequent digital modelling, was collected from all clinically relevant structures of the lower limb.

Figure 10 demonstrates a brief example, taken from an early stage of the dissection of the inguinal canal, of how each polygon-mesh surface is reconstructed from the point cloud data obtained. In this specific example, it can be seen that the surface points collected by the laser scanner have been connected up (automatically by the computer software) by a network of straight lines, to create a three-dimensional triangulated mesh of the tissue surfaces. This model represents the type of graphical output which could be visualised on the laptop computer screen as scanning was being performed.

Figures 11 - 15 provide examples of digital photography and polygon-mesh models, which were derived from selected key stages of the dissection. These include, examples from; Block A: The inguinal canal (Fig. 10); Block C: The anterior and medial compartments of the thigh (Fig. 11); Block D: The anterior and lateral compartments of the leg (Fig. 12); Block E: The gluteal region and posterior compartment of the thigh (Fig. 13); and Block G: The sole of the foot (Fig. 14). In each example given, a digital photograph of the dissected area can be seen on the left and its corresponding polygon mesh model, on the right. The relevant anatomical structures in each case have been labelled using a simple numbering system. Blacked out patches on the polygon mesh models represent deeper areas where the laser stripe could not obtain topographical data, however, as demonstrated in the examples given, these are not associated with any of the relevant structures in each example given.

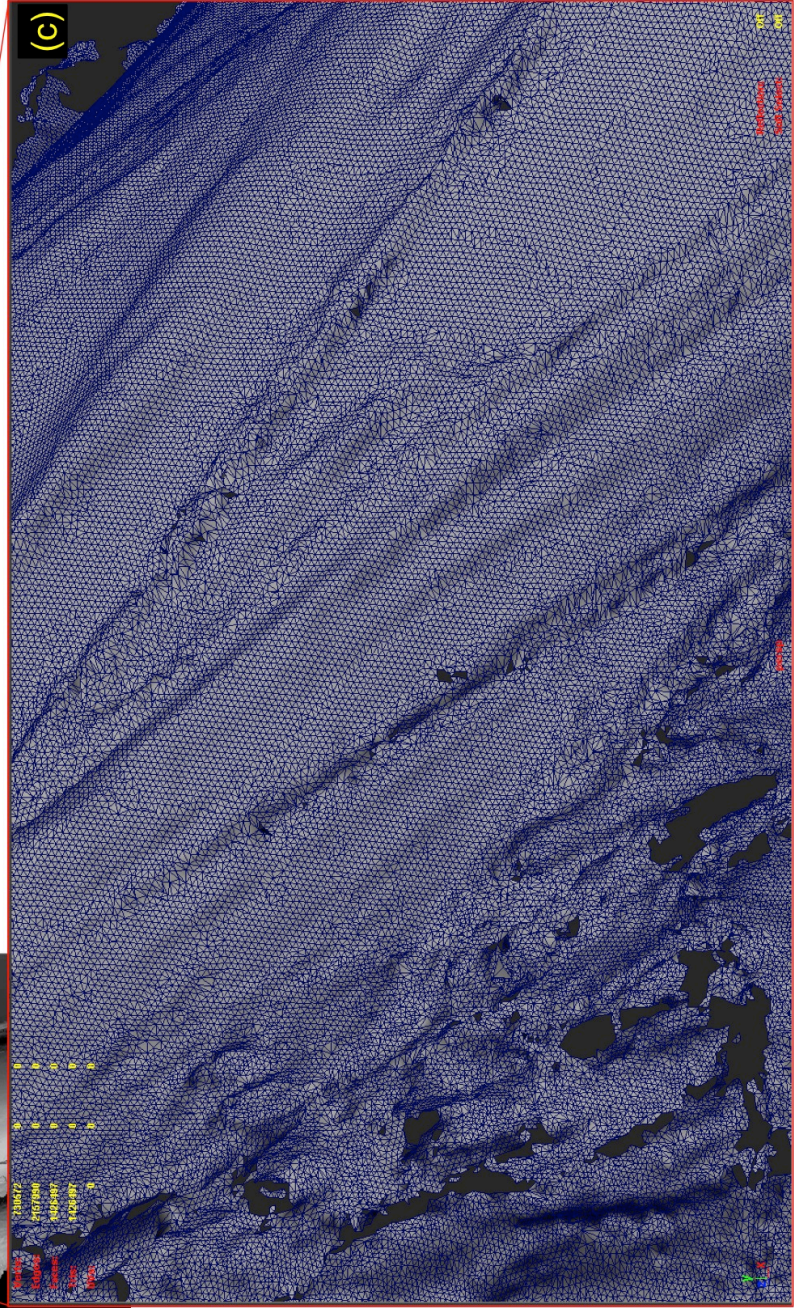
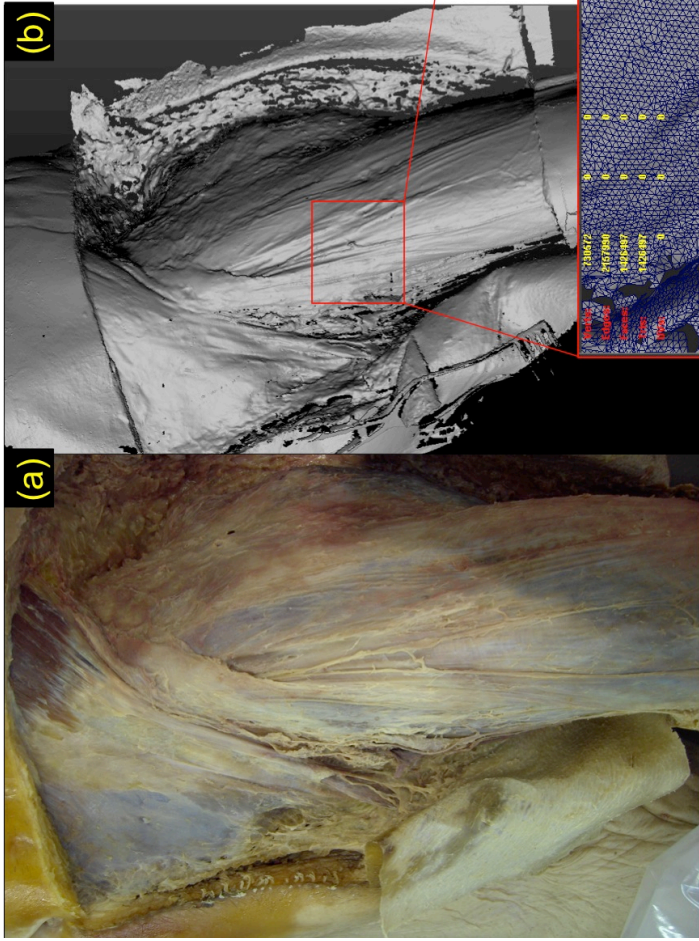


**Figure 10.** An example of how a polygon mesh surface is created from the point cloud data collected at each stage of the cadaveric dissection. (a) Digital photograph of inguinal canal and proximal thigh following dissection Block A(i). (b) Graphical output (polygon mesh) of point cloud data acquired from dissection. (c) Close up of proximal thigh indicating how the triangulated surface is formed from the point cloud data.

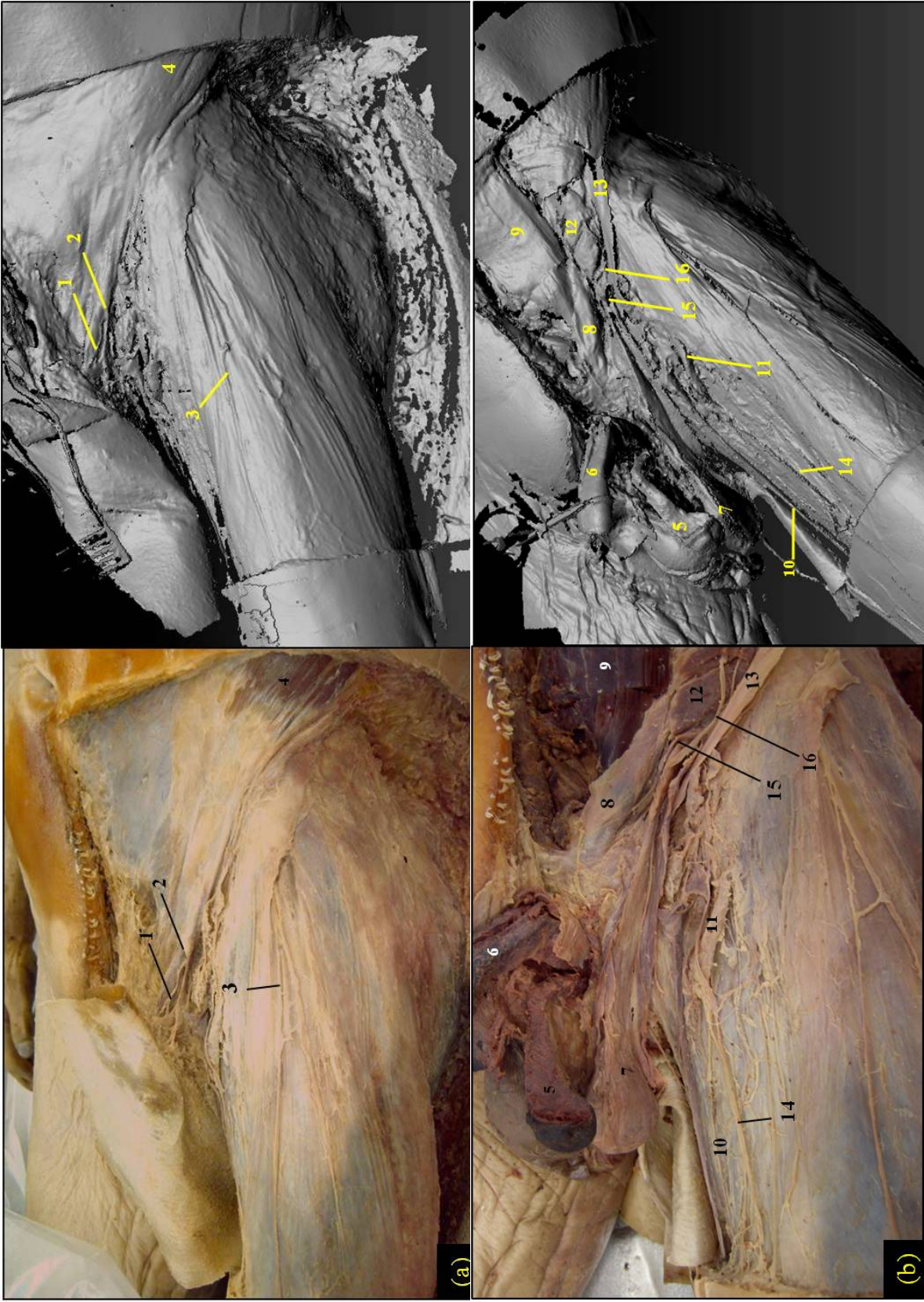
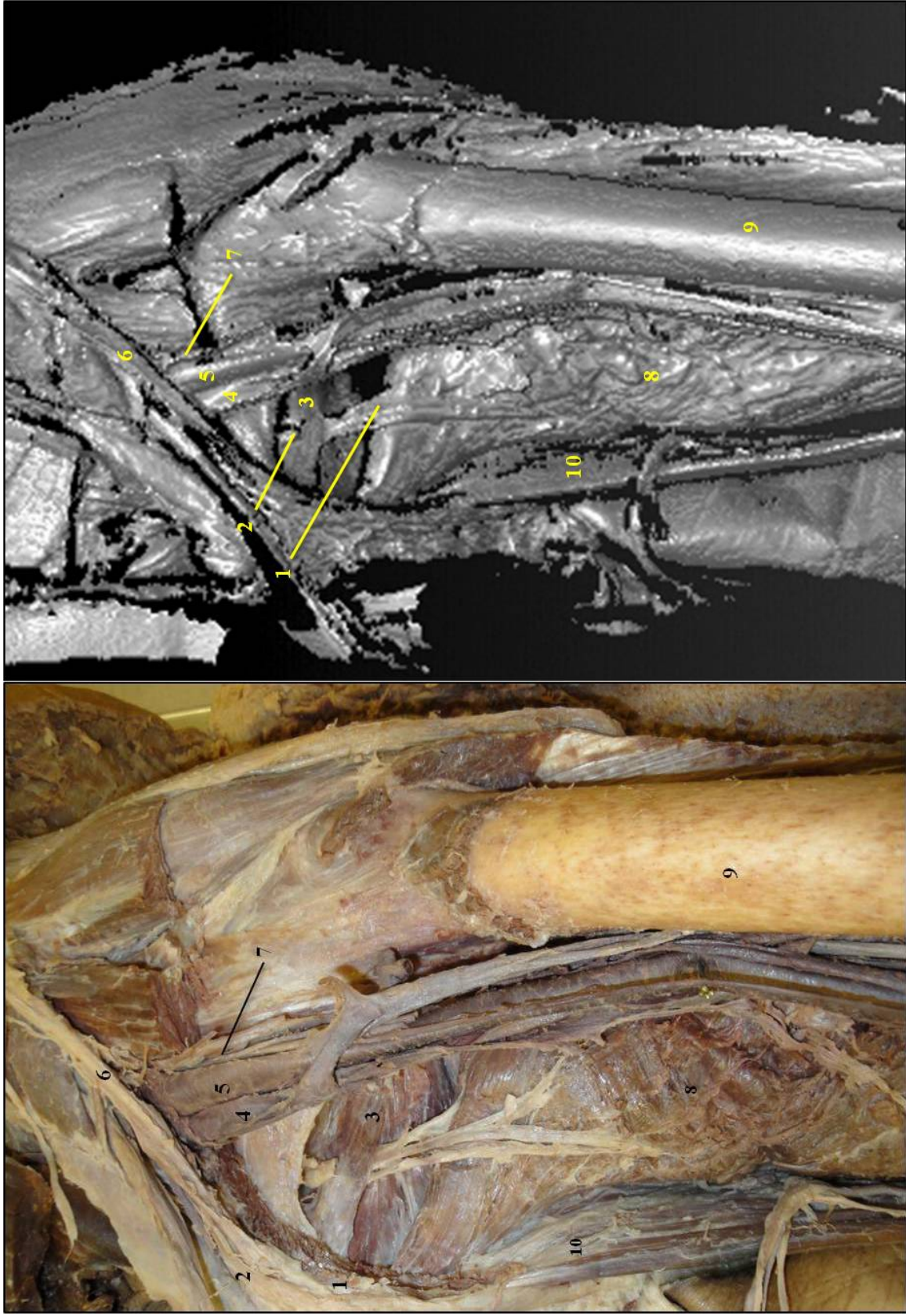
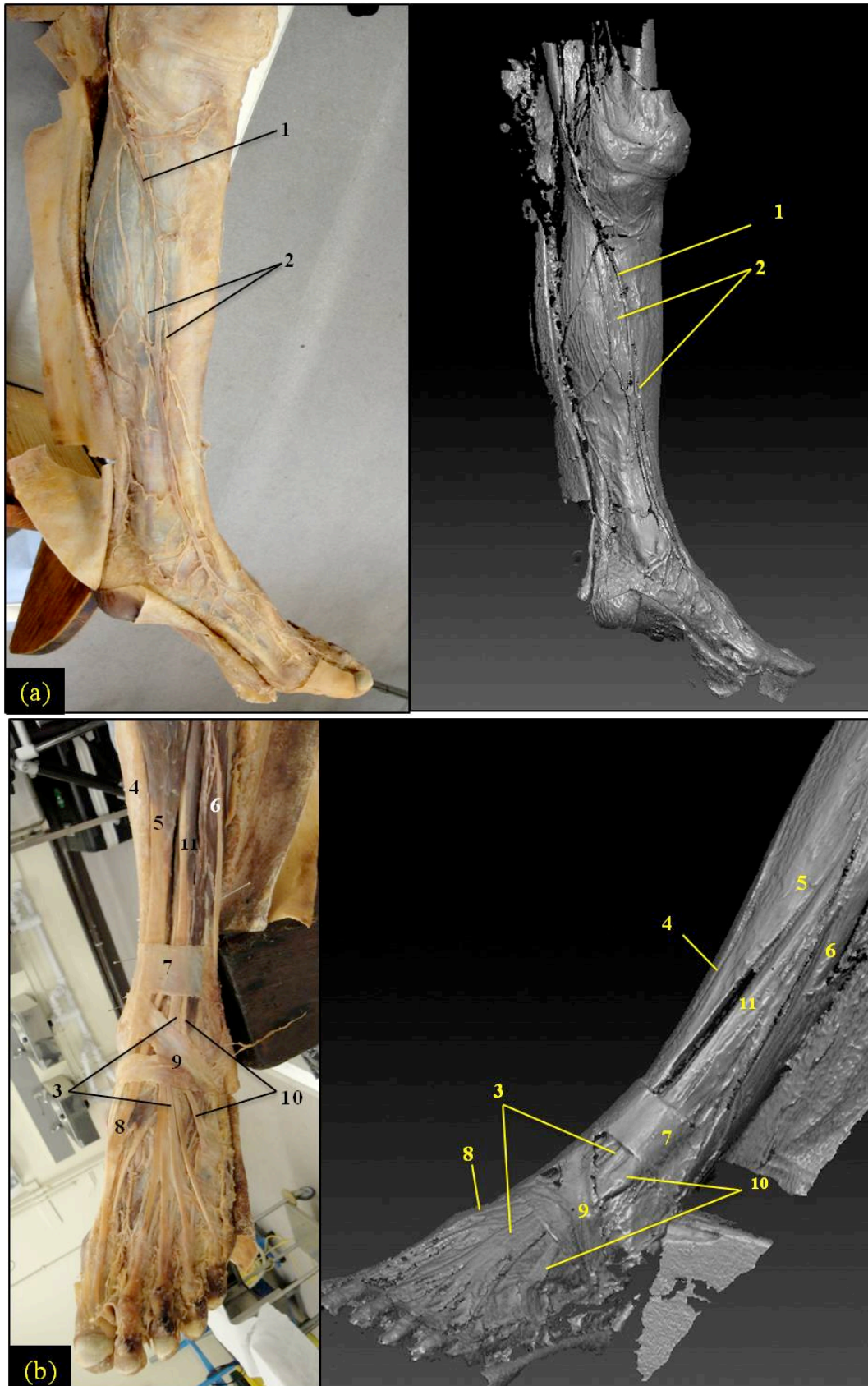


Figure 11. Imaging of selected inguinal canal dissections (Block A) by digital photography and laser scanning. (a) (left): Digital photograph of dissection following Block A(iii), (right): Polygon mesh model derived from laser scanning. (b) (left): Digital photograph of dissection following Block B(iv), (right): Polygon mesh model derived from laser scanning. (1) ilioinguinal nerve; (2) superficial inguinal ring; (3) lateral femoral cutaneous nerve; (4) external oblique; (5) corpus spongiosum; (6) corpus cavernosum; (7) testis; (8) conjoined tendon; (9) rectus abdominis; (10) great saphenous vein; (11) inguinal lymph node; (12) transversus abdominis; (13) inguinal ligament; (14) anterior femoral vein; (15) deep inguinal ring; (16) inguinal nerve.11



**Figure 12. Imaging of anterior thigh dissection from Block C(vi). (Right): digital photograph, (left): Polygon-mesh model acquired from laser scanning. (1) posterior branch of obturator nerve; (2) anterior branch of obturator nerve; (3) obturator externus; (4) femoral vein; (5) femoral artery; (6) inguinal ligament; (7) femoral nerve; (8) adductor magnus; (9) femur; (10) gracilis.**



**Figure 13. Imaging of selected dissections of the anterior and lateral compartment of the leg and dorsum of the foot (Block D). (a) (left): digital photograph following dissection Block D(ii), (right): Polygon-mesh acquired from laser scanning. (b) (left): digital photograph following dissection Block D(iii), (right): Polygon mesh acquired from laser scanning. (1) great saphenous vein; (2) saphenous nerve, (3) extensor digitorum longus; (4) tibia; (5) tibialis anterior; (6) peroneus longus; (7) superior extensor retinaculum; (8) extensor hallucis longus; (9) inferior extensor retinaculum; (10) peroneus tertius; (11) extensor digitorum longus**

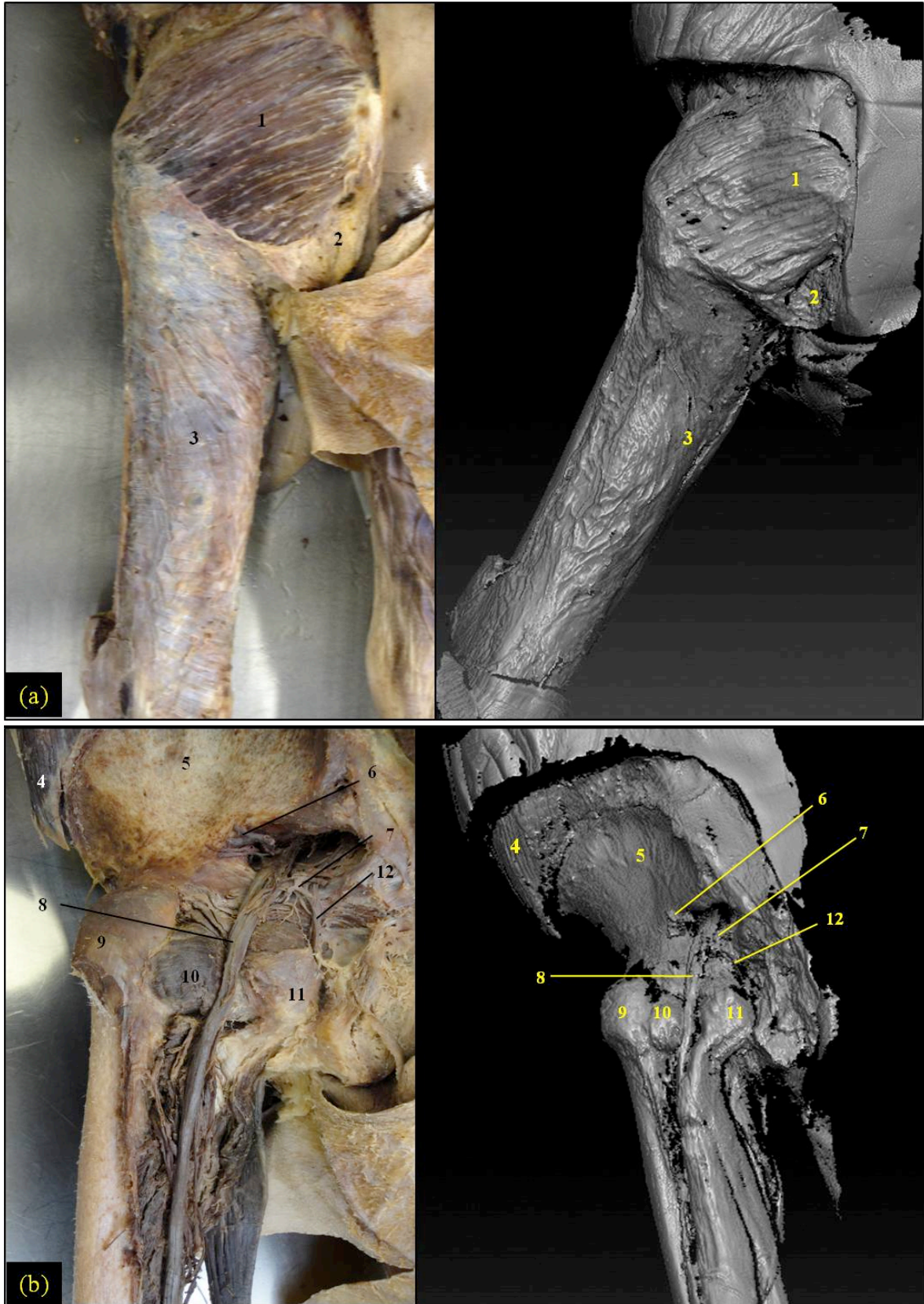


**Figure 14. Imaging of selected dissections from gluteal and posterior compartment of thigh regions (Block E). (a) (left): digital photograph of gluteal region following dissection Block E(ii), (right) Polygon-mesh acquired from laser scanning. (b) (left) : Digital photograph of gluteal region following dissection Block E(vii), (right) polygon-mesh acquired form laser scanning. (1) gluteus maximus; (2) ischiorectal fossa; (3) fascia lata; (4) external oblique; (5) ilium; (6) superior gluteal artery; (7) inferior gluteal artery; (8) sciatic nerve; (9) greater trochanter; (10) quadratus femoris; (11) ischial tuberosity; (12) pudendal artery.**

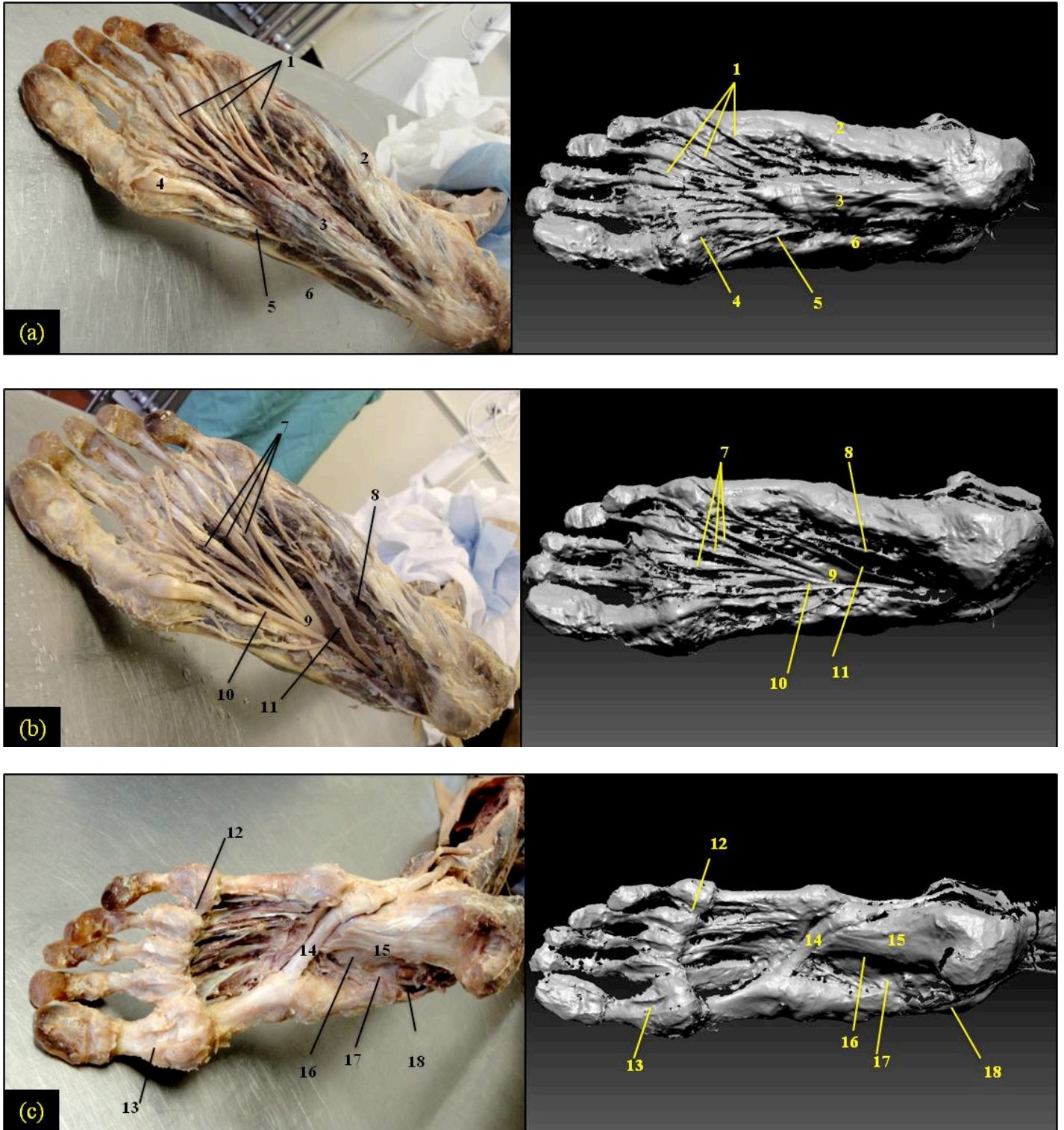


**Figure 15.** Imaging of selected dissections from the sole of the foot (Block G). (a) (left): digital photograph of dissection of first layer of the sole (Block G(iii)), (right): corresponding polygon-mesh acquired by laser scanner. (b) (left): Digital photograph of second layer of the sole of the foot(Block G(iv)), (right) corresponding polygon-mesh. (c) (left) Digital photograph of fourth layer of the sole (Block G(vii)), (right) corresponding polygon-mesh acquired from laser scanning. (1) digital nerves; (2) abductor digiti minimi; (3) flexor digitorum longus (tendon); (4) flexor hallucis longus (tendon); (5) medial plantar nerve; (6) abductor hallucis; (7) lumbricals; (8) lateral plantar artery; (9) flexor digitorum longus; (10) medial plantar nerve; (11) lateral plantar nerve; (12) deep transverse metatarsal ligament; (13) fibrous flexor sheath (opened); (14) tendon of peroneus longus; (15) long plantar ligament; (16) calcaneocuboid ligament; (17) calcaneonavicular ligament; (18) tendon of tibialis posterior.

# 4:Discussion

## **4.1: Overview of Results**

The results show that the unique methodology used for cadaveric data acquisition in this study, incorporating a detailed cadaveric dissection, state of the art laser scanning and simple digital photography, has proven extremely successful in producing a comprehensive and accurate three-dimensional dataset, for the male lower limb.

The first section of results represents various examples from each key stage of the dissection, and demonstrates the level of intricacy and the extent of anatomical detail which was achieved for subsequent data acquisition. Whilst the aim of this study focuses largely on the use of the V5 scanner for obtaining three-dimensional data from the specimen, the quality of the dissection was absolutely paramount to the success of the results obtained. The initial criteria for the cadaveric dissection was that it had to demonstrate all clinically relevant anatomy at a level of detail sufficient for further digital modelling, and be done in such a way as to offer an accurate representation of normal human anatomy. As demonstrated in Figs 1-9, these dissection criteria were successfully met. All clinically relevant anatomy, including that associated with the dermis, musculature, neurovasculature, lymph nodes, ligamentous attachments and bone, was clearly demonstrated for subsequent digital imaging. Each structure was dissected carefully and with precision, and the specimen itself featured no abnormalities with the exception of a small amount of arthritic change on the articulating surfaces of the knee joint, as detailed on page 79. Also noteworthy with regards to the dissection performed in this study, was that the dissection techniques used deviated slightly from standard textbook methods such as those detailed in Gosling et al., (2008) and Zuckerman (1981). Alternative non-traditional dissection techniques were employed in order to expose structures such as the fibrous adductor canal, and the separated quadriceps (not normally demonstrated in standard dissection textbooks) for subsequent data acquisition.

These features make the dissection performed unique to this project, and as a result have enhanced the value of the data obtained.

As can be seen in Figs. 10-15, the second section of results demonstrates that the method of data acquisition used, including both laser scanning and colour digital photography, was successful in accurately obtaining high-resolution topographical, colour and texture data from the cadaveric specimen following each stage of the dissection. Figure 10 clearly demonstrates how the point cloud data obtained, is used (by the scanning software) to create an accurate three-dimensional surface profile of the cadaveric tissues. The Perceptron ScanWorks<sup>®</sup> V5 scanner, capable of collecting surface data at a point-to-point resolution of up to 12  $\mu\text{m}$ , with a measurement accuracy of 24 $\mu\text{m}$  (see Appendices I and II, respectively) was able to collect detailed topographical surface data from all structures listed in the 'Full Account of Cadaveric Dissection' given on pages 22-58 of this report. Notably, this also included finely dissected neurovasculature and lymph nodes. This three-dimensional data, combined with corresponding high resolution (10.1 MP) colour digital photography, has therefore facilitated the acquisition of an extremely comprehensive dataset for the male lower limb, obtained directly from a genuine cadaveric source.

## **4.2: How Can this Data be Used?**

Given the success of this study in producing a comprehensive and accurate three-dimensional dataset for the male lower limb, it is now hopeful that digital design experts within the DDS will be able to utilise this data in the development of high-end virtual reality training applications for both lower limb and inguinal canal regions.

One of the large advantages of the Perceptron ScanWorks® V5 Scanner used in this study is that it can integrate data collection in real-time with a number of industry recognized modelling softwares, such as PolyWorks®, Geomagic® , Rapidform XO™ etc., giving digital experts the flexibility to chose from an array of sophisticated interfaces when using this data to create an optimal interactive training package (see Appendix I).

Though the specifics of data processing beyond cadaveric data acquisition is largely outwith the remit of this report, it is important to highlight the usefulness of this particular dataset in the production of a sophisticated reconstruction, in comparison to those which have been used before. In summary, the topographical surface data obtained from each clinically relevant anatomical structures over the course of this project will be used as accurate three-dimensional scaffolds upon which further digital modelling and enhancement can be performed in the future. Part of this post processing will involve the corresponding colour and texture data from the digital photography component of this study being mapped onto these scaffolds, with the view of eventually creating an accurate and realistic reconstruction of the lower limb for anatomical training. This process will require continuing input from both digital and anatomical experts to ensure that each anatomical structure imaged from the dissection is carefully reconstructed, and that the end product is representative of a real human specimen. This expert contribution, among other things, will ensure that colour and texture data is digitally enhanced where appropriate, to reflect that of true lower limb

anatomy. The combination of this expertise with the use of the three-dimensional cadaveric data collected in this study, demonstrates a unique new approach to the creation of an educational virtual specimen. Whilst processing of the raw data is currently on going, a prototypic virtual reconstruction derived from the first three blocks of dissection, is demonstrated below in Fig. 16.

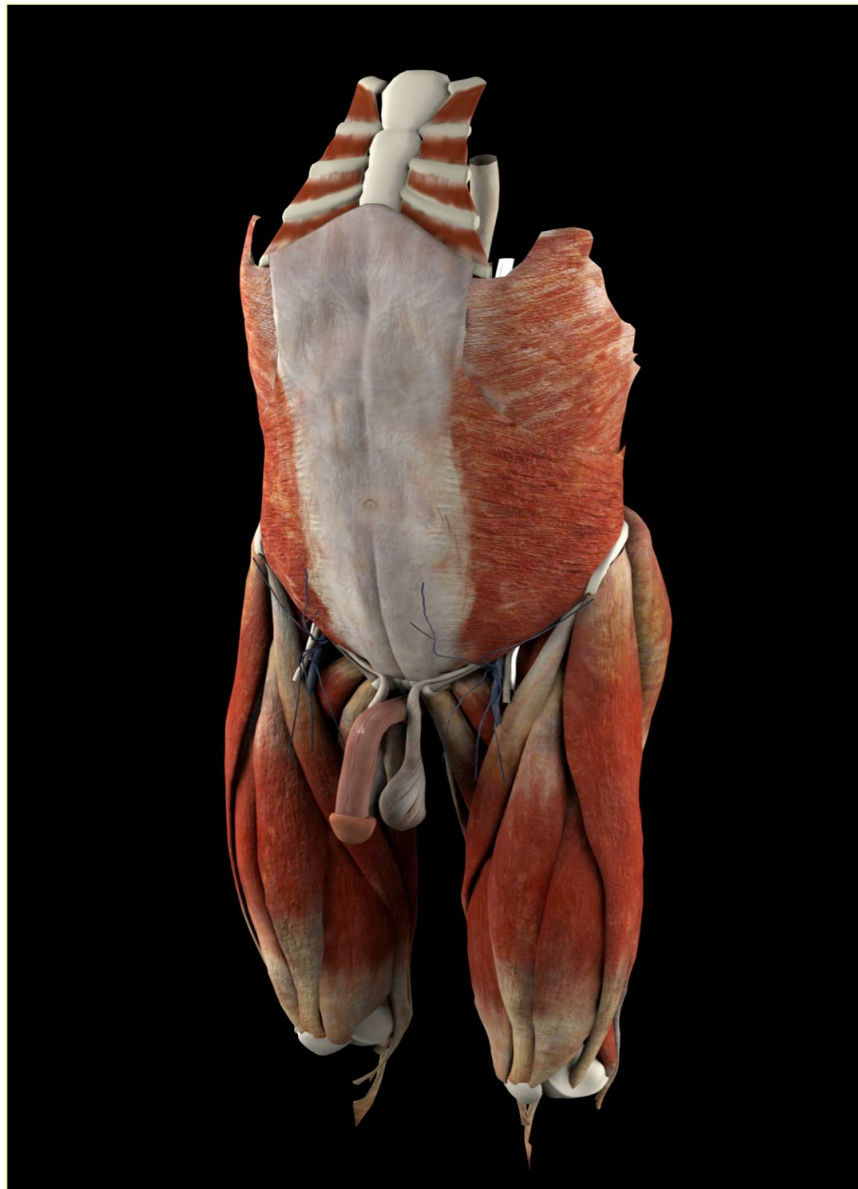


**Figure 16. Prototype reconstruction derived from point cloud data acquired from inguinal canal, external genitalia and anterior thigh dissections by digital design experts at the Digital Design Studio, Glasgow School of Art.**

### **4.3: Previous Work in Cadaveric Data Acquisition**

The concept of digitised cadaveric anatomy, although relatively young, is not new, and given the pressing requirement over recent years to supplement medical training with virtual cadavers, many attempts have been made to collect cadaveric datasets for use in this field. Previous works in this area of research, namely the Visible Human Project (VHP), the Chinese Visible Human (CVH) and the Korean Visible human (KVH), have all pursued the task of digitising cadaveric data by sectioning cadaveric specimens and photographing each slice in sequence. Whilst these cross-sectional datasets have proved extremely useful in many areas of research, there still exists a number of problems associated with their use in creating comprehensive three-dimensional reconstructions for anatomical training (Park et al., 2006; Spitzer & Whitlock, 1998; Zhang et al., 2003).

The National Library of Medicine's Visible Human Project, completed in 1995 at the University of Colorado, was a project that set a profound benchmark in the field of cadaveric data collection, and the first to create full datasets for both the male and female human anatomy. The initial vision of the VHP researchers was to provide a common reference point for the production of anatomical training applications, the development of new medical imaging technologies, and the construction of digital anatomical libraries for access by academics, clinicians and researchers across the globe (Imelińska et al., 2000; Trelease, 1998; Venuti et al., 2004). Following in the footsteps of the pioneering Stanford Visible Female (University of Stanford, 1974), the VHP was the first of its kind to attempt documentation of the complete human anatomy from a real cadaveric source and sparked much enthusiasm amongst educationalists, clinicians and scientific researchers alike. This project has indeed provided a useful source from which research in medical visualisation and anatomical training has benefited greatly, and was in fact already being used by 1400 research, academic,

artistic and industrial establishments in over 43 countries worldwide by its time of completion 1995 (Zhang et al., 2003). The VHP researchers approached the task of cadaveric data acquisition by freezing and cross-sectioning male and female cadavers into two-dimensional slices of millimetre and one-third of a millimetre slices respectively, obtaining a total of 1878 slices for the male, completed in 1994, and 5189 slices for the female in 1995. Prior to cryosectioning, the cadavers were imaged by CT and MRI scanning in both transverse and coronal planes, and these radiographic images were then coupled with colour photographs of the corresponding cryosectioned slices (Spitzer & Whitlock, 1998).

Similarly to the way in which the data from the current study will be used, many subsequent research projects have utilised the Virtual Human Data (VHD) to create three-dimensional reconstructions for anatomical training purposes. The University of Columbia's Vesalius Project is a leading example of how the VHD has been used to create interactive multimedia computer applications for anatomical training. As a result of the Vesalius Project, electronic training applications, derived from the VHD, have been developed for both foot and pelvic anatomy, and successfully incorporated into the anatomy curriculum at Columbia University College of Physicians and Surgeons (Imelińska & Molholt, 2005; Venuti et al., 2004). Other projects which have utilised the VHD for similar purposes, as summarised by Temkin et al. (2006), include the NLM's own AnatQuest, the University of Michigan's iVoxel programme, the Visible Human Server by Ecole Polytechnique Fédérale De Lausanne, The Texas Tech University's W3D-VBS package, the Carnegie Mellon's Volume Browser, and also the Imperial College London's brachial plexus training program (Brenton et al., 2007), to mention but a few. This substantial list demonstrates just a fraction of the impact that the VHP has had on the development of computerised anatomical training.

Despite the profound effect this revolutionary project has had on the prospects of virtual anatomy, and its subsequent use in anatomical training, a number of discrepancies have been

identified in the methodology used to acquire the VHD. Most frequently stipulated by critics as the being the greatest flaw in this methodology, is that before cryosectioning, the male and female cadavers were sectioned into four separate blocks, due to the cryomacrotome table not being of adequate size to accommodate whole cadavers at one time. The instrument used to do this was a relatively thick “backsaw”, which resulted in three distinct junctions of 1.5mm cross-sectional data loss across the thorax, mid thigh, and upper leg regions (Spitzer & Whitlock, 1997; Zhang et al., 2004). It is also reported that during the milling process itself, fragments from delicate or brittle structures such as the teeth, concha nasalis and articulating cartilage were also lost, and that the slicing of tough tendinous tissue caused streaking across individual sections, all of which have implications in three-dimensional processing of the sectional data (Heng, 2007). Various aspects of the cadaveric preparation process, including the freezing of specimens to excessively low temperatures of around  $-70^{\circ}$  C also caused distortion of the neural tissue, blood vessel collapse, and a loss of ear ossicles, and the cadaveric specimens themselves are reported to have presented with a number of anatomical anomalies (Zhang et al., 2003).

Similar projects, such as the KVH and CVH, have since attempted to improve on the VHP methodology of data collection, and also produce datasets that are more typically representative the East Asian population (Park et al., 2006; Zhang et al., 2003). The VKH, initiated in 2000 at Ajou University, Suwon, Republic of Korea adopted a similar approach to collect a full set of cadaveric data for the typical Asian male. Their first attempt in 2001 used a 65 year old who died of cerebroma, and thus was criticised for not representing completely ‘normal’ anatomy. This has however been rectified in a more recent attempt, using a 33 year old cadaver to obtain a total of 8590 cross-sectional images at 0.2 mm intervals (Park et al., 2006; Zhang et al., 2003). Following this, authors of the CVH project, launched in 2001 at the Third Military Medical University in China, claim to have produced the most

comprehensive anatomical dataset from cadaveric material, to date. The methodology used in this study was also similar to that of the VHP, however a larger milling table was used to accommodate the whole cadaver at one time and blood vessels were injected with gelatine to prevent collapse on freezing. Also, milling of the numerous cadavers used was conducted under persistently cool temperatures of  $-25^{\circ}\text{C}$  to prevent crumbling and loss of delicate structures, and digital photographing of the CVH cryosections was performed at a higher resolution than either of the previous studies. As a result, the CVH produced photographic images of 2518 slices for the CVH male, and 3640 slices for the CVH female (Zhang et al., 2003, 2004).

Whilst great advances have been made in the field of cadaveric digitisation in recent years, there remains a great deal of scepticism over the use of previous datasets in the creation of virtual cadavers (Beylot et al., 1996; Nicholson et al., 2006). Though the data collected during the aforementioned studies has indeed been successfully used in the production of an array of computerised training applications to date, researchers who have used the data in this way have frequently reported difficulties in post-processing, storage, and more specifically, in the translation of two-dimensional image slices into sufficiently detailed three-dimensional reconstructions (Imelińska & Molholt, 2005; López-Cano et al., 2007; Temkin et al., 2006). Due to these difficulties, a complete and coherent three-dimensional anatomical library is yet to be produced from the VH dataset since its completion 15 years ago, rendering the initial vision of this project, as yet, unfulfilled (Imelińska & Molholt, 2005).

The greatest problem in translating cross-sectional datasets into useful three-dimensional reconstructions, arise in that the raw data must undergo the laborious and time consuming process of image segmentation. Anatomical image segmentation has been a busy area of research since the advent of modern cross-sectional imaging techniques such as CT and MRI. In this context, image segmentation is defined as the sub-division of a cross-sectional image

into non-overlapping constituent parts by a process of meticulous structure delineation (Kang et al., 2000; Pham et al., 2000). Generally speaking, delineation of an images component structures can be done either manually or using automated algorithms, and usually works on the principle of sorting image pixels into various constituent regions by intensity thresholding or colour differentiation (Pham et al., 2000). In order to reconstruct a three-dimensional anatomical scaffold from cross sectional data (similar to those obtained directly from the cadaveric specimen in this study by way of laser scanning), each slice must be individually segmented into its constituent structures, and then aligned in sequence to create a three-dimensional 'stack' of structure contours. Once this 'stack' has been aligned in sequence, the framework is meshed and then texture mapping and other post-processing can proceed (Brenton et al., 2007, Pham et al., 2000). The quality of the end-reconstruction produced is highly dependant on the success of the image segmentation process, which in turn is determined by the quality of the cross-sectional data, which itself is determined by the size of the slice intervals, the initial photographic resolution, and the precision of slice alignment (Hieu et al., 2010). Taking this into consideration, it is therefore clear why image segmentation of detailed anatomical structures is frequently stipulated in the literature as being the greatest obstacle associated with the use of cross-sectional datasets in the production of three- dimensional virtual cadavers for anatomical training (Boscolo et al., 2002; Cheng et al., 2010; Hamarneh et al., 2005; Ma et al., 2008; Qian et al., 2005; Yushkevich et al., 2006).

A factor which greatly contributes to this problem, applicable to all three of the aforementioned datasets, is that the data obtained was collected from specimens which had been frozen for the purpose of cryosectioning, resulting in poor colour differentiation of the tissues for subsequent photographing. This makes the precise delineation of closely associated structures, such as tendons from surrounding fatty tissue, and bone from

articulating fibrous capsules (notably all constituents of the musculoskeletal system) an exceptionally difficult task (Beylot et al., 1996; Imelińska & Molholt, 2005; Kang et al., 2000; Park et al., 2006; Zhang et al., 2003). This creates a major problem for the development of useful anatomical training devices, as in the case of the Visible Human Male alone, there are musculoskeletal structures present in more than 1800 cross-sectional slides. For this reason, there currently exists a distinctive lack musculoskeletal training applications which have been successfully derived from the cross-sectional datasets described (Kang et al., 2000). Segmentation of the vascular system from the VHD has also suffered as a result of cadaveric freezing, after which many small blood vessels were caused to collapse (Imelińska & Molholt, 2005; Park et al. 2006; Zhang et al., 2003). Deep fascia is another clinically important tissue that, whilst easily displayed by gross dissection, has proved almost impossible to segment from cross-sectional datasets due to its relative thickness. Previous attempts to reconstruct this anatomical layer from the VHD have depended on successful delineation of the underlying musculature (Beylot et al., 1996). Other important anatomical features which can be demonstrated clearly in the dissection room, but not so by cross-sectional photographs, are those which distinguish intramuscular septa from conspicuous connecting membranes within a volume of muscle tissue, posing yet another problem in the reconstruction of musculoskeletal elements from two-dimensional datasets (Beylot et al., 1996).

Given the inevitable complexity of anatomical cross-sections, combined with the problems discussed above, comprehensive segmentation of the data collected by the previous visible human projects cannot be accurately performed using fully automated algorithms. Image segmentation in these cases must therefore be performed, largely by way of manual delineation techniques. Considering then, that image segmentation is often dealt with at the level of digital image pixels, manual techniques can be extremely time-consuming, and in

case of lower resolution datasets, such as the VHD, are not always successful in achieving the high levels of precision required for educational reconstructions (Imelińska & Molholt, 2005; Pham et al., 2000; Sakellariou et al., 2009). Manual segmentation is also subject to human error, and discrepancies at this stage can lead to inaccuracies in the three-dimensional surface contours after the segmented data has been aligned. In the case of the VHD, there are in fact alignment discrepancies within the raw data itself, with there reportedly being six separate shifts in the image sequence. When using data VHD from the any of the affected anatomical regions, misalignment of the cross-sections must be corrected prior to segmentation using the fiducial rod markers present in the raw images, or through surface contour correction after three-dimensional reconstruction is complete (Beylot et al., 1996; Imelińska et al., 2000).

Many researchers have attempted to hasten the process of segmenting these datasets by employing customised semi-automated algorithms. Researchers at the University of Columbia for example, successfully designed a semi-automated colour segmentation algorithm to extract soft tissue structures from the VHD, however the authors reiterate the unlikelihood that fully automated segmentation will ever be able to achieve the level of precision required for the development of high standard anatomical teaching applications. In fact, they state that:

*“until technical challenges related to image processing, visualisation, representation, storage and manipulation of complex colour datasets like the Virtual Human data are resolved, systematic building of anatomy curriculum will never evolve beyond a boutique operation.”*  
(Imelińska et al., 2000).

## **4.4: Advantages of Present Study**

Whilst the visible human datasets described have indeed been heavily scrutinised as a means of gross anatomical teaching, it should not go without mentioning that they have proved invaluable in many other fields of research, including the development of modern radiological imaging techniques, virtual endoscopy and computer assisted surgery (Biasutto et al., 2006; Gorman et al., 1999; Satava, 1996). Also, it should be stipulated that the value of cross-sectional cadaveric datasets as an educational tool for radiological training remains undisputed in this report. The comparison being made in this discussion therefore, is that between the usability of conventional cross-sectional cadaveric data, and the three-dimensional data obtained by laser scanning in this study, for the sole purpose of creating a virtual specimen for anatomical training. In light of this, it can be argued that the three-dimensional dataset acquired by way of cadaveric laser scanning in this study offers four main advantages:-

### **(1) High resolution and accuracy**

By using the Perceptron ScanWorks<sup>®</sup> V5 scanner in conjunction with a carefully planned and high precision cadaveric dissection like the one documented in this study, topographical surface data can be acquired from the finest of gross anatomical structures such as delicate neurovasculature and small lymph nodes, at a point-to-point resolution of up to 12 $\mu$ m (see Appendix I). Additionally, Perceptron guarantee rigorous factory rectification and testing of equipment, ensuring that the scanner can perform high-resolution data acquisition from each anatomical structure, with a measurement accuracy of 24 $\mu$ m  $2\sigma$  (see Appendix II).

## (2) Requirement for complex image segmentation is eliminated

Notably one of the main advantages to the method of cadaveric data acquisition used in this study is that it is able to facilitate the collection of three-dimensional digital data, directly from the cadaveric source. In comparison to cross-sectional methods, laser-facilitated data collection eliminates the requirement for technically challenging data segmentation to be performed on the data prior to three-dimensional reconstruction. This means that any anatomical structure which is successfully imaged in 3D by way of scanning, however fine or conspicuous, is not then lost at a later stage in post-processing i.e. during cross sectional image segmentation.

## (3) Potential for improved realism of end product

By obtaining three-dimensional data directly from the surface of the cadaveric tissues, there is great potential for the finished digital specimen to be a significantly more visually representative of that which would be found in the traditional dissection room compared to that created from cross-sectional data. As previously discussed, certain clinically important anatomical structures, such as thin fascial layers and connective membranes, can be demonstrated extremely well by gross dissection, yet are sometimes barely visible on a cross-sectional slide. By using the method of data acquisition documented in this study, high-resolution topographical and texture information can be obtained directly from the anatomical surfaces, and this will inevitably aid in the production of a realistic end product for anatomical training. An excellent example of this is demonstrated in Fig.11, where it can be seen that surface data was successfully acquired from the deep fascia of the thigh and the investing layers of the inguinal canal. By comparison, Lopez-Cano et al. (2007), attempted to create a real-time reconstruction of the inguinal canal for surgical education using VHD,

however encountered great difficulties in acquiring accurate data for the insertion points of the aponeurotic layers due to the insufficient resolution of the cross-sectional data. As a result they had to incorporate data from other sources to complete their digital reconstruction of the inguinal canal. The three-dimensional surface data acquired from each carefully dissected aponeurotic layer in this study, combined with corresponding digital photography, will provide a useful dataset from which an anatomically accurate reconstruction of the spatially complex inguinal canal can be developed. If successful, this digital specimen can then be utilised to create an interactive training tool for surgical rehearsal in the future. Another potential advantage to the unique methodology used in this study, if indeed it is successful in improving the realistic qualities of digital cadavers in the future, is that the discrepancies which currently exist between the views of traditional and modern educators regarding virtual training devices in medical education, could perhaps one day be resolved.

#### (4) No uncontrolled loss, or deformation of cadaveric data

The only physical contact that was had with the cadaver throughout the duration of this study was that between the specimen and the author. The dissection component of this project underwent rigorous planning in the weeks prior to the beginning of the process, and all of the initial dissection criteria were achieved as a result. Unlike previous studies, where important anatomical data has been lost during the harsh milling process, or where tissues have streaked across the photographed slices, the non-contact nature of laser-facilitated data acquisition resulted in no uncontrolled or unexpected loss of cadaveric data. Also, by not approaching data acquisition via conventional sectioning methods, the problem of slice misalignment, encountered in previous projects, was not a risk factor in this study. Instead, registration or alignment of point cloud data was performed by the Cimcore Infinite 2.0 (Seven axis) PCMM

Arm, which too is issued with assured factory rectification and guaranteed performance accuracy (see Appendices III and IV for Cimcore accuracy details).

As a result of the unique methodology used in this study, accurate high-resolution three-dimensional surface data was successfully obtained from all clinically relevant anatomy of the male lower limb. Combining this data with both high-resolution colour digital photography, and continued expert input, a comprehensive reconstruction of the lower limb can now be developed for the purpose of gross anatomical training and surgical rehearsal, in the absence of many of the limitations associated with the use of cross-sectional data.

## **4.5: Potential for Research Development**

Whilst this study has proved very successful in demonstrating a novel method of cadaveric data acquisition for potential use in three-dimensional gross anatomical training, there are various factors which should be considered for the development of this research in the future.

One of these considerations, though necessary for the preservation of cadaveric tissue and prevention of mould growth over the course of the dissection period, is that the embalming procedure used in this study caused slight alterations to the colour and texture properties of the cadaveric tissues. As discussed, alteration of these tissue properties should be addressed during the post-processing stages of the digital reconstruction under the guidance of qualified experts. Also, the collection and use of additional photographic information from fresh cadaveric, or even living tissues in the future could add greatly to the value of a realistic end product.

Another important consideration when using this data for the purpose of anatomical training is that the specimen used, presented a small amount of arthritic change on the articulating surfaces of the patella, proximal tibia and distal femur. This data can be rectified during post-processing, where the texture of healthy cartilage can be mapped onto the affected areas of the scan data. Whilst imaging of pathological anatomy was outwith the remit of this particular study, this feature indicates another potential use for laser scanning in the development of educational reconstructions, i.e. those for teaching pathological anatomy.

There are also a number of important considerations which should be made when comparing the methodology used in this study to that used in cross-sectional data acquisition projects. An important consideration for example, is the end-use of the data. The hypothesis made in this report is that three-dimensional data acquisition using the Perceptron ScanWorks<sup>®</sup> V5

scanner is a useful alternative methodology for the collection of data which can be used in the production of more realistic and accurate digital cadavers for gross anatomical training in the future. This hypothesis is made largely on the basis that it bypasses the difficult task of image segmentation, and is capable of extracting data from the fine anatomical structures at extremely high resolutions. It is however noteworthy that for radiological training, cross-sectional datasets and radiological images of living anatomy are unrivalled by this study alone. This therefore indicates another potential line of development for this research, in that coupling this technology with corresponding CT and MRI scanning of the specimen prior to dissection could add exceptional value to datasets obtained by this method in the future. It is also important to recognise that the methodology used to acquire cadaveric data in the previous studies was designed to obtain full human datasets for both male and female anatomy in a relatively short space of time for use in various disciplines, including those outwith the field of 'digital cadavers'. This study focused on a single anatomical region, with the view of demonstrating a potential new method of cadaveric data acquisition for subsequent three-dimensional modelling, only. A summary of the main differences between the two methods of cadaveric data acquisition discussed in this report is given in Table. 1, on page 109.

The next obvious step for this project therefore, is to acquire cadaveric data, using this unique methodology, from other anatomical regions of the body. In conjunction with this project, a similar head and neck study, involving collaboration between the Digital design Studio, Glasgow School of Art, the Laboratory of Human Anatomy, University of Glasgow and the University of Glasgow's Dental School, is currently underway. This project is utilising the same method of data acquisition to obtain cadaveric data from all clinically relevant anatomical structures of a carefully selected head and neck specimen. The three-dimensional dataset obtained in this case will be used to produce a sophisticated digital reconstruction of

the head and neck, which can then be used in medical, dental and craniofacial surgical training.

## A Comparison of Methods in Cadaveric Data Acquisition

	<b>Previous Cross-Sectional Cadaveric Data Acquisition Projects (VHP, CVH and KVH)</b>	<b>Laser facilitated Cadaveric Data Acquisition Method Used in This Study</b>
<b>Method of data acquisition:</b>	Freezing and sectioning of cadaveric specimen, followed by photography of anatomical slices (Accompanied with CT and MRI scanning)	Embalming and dissection of cadaveric specimen followed by laser-scanning of dissected tissues  (Accompanied with digital photography)
<b>Main equipment used for data acquisition</b>	Digital camera	Perceptron ScanWorks <sup>®</sup> V5 scanner
<b>Main type of data collected:</b>	Two-dimensional anatomical cross-sections	Three-dimensional point clouds
<b>Data resolution measured in:</b>	Pixels	Distance between laser points
<b>Maximum resolution obtainable:</b>	VHP: 2490368 pixels/slice KVH:61043290 pixels/slice CVH: 6291456 pixels/slice	Point-point-resolution up to 12 $\mu$ m/scan
<b>Requirement for image segmentation prior to reconstruction:</b>	YES	NO
<b>Data alignment:</b>	Alignment of anatomical sections in sequence. Done using fiducial rods in raw data or surface contours of post-segmented data	Translation of point cloud profiles from different scans into common coordinate frame. Done during data acquisition process using CMM arm
<b>Main advantage in medical education:</b>	Useful for teaching of cross-sectional anatomy for radiology training	Useful in creation of realistic digital specimens for three-dimensional anatomical training and surgical rehearsal

**Table 1.** A summary of the main differences between previous cross-sectional cadaveric data acquisition projects and the laser-facilitated approach documented in this study.

## **4.6: Summary and Conclusion**

Under the pressures of a growing medical curriculum, and a reduction in the time available for cadaveric dissection in both undergraduate and post graduate curriculums, anatomical teaching is becoming increasingly dependant on supplementation from virtual anatomical training aids. In light of these pressures, a great deal of research has been invested in the acquisition of cadaveric data to create realistic virtual specimens for this purpose. Until now however, the educational value of these training methods have been questioned due to their poor detail and lack of realistic qualities. The problems associated with the usability of previous cadaveric datasets for the development of adequate three-dimensional reconstructions, stem from the methodology used to acquire the cadaveric data. In each case, this is done by serially sectioning cadaveric specimens, and photographing the individual slices. To create volumetric structures from this data, these slices must undergo a laborious segmentation process, which is extremely complex and not always successful in adequately reconstructing finer anatomical structures which are none the less important in anatomical teaching.

The aim of this study therefore was to approach cadaveric data acquisition, for the purpose of creating a three-dimensional cadaveric specimen, by obtaining three-dimensional data directly from cadaveric tissues with a Perceptron ScanWorks<sup>®</sup> V5 laser scanner.

In order to do this, a carefully planned dissection of the lower limb was performed, and laser scanning of all clinically relevant structures was undertaken at each stage. In addition to the three-dimensional data acquired by laser scanning, colour and texture information was also collected from the cadaveric tissues by way of high-resolution digital photography.

As a result, a comprehensive three-dimensional dataset was acquired from all clinically relevant anatomy of the lower limb. Data was obtained at extremely high point to point resolutions, and with a measurement accuracy of  $24\mu\text{m}$ ,  $2\sigma$ .

By obtaining three-dimensional cadaveric data in this way, conventional image segmentation for the production of a digital specimen will not be necessary, and finely dissected gross anatomical structures can be documented with high precision. Using the corresponding photographic data, combined with continued expert input, the topographical data obtained from this study can be processed further to create an accurate and realistic virtual reconstruction of the lower limb for the purpose of three-dimensional anatomical training and surgical rehearsal. Whilst the results of this study create a promising prospects for the future development of virtual cadavers, the value of cross sectional datasets is not challenged as the best means of radiological training in this report.

Regardless of the means used to digitise cadaveric data for anatomical training, whether it is by photographing cross-sections or laser-facilitated three-dimensional scanning, the need to rectify the deficits in anatomical teaching in medical education is pressing. Further processing and thorough evaluation of virtual anatomy as an effective means of learning will be an important challenge for digital designers and medical educationalists of the future.

# References

- Beylot, P., Gingins, P., Kalra, P., Thalmann, N.M., Maurel, W., Thalmann, D., Fasel, J. (1996) 3D Interactive Topographical Modeling using Visible Human Dataset. *Eurographics*. 15(3): 33-44
- Biasutto, S.N., Causa, L.I., Criado del Río, L.E. (2006) Teaching anatomy: Cadavers vs. computers? *Ann Anat*. 188:187-190
- Boscolo, R., Brown, M.S., McNitt-Grey, M.F., (2002) Medical Image Segmentation with Knowledge-guided Robust Active Contours. *RadioGraphics*. 22:437-448
- Brenton, H., Hernandez, J., Bello, F., Strutton, P., Purkayastha, S., Firth, T., Darzi, A. (2007) Using multimedia and Web3D to enhance anatomy teaching. *Computers and Education*. 49:32-53
- Cahill, D.R., Leonard, R.J., Marks, S.C Jr. (2000) A comment on recent teaching of human anatomy in the United States. *Surg Radiol Anat*. 22:69-71
- Cheng, G., Li, X.C., Wu, G.Q., Zhang, S.X., Xiong, X.F., Tan, L.W., Yang, R.G., Li, K., Yang, S.Z., Dong, J.H. (2010) Three-Dimensional reconstruction of the Digitized Human Liver: used on Chinese Visible Human. *Chinese Medical Journal*. 23(2): 146-150
- Cottam, W.W. (1999) Adequacy of Medical School Gross Anatomy Education as Perceived by Certain Postgraduate Residency Programs and Anatomy Course Directors. *Clinical Anatomy*. 12:55-65
- Digital Design Studio, 2007. Medical Visualisation Network [online] Available at: <<http://www.medicalvisualisation.co.uk/>> [Accessed 15<sup>th</sup> July 2010]
- Europac3Dimensional, 2011. Case Studies [online] Available at: <<http://www.europac3d.com/casestudies.html>> [Accessed 5th June 2011]
- Evans, D.J.R., Watt, D.J. (2005) Provision of Anatomical Teaching in a New British Medical School: Getting the Right Mix. *The Anatomical Record (Part B:New Anat.)*. 284B:22-27
- Fagan, S.P., Awad, S.S. (2004) Abdominal wall anatomy: the key to a successful inguinal hernia repair. *The American Journal of Surgery*. 188: 3S-8S
- Fasel, J.H.D. (1993) Elementary anatomy for the future general practitioner: the arteries. *Medical Teacher*. 15(4):341-349
- Finkelstein, P., Mathers, L. (1990) Post-Traumatic Stress Among Medical Students in the Anatomy Dissection Laboratory. *Clinical Anatomy*. 3:219-226
- Garg, A., Norman, G., Spero, L., Taylor, I. (1999) Learning anatomy: do new computer models improve spatial understanding? *Medical Teacher*. 21(5): 519-522
- Gerth, R.J., Brueckner, S. A. (2005) The Digital Body Development System. International Automotive Body Congress, Sept. 21-23, Ann Arbor, Michigan

- Gerth, R.J. (2005) Virtual functional Build For Body Assembly. ASME 2005 Mechanical Engineering Congress and Exposition. Nov 5-11, Orlando, Florida
- Gorman, P.J., Meier, A.H., Krummel, T.M. (1999) Simulation and Virtual Reality in Surgical Education Real or Unreal? *Arch Surg.* 134:1203-1208
- Gosling, J. A. et al. (2008) *Human Anatomy, Color Atlas and Textbook.* 5th Ed. Mosby
- Hamarneh, G., Yang, J., McIntosh, C., Langille, M. (2005) 3D Live-Wire-Based Semi-Automatic Segmentation of Medical Images. *Proceedings of 2005 SPIE Medical Imaging Conference: Image Processing (Vol 5747):* pp. 1597-1603
- Heng, P.A. (2007) Advances in Visible Human Based Virtual Medicine. *Digital Human Modeling.* 4561: 623-632
- Hieu, L.C., Sloten, J.V., Hung, L.T., Knanh, L., Soe, S., Zlatov, N., Phuoc, L.T., Trung, P.D. (2010) Medical Reverse Engineering Applications and Methods. 2nd International Conference on Innovations, recent Trends and Challenges in Mechatronics, Mechanical Engineering and New High-Tech Products Developments. Sep 23-24, Bucharest, Romania
- Imelińska, C., Downes, M.S., Yuan, W. (2000) Semi-automated color segmentation of anatomical tissue. *Computerized Medical Imaging and Graphics.* 24:173-180
- Imelińska, C., Molholt, P. (2005) Incorporating 3D Virtual Anatomy Into the Medical Curriculum. *Communications of the ACM.* 48(2):50-54
- Jastrow, H., Vollrath, L. (2003) Teaching and Learning Gross Anatomy Using Modern Electronic Media Based on the Visible Human Project
- Kang, H. S., Kim, B. H., Ryu, F.W., Hong, S.H., Chung, H. W., Cho, S.Y., Kim, Y.H., Hwang, S.I., Feong, D.K., Shin, Y. G. (2000) The Visible Man: Three- Dimensional Interactive Musculo-skeletal Anatomical Atlas of The Lower Extremity. *RadioGraphics.* 20: 279-286
- Kilroy, D., Driscoll, P. (2006) Determination of required anatomical knowledge for clinical practice in emergency medicine: national curriculum planning using a modified Delphi technique. *Emerg. Med. J.* 23:693-696
- Kluchova, D., Bridger, J., Parkin, I.G. (2000) Anatomy into the future. *Bratisl Lek Listy.* 101(11):626-629
- López-Cano, M., Rodríguez-Navarro, J., Rodríguez-Baeza, A., Armengol-Carrasco, M., Susín, A. (2007) A real-time dynamic 3D model of the human inguinal region for surgical education. *Computers in Biology and Medicine.* 37:1321-1326
- Ma, Z., Tavares, J.M.R.S., Jorge, R.N. (2008) Segmentation of Structures in 2D Medical Images. 5th European Congress on Computational Methods in Applied Sciences and Engineering. June 30- July 5, Venice, Italy
- Malamed, S., Seiden, D. (1995) The Future of Gross Anatomy Teaching. *Clinical Anatomy.* 8:294-296

- Malomo, A.O., Idowu, O.E., Osuagwu, F.C. (2006) Lessons from History: Human Anatomy, from the Origin to the Renaissance. *Int. J. Morphol.* 24(1):99- 104
- McLachlan, J.C., Bligh, J., Bradley, P., Searle, J. (2004) Teaching anatomy without cadavers. *Medical Education.* 38:418-424
- Mitchell, R., Batty, L. (2009) Undergraduate perspectives on the teaching and learning of anatomy. *ANZ J Surg.* 79:118-121
- Moosman, D.A., Arbor, A. (1980) A Surgeon's View: The Decline and Perhaps the Fall of Gross Anatomy Instruction. *The American Journal Of Surgery.* 140:266-269
- Moxham, B.J., Plaisant, O. (2007). Perception of Medical Students Towards the Clinical Relevance of Anatomy. *Clinical Anatomy.* 20:560-564
- Newell, R.L.M.(1995) Follow The Royal Road. *Clinical Anatomy.*8:124-127
- Nicholson, D. T., Chalk, C., Funnel, W.R.J., Danial, S.J. (2006) Can Virtual Reality Improve Anatomy education? A randomized controlled study of a computer-generated three-dimensional anatomical ear model. *Medical Education.*40(11): 1081-1087
- Older, J.(2004) Anatomy: A Must For Teaching the Next Generation. *Surg J R Coll Surg Edinb Irel.*2:79-90
- Park, J. S., Chung, M. S., Hwang, S.B., Shin, B.S. (2006) The Visible Korean Human: Its Techniques and Applications. *Clinical Anatomy.* 19(3):216-224
- Patel, K.M., Moxham, B.J. (2006) Attitudes of Professional Anatomists to Curricular Change. *Clinical Anatomy.* 19:132-141
- Perceptron, 2011. Scanworks [online] Available at: <http://www.perceptron.com/index.php/en/-industrial/3d-scanning-solutions-g/manual-3d-scanning.html> [Accessed 5th June 2011]
- Pfeifer, N., Briese, Ch. (2007) Laser Scanning – principles and Applications. *Geo-Siberia, 3rd International Exhibition & Scientific Congress on Geodesy, Mapping, Geology, Geophysics, Cadaster.* April '07, Novosibirsk, Russia
- Pham, D.L., Xu, C., Prince, J.L. (2000) Current Methods in Medical Image Segmentation. *Annual Review of Biomedical Engineering.* 02: 315-337
- Prince, K.J.A.H., van Mameren, H., Hylkema, N., Drukker, J., Scherpbier, A.J.J.A., van der Vleuten, C.P.M. (2003) Does problem-based learning lead to deficiencies in basic science knowledge? An empirical case on anatomy. *Medical Education.* 37:15-21
- Pryde, F.R., Black, S.M. (2005) Anatomy In Scotland: 20 Years Of Change. *SMJ.* 50(3):96-98
- Qian, L., Hui, G., Qingming, L. (2005) Parallel Visualization of Visible Chinese Human with Extremely Large Datasets. *27th Annual International Conference of the IEEE- EMBS Engineering in Medicine and Biology Society,* Sep 1-4, Shanghai, China
- Rizzolo, L.J. (2002) Human Dissection: An Approach to Interweaving the Traditional and Humanistic Goals of Medical Education. *The Anatomical Record (New Anat.).* 269:242-248

Rizollo, L.J., Stewart, W.B. (2006) Should We Continue Teaching Anatomy by Dissection When...?. *Anat Rec (Part B: New Anat)*. 289B:215-218

Royal College of Physicians Surgeons Glasgow (RCPSG). 'About Us', [online] Available at: <[://www.rcpsg.ac.uk/About\\_Us/Pages/default.aspx](http://www.rcpsg.ac.uk/About_Us/Pages/default.aspx)> [Accessed: 8<sup>th</sup> June 2011]

Sakellariou, S., Ward, B.M., Charissis, V., Chanock, D., Anderson, P (2009) Design and Implementation of Augmented Reality Environment for Complex Anatomy Training: Inguinal Canal Case Study. *Virtual and Mixed Reality*: 605-614.

Satava, R.M. (1996) Virtual Endoscopy Diagnosis using 3-D visualization and virtual representation. *Surg Endosc*. 10:173-174

Shaw-Dunn, J. (1995) Follow the Radical Road: Comment on R.L.M Newell's Paper. *Clinical Anatomy*. 8:131-133

Spitzer V.M., Whitlock D.G. (1998) *Atlas of the Visible Human Male: Reverse Engineering of the Human Body*. Sadbury, Jones & Barlett

Standing, S.(2009) New Focus on Anatomy for Surgical Trainees. *ANZ Journal of Surgery*.79(3):114-117

Temkin, B., Acosta, E., Malvankar, A., Vaidyanath, S. (2006) An Interactive Three-Dimensional Virtual Body Structures System for Anatomical Training Over the Internet. *Clinical Anatomy*. 19: 267-274

Trelease, R. (1998) The Virtual Anatomy Practical: A Stereoscopic 3D Interactive Multimedia Computer Examination Program. *Clinical Anatomy*. 11:89-94

Turney, B.W. (2007) Anatomy in a modern medical curriculum. *Ann R Coll Surg Engl*. 89:104-107

University of Stanford, 1974. Stanford Visible Female, [online] Available at: <<http://lucy.stanford.edu/backgr.html>> [Accessed 3rd June 2011]

Venuti, J., Imelińska, C., Molholt, P. (2004) New Views of Male Pelvic Anatomy: Role of Computer generated 3D Images. *Clinical Anatomy*. 17:261-271

Ward, B.M., Charissis, V., Rowley, D., Anderson, P., Brady. (2009) An Evaluation of Prototype VR Medical Training Environment: Applied Surgical Anatomy Training Environment for Malignant Breast Disease. *Studies in Health Technology and Informatics*. 132: 550-555

Yushkevich, P. A., Piven, J., Hazlett, H.C., Smith, R.G., Ho, S., Gee, J.C., Gerig, G. (2006) User-Guided 3D Active Contour Segmentation of Anatomical Structures: Significantly Improved Efficacy and Reliability. *Journal of Neuroimaging*. 31:1116-1128

Zhang, S.X., Heng, P.A., Liu, Z.J., Tan, L.W., Qiu, M.G., Li, Q.Y., Liao, R.X., Li, K., Cui, G.Y., Guo, Y.L., Yang, X.P., Liu, G.J., Shan, J.L., Liu, J.J., Zhang, W.G., Chen, X.H., Chen, J.H., Wang, J., Chen, W., Lu, M., You, J., Pang, X.L., Xiao, H., Xie, Y.M. (2003) Creation of the Chinese Visible Human Data Set. *The Anatomical Record (Part B: New Anat.)* 275B:190-195

Zhang, S.X., Heng, P.A., Liu, Z.J., Tan, L.W., Qui, M.G., Li, Q.Y., Liao, R.X., Li, K., Cui, G.Y., Guo, Y.L., Yang, X.P., Liu, G.J., Shan, J.L., Liu, J.J., Zhang, W.G., Chen, X.H., Chen, J.H., Wang, J., Chen, W., Lu, M., You, J., Pang, X.L., Xiao, H., Xie, Y.M., Cheng, J.C.Y. (2004) The Chinese Visible Human (CVH) datasets Incorporate Technical and Imaging Advances on Earlier Digital Humans. *Journal of Anatomy*. 204(3): 165-173

Zuckerman, S. Z. (1981) *A New System of Anatomy: A Dissection Guide and Atlas*. 2nd Ed. USA. Oxford University Press

# Appendices

# Appendix I: ScanWorks V5 Data Sheet



## SENSOR SPECIFICATIONS

Dimensions	115 mm x 100 mm x 80 mm
Mass	438 g
Profile density	7640 points/line
Update frequency	60 Hz
Scan rate	458400 points/second
Mean point to point resolution	0.0137 mm
Stand-off	100 mm
Depth of field	110 mm
Near field width	93 mm
Mid field width	105 mm
Far field width	140 mm
Measurement accuracy <sup>1</sup>	0.0240 mm 2 $\sigma$ corner test
Feature resolution <sup>2</sup>	0.0045 mm 2 $\sigma$ sphere test
Sensor feature repeatability <sup>2</sup>	0.0050 mm 2 $\sigma$ sphere test
Safety	Class 2M, 660 nm laser
Certifications	UL, CSA, CE
Environmental Protection	10°C to 40°C Sensor IP64 / Enclosure IP31

<sup>1</sup> NIST standard  
<sup>2</sup> OSIS standard  
 Perceptron is registered to ISO9001:2000 standards  
 Specifics are subject to change without notice.



## SCANWORKS® ADVANTAGES

**PRINCIPLE**  
 The ScanWorks® portable scanning system combines the ease-of-use of portable CMM arms with the sophistication of Perceptron's scanning technology. The ScanWorks® V5 sensor uses solid state, non-contact, laser-based technology. Using triangulation, the scanner captures profiles generated by the intersection of a projected laser plane and the target topography. Users can easily control data collection through buttons on the portable CMM. For each profile, the arm position is used to translate the profile data into a common coordinate frame. Once translated, the profile is married with the other profiles to produce digital 3D part topography.

**SPEED**  
 A maximum of 7640 points along the laser line at a rate of 60Hz provides the user with unparalleled scan data density. This incredible rate of up to 458400 points per second gives a minimum point to point resolution of 12µm.

**LARGE FIELD OF VIEW**  
 Having a maximum width and depth of field of 140mm and 110mm, respectively, enables users of the ScanWorks® V5 sensor to rapidly capture large, geometrically complex, areas.

**PROJECTED RANGEFINDER**  
 Several features are available to guide the user when scanning. Most notable is the ScanWorks® V5 proprietary field of view projection. The sensor projects an accurate trapezoidal representation of the field of view showing the extents as well as optimal scanning offset distance. This enables the user to quickly become familiar with good scanning practices and minimize redundant overlapping data. This system is backed up by an audible tone which changes frequency depending on depth of field and a graphical output.

**DYNAMIC RANGE**  
 The ScanWorks® V5 sensor has just the same ability to capture accurate data on dark and reflective surfaces as the proven ScanWorks® V4i sensor. Its class-leading dynamic range negates the need for harmful white powder sprays and paints. The addition of advanced software filters enables dynamic reflection removal and hardware filters make the sensor impervious to ambient light.

**ACCURACY**  
 Field calibration of the sensor is entirely independent of the hard probe. Within a few minutes, the user can precisely align the sensor to the PCMM co-ordinate frame without having to calibrate the hard probe first. Factory rectification of the V5 sensor ensures measurement accuracy of 24µm 2 $\sigma$  throughout the entire field of view.

**REAL-TIME INTEGRATIONS**  
 Direct integrations with InnovMetric™ PolyWorks®, Geomagic®, Rapidform XO™ and Delcam PowerINSPECT allow the user to scan within a familiar interface. Time consuming file management becomes a thing of the past because the data is captured real-time within your preferred reverse engineering or inspection suite.

**USABILITY**  
 The lightweight ergonomic design of the ScanWorks® V5 scanning solution makes easy work of even the most arduous measurement tasks. With the PCMM's hard probe exposed at all times, at the flick of a switch, the user can alternate between non-contact and contact measurement. This feature can be extremely useful when setting up alignments or datum features.

**PORTABILITY**  
 The ScanWorks® V5 sensor is transported in a wheeled flight case similar in size to a small suitcase. Along with the PCMM and laptop computer, the entire scanning solution easily fits into a family car. Magnetic mounts on the PCMM base ensure a robust setup in a manufacturing environment. When a magnetic surface is not on hand, a range of tripods is available at extra cost.

**VERSATILITY**  
 ScanWorks® V5 is suitable for numerous industries and applications, from the factory floor to inspection rooms and laboratories. Industries where ScanWorks® is delivering value and cost savings include:  
 Aerospace, animation, automotive, consumer products, cultural heritage, forging, investment casting, mould & die, plastics, prototyping and stamping.

**SUPPORT**  
 Perceptron provides unparalleled service and support to our scanning solution users. With both ISO9001 and QS9000TE certifications and through a network of qualified Value Added Resellers, Perceptron provides a combination of excellent large, medium and small enterprise support on a local level.



Perceptron is a global public company with offices in the Americas, Europe and Asia and over 25 years of experience in 3D non-contact applications. Producing over 5000 sensors each year, Perceptron has a worldwide base of installations in major manufacturing companies. We are committed to consistently exceed customer's expectations by providing continuous improvement in products, processes and services.  
 Formed in 1981 to help the automotive industry monitor and control the dimensional quality of automobile bodies and subassemblies, laser-based monitoring technologies have become the core competency of the company. Both in-line and end-of-line process measurement have grown into a group of flexible systems that provide monitoring and quality assurance throughout the entire manufacturing process. Perceptron's products are proven and reliable for improving productivity and quality, and reducing scrap, rework, and costs.  
 Today's computer power and innovation by software partners in CAD/CAM, inspection, solid modelling, rapid prototyping, reverse engineering and more are taking us to new and exciting places. We are involved with government-sponsored programs, such as NIST, for advanced product and process development. We are an active member of the OSIS group working to create industrial standards for scanning systems. We continue to look for better ways to design, produce, and deliver superior products that help our customers be more competitive in an increasingly global competitive environment.

<b>Global Headquarters</b> Perceptron Inc. 47827 Halyard Drive Plymouth, MI 48170 USA Tel: +1 734 414 6100 Fax: +1 734 414 4700 www.perceptron.com Copyright 2010	<b>European Headquarters</b> Perceptron GmbH Stahlgruberring 7 81829 Munich Germany Tel: +49 89 960 980 Fax: +49 89 960 98101 International Inquiries: European Inquiries:	<b>Asian Headquarters</b> Perceptron Asia Pte. Ltd. 18 Boon Lay Way #10-143 TradeHub 21 Singapore 609966 Tel: +65-6795 5280 Fax: +65-6795 1937 3dscanning@perceptron.com inquiry@perceptron.de
---	--	--

# Appendix II: Perceptron Accuracy Statement



## Knowledge Base Document

KBD0012

### V-Series Accuracy, Standards and Traceability

#### Description

The purpose of the document is to explain the methodology and standards used in the V-Series Sensor accuracy statement.

Measurement accuracy <sup>1</sup>	0.0240 mm 2 $\sigma$ corner test
Feature resolution <sup>2</sup>	0.0045 mm 2 $\sigma$ sphere test
Sensor feature repeatability <sup>2</sup>	0.0050 mm 2 $\sigma$ sphere test

<sup>1</sup> NIST standard  
<sup>2</sup> OSIS standard

#### Background

Due to a lack of standardization in the non-contact measurement field, manufacturers of said optical scanning equipment have used different methods to measure the accuracy of the systems they produce. Comparing sensors by their accuracy statements can be both confusing and difficult as different methods and statistical values are being used across the industry. This document will try to explain the methods used by Perceptron, but the best test of scanning equipment is the benchmark. By comparing the different equipment in real part measurement situations you can gauge for yourself what the devices can and cannot do.

Perceptron is an ISO 9000 Certified company that has been in the dimensional measurement field in the automotive manufacturing sector since its inception in 1981 and has complied with the standards as set forth by the **National Institute of Standards and Technology (NIST)** for that industry. Because of this background Perceptron has vast experience in the necessity and implementation of traceability and standards in measurement. When Perceptron entered into the CMM/PCMM scanning sensor business in the 1990s there were no such standards for the optical measurement industry to gauge sensor performance against. Perceptron has made the effort to be compliant with existing standards that are applicable to scanning and has joined organizations such as the committee for **Optical Sensor Interface Standards (OSIS)** that have been formed in an attempt to create more uniform standards.

#### Organizations

Several organizations involved in the standards community are mentioned in the Accuracy Statement and this document. Below is a list of the organizations and who they are.

##### International Organization for Standardization (ISO)

The ISO is a non-governmental organization made up of a network of the national standards institutes of 158 countries, one member per country, with a Central Secretariat in Geneva, Switzerland, that coordinates the system. It is also the world's largest developer and publisher of International Standards in an attempt to standardize manufacturing and measurement on a worldwide basis.

##### National Institute of Standards and Technology (NIST)

NIST is a non-regulatory federal agency within the U.S. Department of Commerce which was founded at the beginning of the 20<sup>th</sup> century to promote U.S. innovation and industrial competitiveness by advancing measurement science, standards, and technology. NIST has a long history as the United States standards keeper for measurements of mass, force, vibration, and other quantities. NIST is also the United States representative to ISO.

## International Association of Coordinate Measuring Machine Manufacturers (IACMM)

The IACMM was founded as an international non-profit group to promote standardization in manufacturing and training in CMM technology and use. This association was made up by a consortium of most of the major CMM manufacturers including Zeiss, Hexagon, LK, Wenzel and Mitutoyo.

## Optical Sensor Interface Standard (OSIS)

One of the first programs that grew out of the IACMM was a committee made up by IACMM members and representatives from different optical sensor manufacturers including Perceptron to standardize the optical probe solutions used on Coordinate Measuring Machines. The committee and the Standard came to be known by the acronym OSIS. The OSIS committee broke the project into 3 work groups:

- Workgroup 1: Mechanical and electrical interface
- Workgroup 2: Data interface (software integration)
- Workgroup 3: Specifications, classifications and performance verifications

## Accuracy, Sigma and Statistics

The biggest problem in comparing accuracy between manufacturers is “What artifact was measured” and “How was it being measured”? Most manufacturers will not go into detail on how they have derived their accuracy and repeatability, this makes accuracy comparison even more difficult.

As seen in the statement above all results are shown in a sigma value as represented by the  $\sigma$  symbol. This value is referencing the distribution of the results in deviation to a mean. The higher the sigma value (see chart to right) the greater the percentage of the population is being represented. So as an example the Perceptron feature resolution states that the over 95% of the results for that test were within +/- 4.5 microns (.000177 inch).

### Percentages

1 $\sigma$	68.26894921371%
2 $\sigma$	95.44997361036%
3 $\sigma$	99.73002039367%
4 $\sigma$	99.99366575163%
5 $\sigma$	99.99994266969%
6 $\sigma$	99.99999980268%

Considerations other than the population size used and what is being measured that should be taken into account when comparing accuracy statements is the size of the Field of View (FOV). To create more accurate systems some manufacturers’ severely reduce or clip the size of the FOV in order to get higher resolution making the sensor harder to use and requiring more time to gather the points.

## The OSIS Shell

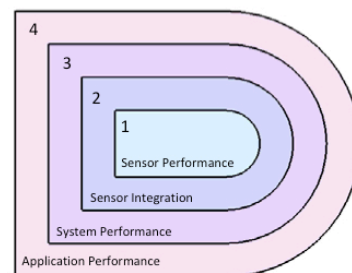
As mentioned, Workgroup 3 of the OSIS committee was organized to create standards for specifications, classifications and performance verifications. Out of this group came the 4 shell approach for performance verification.

**Shell 1:** Sensor Performance – Testing done by isolating the sensor from the rest of the integrated system. All testing is done in the sensor FOV using a traceable artifact.

**Shell 2:** Sensor Integration - The sensor is tested on mover using all components such as cables and software but using a traceable artifact under laboratory conditions.

**Shell 3:** System Performance - Complete system with mover testing done under laboratory conditions on traceable artifact using standards such as ANSI/ASME B89, ISO 10360, VDI 2617 part 6, 6.1 and 6.2

**Shell 4:** Application Performance - Complete system with mover testing done under real world conditions on real world part.

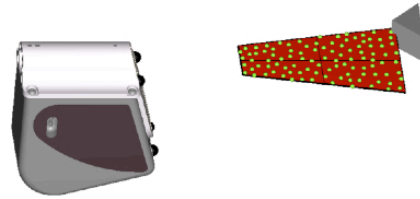


## The Perceptron Accuracy Statement

The Perceptron Accuracy Statement is broken down into 3 parts, Measurement Accuracy, Feature Resolution and Sensor Feature Repeatability. The Accuracy Statement further associates these tests to either NIST or OSIS. This section will describe each test and explain the association.

- **Measurement Accuracy (NIST)**

This test is done by moving the sensor through the FOV resolving a corner point in 96 random locations, (24 positions in 4 quadrants) with each position measured 10 times for repeatability. In this test the sensor is being moved, which means the accuracy of the machine needs to be traceably maintained. This means in order to meet ISO/NIST standards the test stand must be checked twice a year by use of a Laser Interferometer which also has to be calibrated once a year by the OEM.



*Sensor is moved to measure 96 positions*

- **Feature Resolution & Sensor Feature Repeatability (OSIS)**

As mentioned in the OSIS shell paragraph, the 1<sup>st</sup> shell deals specifically with sensor performance by isolating the sensor and measuring a known artifact. Perceptron has made this test even more stringent by including the portion of Shell 3 that requires the testing be done using the applicable portions of the ANSI/ASME B89, ISO 10360, VDI 2617 standards dealing with ball bars and ball plate testing.

**ANSI B89 Excerpts**

Requires multiple static measurements of the position of a fixed ball. The range (largest minus smallest) is the machine's repeatability.

Measurements of a ball bar at multiple positions and orientations in the machine's working volume. This value is the machine's volumetric performance.



*NIST traceable ball plate used for accuracy testing*

## Additional Accuracy Testing

The results used in the accuracy statement are not from the only tests done on the Perceptron sensor, other tests include:

- Flatness on both matte and shiny surfaces
- Gap on both sharp and rounded edges
- Electronic noise
- Laser line quality
- Laser line skew
- Image repeatability

Many of the tests used are based on the OSIS Cube Artifact, designed specifically for checking the quality of non-contact sensors.



*OSIS Cube Artifact*

# Appendix III: Cimcore Infinite 2.0 Arm Data Sheet



EuroPac 3Dimensional  
3 Cranham Court  
Arden Square  
Crewe Business Park  
Crewe Cheshire  
CW1 6HA  
United Kingdom  
[www.europac3d.com](http://www.europac3d.com)

DATA SHEET

Measuring the future in 3D

## INFINITE 2.0 from cimcore



Back view of base

### The NEW INFINITE 2.0

is Cimcore's easiest to use and most accurate articulating arm ever. New handling and performance features – along with patented infinite rotation, quick-change probes, exclusive wireless connectivity and battery power – provide **INFINITE** portability and measuring power. **INFINITE 2.0** plus models, with unsurpassed repeatability and volumetric accuracy, are ideal for the most demanding inspection tasks.

1. Patented **infinite rotation** of principle axes allows inspection in difficult-to-reach areas.
2. With the new Bridge-CMM class TESA kinematic multiwire probe joint, you get unsurpassed measuring performance. **Carbon fibre probes** feature automatic probe recognition.
3. A new smaller, **easy-grip head** features an LED work light and an integrated digital camera which allows the operator to graphically document a setup.
4. **New SpinGrip** infinite-rotating grips at elbow and forearm provide two low friction grip positions for better ergonomics. SpinGrips allow the CMM to 'float' in the operator's hands, maximising accuracy and minimising operator fatigue.
5. **Heidenhain encoders**, manufactured to our specifications, offer 'wide track' bearing support which enhances performance.
6. **Advanced carbon filter** arm tubes are strong, lightweight, thermally stable and feature a lifetime warranty.
7. An improved, **low profile Zero-G counterbalance** reduces operator fatigue and delivers effortless control in all positions, including above and below centre line.
8. An upgraded 802.11g **WIFI connection** – transmitting up to 6 times farther and 50 times faster than Bluetooth – allows the operator to position the computer where it is most convenient.
9. A **Li-Ion battery** allows on site inspection with AC power or cables. A sealed battery cover prevents contamination of the battery compartment or accidental dislodging of the battery.
10. A **quick-clip probe holster** keeps three spare probes and the change key safe and handy.
11. The **universal mounting system** attaches to a variety of bases, and includes a magnetic mount for a smaller footprint and simplified set up.

T: +44 (0)1270 216000 F: +44 (0)1270 216123 E: [sales@europac3d.com](mailto:sales@europac3d.com)



G800208

PORTABLE MEASURING ARMS

[www.europac3d.com](http://www.europac3d.com)

## INFINITE 2.0 SEVEN AXIS CMM WITH PERCEPTON V5 NON-CONTACT LASER SCANNER



The Cimcore Infinite 2.0 measuring arm is also available in seven axis form, allowing for maximum flexibility of movement when used with a scanning head. EuroPac 3D supply Perceptron laser scanners which provide a class leading data collection of 458,000 points per second and point resolution of 4.5 microns. This combination of arm and laser is perfect for Reverse Engineering, Inspection and Digital Modelling.

INFINITE 2.0 (SIX AXIS)						
Measuring Range	1.2m	1.8m	2.4m	2.8m	3.0m	3.6m
Point Repeatability	0.010mm	0.016mm	0.020mm	0.029mm	0.034mm	0.050mm
Volume Length Accuracy	0.016mm	0.023mm	0.029mm	0.041mm	0.050mm	0.068mm
Arm Weight	6.89kg	7.57kg	7.82kg	7.97kg	8.22kg	8.65kg

INFINITE 2.0 (SEVEN AXIS)					
Measuring Range	1.8m	2.4m	2.8m	3.0m	3.6m
Point Repeatability	0.024mm	0.028mm	0.045mm	0.050mm	0.070mm
Volume Length Accuracy	0.035mm	0.040mm	0.064mm	0.071mm	0.100mm
Arm Weight	8.05kg	8.33kg	8.33kg	8.85kg	9.13kg

INFINITE 2.0 PLUS (SIX AXIS)		
Measuring Range	2.4m	3.6m
Point Repeatability	0.017mm	0.043mm
Volume Length Accuracy	0.025mm	0.058mm
Arm Weight	7.82kg	8.65kg

INFINITE 2.0 PLUS (SEVEN AXIS)					
Measuring Range	1.8m	2.4m	2.8m	3.0m	3.6m
Point Repeatability	0.019mm	0.020mm	0.029mm	0.035mm	0.048mm
Volume Length Accuracy	0.025mm	0.026mm	0.045mm	0.050mm	0.068mm
Arm Weight	8.05kg	8.33kg	8.33kg	8.85kg	9.13kg

Humidity: 5% - 95% noncondensing  
 Shock & Impact: 6ms, < 1000 ms/s<sup>2</sup>  
 Certification: CE compliant  
 Vibration: (55 to 2000HZ): < 100 ms/s<sup>2</sup>  
 Power Requirement: Universal worldwide voltage | 110-240

T: +44 (0)1270 216000 F: +44 (0)1270 216123 E: [sales@europac3d.com](mailto:sales@europac3d.com)



G800208

# Appendix IV: Description of Cimcore Accuracy Terminology



## **CIMCORE**

**CIMCORE is a brand of Hexagon Metrology for portable measuring arms. CIMCORE Arms are sold and supported through a worldwide network of independent distributors that bring local support and expertise.**

**CIMCORE brand products are built in ISO certified Hexagon Metrology factories located in Carlsbad, CA and Montoire, France.**

**The Volumetric Accuracy Test** most accurately represents the reasonable expectations for machine performance in practical measuring applications since it involves measuring a certified length standard many times in several locations and orientations and compares the resultant measurements to the actual length. The Volumetric Length Accuracy Test is the most appropriate test for determining machine accuracy and repeatability. The result is the maximum deviation of the measuring distance less the theoretical length.

**The Point Repeatability Test** is the reference test to determine measurement arm repeatability with ball probe. The cone is in front of the machine. Points are measured from multiple approach directions. The average point and the deviation of each point to the average center are calculated. The result is the maximum range divided by two.

### **Ambient conditions**

Working temperature: 0°C - 50°C (32°F – 122°F)  
Storage temperature: -30° -70° C (-22°F – 158°F)  
Relative humidity: 10% - 90% non-condensing  
Operational elevation: 0-2000 m (0-6600 ft)

### **Marks of conformity**

CE Compliance: Yes

### **Power requirement**

Universal worldwide voltage 110V-240V

## Appendix V: LHA Embalming Protocol

- Cadavers presented to the Anatomy dept for dissection are initially embalmed using arterial injection and embalming completed by subcutaneous spot injection.
- Name tags, garments, jewellery and hair: removed.
- Cadaver tagged with correct year/ body number as required by the Anatomy Act 1984 (amended 2006).
- Mouth sutured and eye caps placed between eye and eyelid.
- Incision made immediately above clavicle and carotid artery raised/opened to accept large bore cannula.
- 3 litres of Industrial Methylated Spirits (IMS) injected to prevent rapid fixation of blood by formaldehyde (to prevent artery blockage).
- 25-30 litres of embalming fluid\* injected using “PORTIBOY” Mark V high pressure injection pump (between 30psi and 50psi).
- Cadaver left over night to allow settling of fixative.
- Areas of poor fixation to be subcutaneously spot injected using open ended cannula (connected to embalming pump).
- Carotid incision sutured.
- Cadaver washed, placed in transparent body bag, tagged and refrigerated at 4°C for approximately 6 weeks prior to use.

\* Cambridge Formulation Embalming Fluid:

Solution	ml/litre
IMS	625ml
Phenol (80%)	125ml
Formaldehyde (37%)	75ml

Add to mixture:

Phenoexetol (mould growth inhibitor)	5ml
--------------------------------------	-----

